An investigation into the sources of iron and iron(II) in HNLC high-latitude oceans

by

Christina Schallenberg
M.Sc., Dalhousie University, Halifax, 2003

A Dissertation Submitted in Partial Fulfillment of the
Requirements for the Degree of

DOCTOR OF PHILOSOPHY

in the School of Earth and Ocean Sciences

An investigation into the sources of iron and iron(II) in HNLC high-latitude oceans

by

Christina Schallenberg
M.Sc., Dalhousie University, Halifax, 2003

Supervisory Committee

Dr. Jay T. Cullen, Supervisor
(School of Earth and Ocean Sciences)

Dr. Roberta Hamme, Departmental Member
(School of Earth and Ocean Sciences)

Dr. James Christian, Departmental Member
(School of Earth and Ocean Sciences)

Dr. David Harrington, Outside Member
(Department of Chemistry)

Dr. Philippe Tortell, Additional Member
(Department of Earth, Ocean & Atmospheric Sciences, University of British Columbia)

Supervisory Committee

Dr. Jay T. Cullen, Supervisor
(School of Earth and Ocean Sciences)

Dr. Roberta Hamme, Departmental Member
(School of Earth and Ocean Sciences)

Dr. James Christian, Departmental Member
(School of Earth and Ocean Sciences)

Dr. David Harrington, Outside Member
(Department of Chemistry)

Dr. Philippe Tortell, Additional Member
(Department of Earth, Ocean & Atmospheric Sciences, University of British Columbia)

ABSTRACT

High nutrient, low chlorophyll (HNLC) regions, where the availability of iron (Fe) limits primary production, comprise approximately 40% of the global ocean. Variability in Fe supply to these regions has the potential to impact Earth's climate by affecting the efficiency of the biological carbon pump, and thereby carbon dioxide uptake by the oceans. Characterizing Fe sources to HNLC regions is thus crucial for a better understanding of the connections and feedbacks between the ocean and climate change.

This work addresses the question of Fe supply to two HNLC regions: the Southern Ocean and the subarctic northeast (NE) Pacific Ocean. In both regions, dissolved Fe (dFe) and the reduced form of iron, Fe(II), were measured in the water column. In

the Southern Ocean, measurements were undertaken under the seasonal pack ice in the East Antarctic south of Australia. The results indicate that the sea ice represents a significant dFe source for the under-ice water column in spring, and that the Fe delivered from brine drainage and sea ice-melt likely contributes to the formation of the spring bloom at the ice edge. Shelf sediments were also found to supply dFe to the water column. Their effect was most pronounced near the shelf break and at depth, but offshore transport of Fe-enriched waters was also implicated. Fe(II) concentrations in spring were very low, most likely due to a lack of electron donors in the water column and limited solar radiation underneath the sea ice.

Repeat measurements along a transect in the subarctic NE Pacific indicate that shelf sediments supply dFe and Fe(II) at depth, but their influence does not appear to extend offshore beyond several hundred kilometres. Episodic events such as the passage of sub-mesoscale eddies may transport subsurface waters a limited distance from the shelf break, supplying Fe(II) in a depth range where upwelling and deep mixing could bring it to the surface. Offshore, dFe shows little variability except in June 2012, where an aerosol deposition event is suspected to have increased dFe concentrations at depth. Fe(II) concentrations offshore are generally low, but show transient maxima at depth that likely result from remineralization processes in the oxygen deficient zone that stretches from ∼600 to 1400 m depth in the subarctic NE Pacific. Elevated Fe(II) concentrations at depth were also observed in conjunction with the aerosol deposition event, which might indicate Fe(II) production associated with settling particles. However, the aerosol deposition event, which most likely stemmed from forest fires in Siberia, did not appear to trigger a phytoplankton bloom in surface waters, possibly due to a lack of Fe fertilization from the deposited material, or due to toxic effects on the resident phytoplankton community.

Dust deposition from the atmosphere is considered a major Fe supply mechanism to remote HNLC regions, but the factors affecting Fe solubility of dust are poorly constrained. A laboratory experiment was conducted to test whether the presence of superoxide, a reactive oxygen species, enhances the dissolution of dust from different geographic source regions. The results indicate that superoxide may promote Fe solubilization from the dust sources tested, and that the effect of exposure to superoxide is on par with the Fe solubilizing effect of photochemical reactions. Given the possibility of widespread superoxide production by heterotrophic bacteria at all depths of the ocean, this finding suggests that significant Fe dissolution of dust particles could occur throughout the water column, not only in the well-lit surface layer.

Contents

List of Tables

List of Figures

ACKNOWLEDGEMENTS

On the long list of people to whom I extend my gratitude, surely Jay deserves to be mentioned first. Jay, it's an honour to be your first PhD student, and I can't tell you how much I appreciate your guidance and patience throughout this journey that was my PhD project. Thank you for bearing with me when I declared that "it had all been done", having managed to convince myself that there were no interesting research questions left in my field. Thank you also for standing by me to trouble-shoot a perfectly working superoxide system for months on end. I won't lie and say it was all a blast, the superoxide chapter certainly wasn't, but all in all it's been a great time of my life, and I'm especially grateful for your trust in me, for granting me a lot of personal freedom, and for a healthy work-life balance in your supervisory model. Last but not least, I want to thank you for inviting me — along with our lab group — into your family: Tracy, this is also a shout-out to you! I will forever remember with fondness the Beer and Cheese nights, Feats of Strength, and games of Settlers.

Next I would like to thank my supervisory committee: Roberta, Jim, David, Phil — you were all there for me when I needed to discuss a particularly tricky aspect of my data, and I thank you for that. All along I've considered you more of a "support team" than a supervisory committee, and I'm grateful for all your help, advice and comments throughout the years, and for not holding it against me when my research has been outside your comfort zone.

My thesis would not have been complete without the research that I was able to do in Tasmania. My gratitude extends to Andy Bowie for taking a chance on me and sending me to the Antarctic, and also to Delphine Lannuzel and Pier van der Merwe for their support in generating and interpreting my data.

Back in Victoria, my student life was much enriched by the members of the Cullen lab group. I would like to especially acknowledge Dave, Sarah and Trish, as well as the industrious and stealthy Beer Fairy. Special thanks to Dave, not only for expanding my knowledge of aquatic chemistry to the intricacies of beer brewing, but also for teaching me in the most gentle way possible what does — and does not — constitute a limerick. I shall never forget. Thanks also for ruining my beer taste buds forever, and for wearing short shorts in the bubble, among many other things that have made lab life happier over the years. I'm glad you took a chance on our group, even though our score in your excel spreadsheet wasn't that stellar.

There are also many people "behind the scenes" without whom this work would

not have been possible. This includes the SEOS office, with special thanks to Allison for being so incredibly patient and always helpful, and for lending an ear when needed. As well, I spent a lot of time on Coastguard and research vessels, and would be virtually without data were it not for the help of the captains and crews of these vessels, and some wonderful chief scientists, with special mention of Marie Robert who has been incredibly accommodating of our trace metal requirements. The friendly people of the Institute of Ocean Sciences have been instrumental to the success of all these cruises, and so have the members of the respective "trace metal gangs". At UVic, our lab gets a lot of support from the good people at Science Stores, the Mechanical Shop and the Electronics Shop, and I'm very grateful for that. I would also like to acknowledge the assistance of DT Abbey in getting me through the last stages of thesis writing.

Finally, I need to thank the people who had nothing to do with the thesis work itself, but who have everything to do with the success of this endeavour. My family and friends, both near and far: You make it all worthwhile, and you've carried me through when I was wondering what the heck I am doing. Thank you for being part of this journey, for believing in me, for listening to my rants, for taking me to the spa, for making me laugh and for letting me cry. I couldn't have done this without your love and support. And of course thank you, Klaus, for so many more things than fit into this paragraph.

I dedicate this dissertation to my parents, who have supported me with their love and trust throughout my meandering life journey, and who have set me free to make my home in Canada.

Chapter 1

Introduction

In this chapter, I present background information on iron (Fe) in the ocean, providing not only a framework but also a motivation for studying this essential micronutrient's behaviour in the marine environment. There is particular uncertainty about the sources and cycling of Fe in the ocean, with implications for the global carbon cycle on glacial-interglacial timescales. Thie general introduction is followed by a section where I briefly describe the motivation for the individual chapters of my thesis.

1.1 Iron in the ocean

It is estimated that in about 40% of the world's oceans, the micronutrient iron (Fe) is in such low supply that it limits primary productivity (Moore et al., 2002). These Fe-limited regions are often termed high nutrient, low chlorophyll (HNLC) because macronutrients are underutilized compared to other oceanic regions where Fe is in sufficient supply (see Figure 1.1). The low Fe concentrations in HNLC regions result from both low Fe input and low solubility of the metal. Fe is only sparingly soluble in oxygenated seawater (Liu and Millero, 2002) and it has a short residence time due to precipitation reactions and significant scavenging loss onto particle surfaces (Boyd and Ellwood, 2010).

However, the solubility of Fe in seawater is greatly enhanced by the presence of organic ligands. More than 99% of the dissolved Fe (dFe) in the oceans is complexed by organic ligands, raising the solubility of Fe by more than an order of magnitude (Boye et al., 2001; Gledhill and Buck, 2012; Gledhill and van den Berg, 1994; Kuma et al., 1996; Rue and Bruland, 1995; Wu and Luther III, 1995). Marine organic

ligands are still poorly characterized, and their sources likely range from river input and sedimentary processes to biological production (Gledhill and Buck, 2012). In regions with high Fe supply, organic ligands are thought to play an important role in setting the solubility limit for Fe (e.g., Baker and Croot, 2010; Thuróczy et al., 2012).

1.2 Iron and the biological carbon pump

Changes in the supply of iron to the oceans have the potential to affect the global carbon cycle because they have a direct impact on the ability of phytoplankton to take up carbon dioxide (CO_2). The biological carbon pump is the process whereby the uptake of CO_2 by phytoplankton is followed by the sinking of cells to the ocean interior, where the fixed CO_2 is cut off from communication with the atmosphere for centuries to millennia (Falkowski et al., 1998; Sunda, 2010). The availability of Fe in the surface ocean may thus exert a direct control on the Earth's climate.

This possibility prompted John Martin (1990) to formulate the "iron hypothesis", which proposes that increased Fe supply to the Southern Ocean during glacial periods may have contributed to the ∼80 ppm atmospheric CO_2-drawdown recorded in ice cores. Numerous mesoscale Fe-addition experiments have been conducted since, confirming that Fe infusions in HNLC regions of the ocean do indeed enhance primary productivity (e.g., Boyd et al., 2000, 2007; Coale et al., 2004; Smetacek et al., 2012). While the evidence regarding sustained CO_2-drawdown from these experiments remains controversial, studies exploring carbon export resulting from natural Fe fertilization in the Southern Ocean have found indicators of substantial carbon sequestration (e.g., Blain et al., 2007; Pollard et al., 2009).

1.3 Iron supply to the ocean

The role of Fe in limiting the biological carbon pump highlights the importance of understanding the sources of Fe to the ocean, and how they may have varied through time. The Fe supply to HNLC regions is of particular interest in this respect, as these areas have the strongest potential to influence the global carbon cycle via the biological carbon pump (Measures et al., 2012).

The sources of Fe to the ocean are numerous, with river input and shelf sediments important contributors in coastal waters (Buck et al., 2007; Elrod et al., 2004; Johnson et al., 1999). Hydrothermal vents also make a substantial Fe contribution, but their

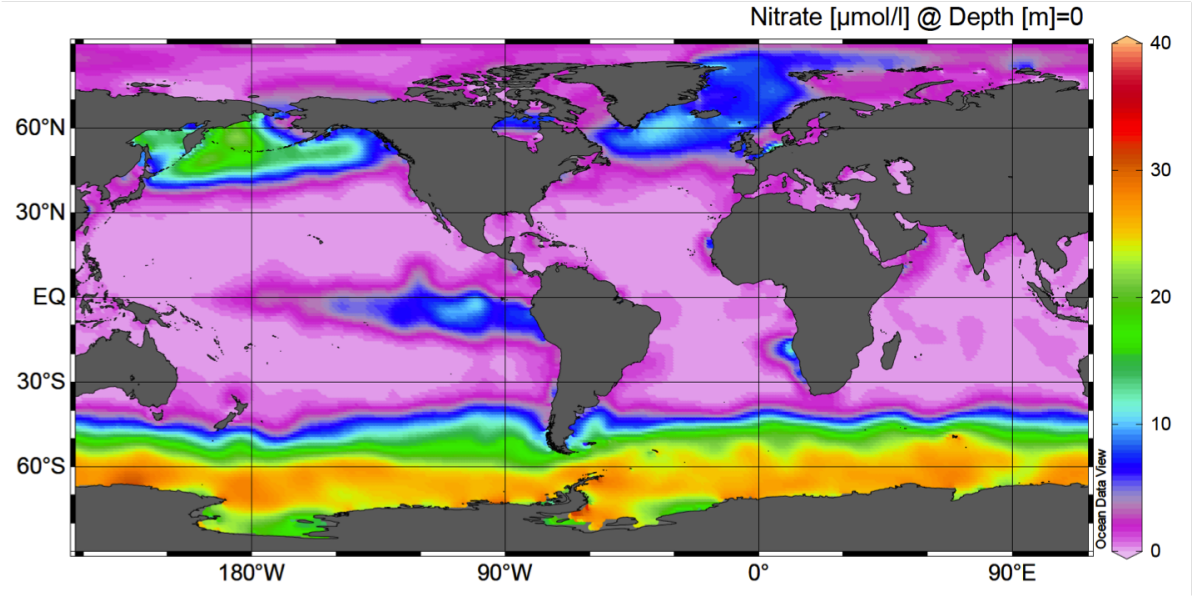

Figure 1.1: Global map of surface nitrate concentrations in the ocean. HNLC areas are evident as regions where nitrate concentrations are elevated.

impact on phytoplankton is limited because the Fe input is restricted to the deep ocean (Tagliabue et al., 2014, 2010). In the open ocean, eolian deposition of terrigenous dust can play an important role and is the mode of Fe supply that is implicated in the "iron hypothesis" (Jickells et al., 2005; Martin, 1990; Moore and Braucher, 2008). However, in the contemporary open ocean, sedimentary sources are estimated to contribute at least as much Fe to the global ocean inventory as dust input (Moore and Braucher, 2008).

In addition to desert dust, there are other aerosol sources such as forest fires and volcano eruptions that can supply Fe to the surface ocean (e.g., Guieu, 2005; Hamme et al., 2010; Ito, 2011). In the northeast subarctic Pacific, wind-mobilized glacial flour may also have a role to play (Crusius et al., 2011; Schroth et al., 2009). While deposition of aerosols in the open ocean is not in question, the effect on the dissolved Fe inventory of the ocean is much less certain. For example, the Fe solubility estimates for atmospheric dust span several orders of magnitude (Boyd et al., 2010), and mesocosm studies suggest that the deposition of dust in seawater can in fact lead to a decrease of dissolved Fe in surface waters through adsorptive scavenging to particle surfaces (Wagener et al., 2010).

There are additional Fe sources to HNLC regions that operate on different time

and spatial scales. For example, in the northeast subarctic Pacific, mesoscale eddies can transport considerable amounts of dissolved and particulate Fe from their coastal source region to the HNLC open ocean (Brown et al., 2012; Johnson et al., 2005; Lippiatt et al., 2011; Xiu et al., 2014). Though relatively small in area, i.e. with diameters no more than ∼200 km, the Fe-fertilizing effect of such mesoscale eddies may continue for more than a year (Johnson et al., 2005). In the Southern Ocean, sea ice, icebergs and melting glaciers may provide significant local Fe input (Gerringa et al., 2012; Lannuzel et al., 2014; Lin et al., 2011; Raiswell et al., 2008; Vancoppenolle et al., 2013).

1.4 Bioavailability of Fe

Iron can take many different forms in the ocean. In terms of size classes, there are three phases, conventionally defined as follows (e.g., Cullen et al., 2006; Wu et al., 2001):

- the particulate phase (>0.4 μm)
- the colloidal phase (<0.4 μm and >0.02 μm)
- the soluble phase (<0.02 μm)

The colloidal and soluble phases are frequently combined, with dissolved Fe (dFe) operationally defined as either <0.2 μm or <0.4 μm. In this thesis, dFe is defined as <0.2 μm. The colloidal phase can make up a substantial portion of the dFe pool in the ocean (Bergquist et al., 2007) and may show behaviour distinct from the soluble phase. For example, Cullen et al. (2006) found that colloidal Fe may be inert to ligand exchange with the soluble phase. Both the colloidal and the soluble Fe pool largely consist of organically bound Fe, but partitioning between the two phases cannot be fully explained by organic ligand distributions (Cullen et al., 2006).

The bioavailability of the different forms of Fe in the ocean is still being investigated (Shaked and Lis, 2012). While the dissolved phase is generally assumed to be the primary pool that phytoplankton tap into, some species may also be able to access particulate Fe (e.g., Rubin et al., 2011). In the dissolved fraction, colloidal Fe may be less bioavailable than the soluble phase (e.g., Chen and Wang, 2001), and organically bound Fe is less accessible than inorganic Fe (Lis et al., 2014; Maldonado and Price, 1999; Maldonado et al., 2005).

The most bioavailable species of Fe in the ocean is assumed to be the reduced form of Fe, Fe(II). This is largely due to the fact that reduction of Fe appears to be an intermediate step in the Fe-uptake mechanism employed by various phytoplankton (Kranzler et al., 2011; Lis et al., 2014; Maldonado and Price, 2001; Shaked et al., 2005). Photochemical reduction of organically bound Fe also decreases ligand binding strength, rendering the complexed Fe more labile and increasing its bioavailability (Barbeau et al., 2001).

1.5 Iron(II) in the ocean

While Fe(II) is the more soluble form of inorganic iron, it is usually present at very low concentrations in oxygenated seawater because it is thermodynamically unstable under oxic conditions (Millero et al., 1987). In order for detectable steady-state concentrations of Fe(II) to be present, its production must exceed loss terms such as oxidation and biological uptake, and/or Fe(II) must be stabilized, for example by organic ligands (Croot et al., 2001; Roy et al., 2008). The Fe(II) half-life in the surface ocean is typically on the order of minutes and is strongly dependent on temperature, with half-lives $\sim$30 minutes in waters around 5°C, and $<$1 minute at 25°C.

In the surface ocean, photochemical reactions are a common pathway for the production of Fe(II) (Rijkenberg et al., 2005; Sarthou et al., 2011). These reactions involve organic molecules that have the ability to absorb light and act as electron donors (e.g., Barbeau et al., 2001). In addition, Fe reduction at cell surfaces may be a source of Fe(II) (Lis et al., 2014; Maldonado and Price, 2001). The superoxide anion, O_2^-, is thought to be a common intermediate in the photochemical reduction of Fe (Fan, 2008; Garg et al., 2007b; Rose and Waite, 2006), and it may also play a role in biological Fe reduction and aid iron acquisition (Garg et al., 2007a; Rose, 2012; Rose et al., 2005).

The known Fe(II) sources in the deep ocean include hydrothermal vents, remineralization processes and benthic fluxes from anoxic sediments (Lohan and Bruland, 2008; Sarthou et al., 2011; Sedwick et al., 2014; Statham et al., 2005). The recent discovery of widespread superoxide production by heterotrophic bacteria ubiquitous in the ocean (Diaz et al., 2013) may point to an additional pathway for Fe(II) production at depth.

1.6 Thesis motivation and outline

For my research, I have sought to investigate the sources of Fe to HNLC regions of the ocean. Specifically, I have focused on two areas: the seasonally ice-covered Southern Ocean and the subarctic northeast Pacific Ocean. The Southern Ocean is the largest HNLC area on the planet, and up to 40% of its surface is seasonally covered by sea ice (Comiso, 2010). Sea ice is enriched in Fe compared to seawater, and the seasonal sea ice-melt represents an important Fe source to the Southern Ocean (Lannuzel et al., 2010). I have measured dFe and Fe(II) concentrations under the pack ice in the East Antarctic in spring, with the goal to investigate the Fe contribution from sea ice in the context of other Fe sources to the Southern Ocean (**Chapter 2**).

In the HNLC subarctic Pacific Ocean, repeat measurements of dFe and Fe(II) concentrations along a transect from coastal to open ocean waters have allowed me to assess the variables and supply terms that shape the distribution of dFe and Fe(II) in this area (**Chapter 3**). The presence of an oxygen deficient zone (ODZ) between 600 and 1400 m depth adds to the complexity of this oceanic region and considerably slows Fe(II) oxidation rates. Fe(II) concentrations and their variability through time not only point to reductive dFe sources such as anoxic sediments, but are also noteworthy in their own regard due to the higher bioavailability of Fe(II) relative to Fe(III). Of particular interest in Chapter 3 is the potential role of particles as a source of Fe(II), which partly motivated the experiment described in Chapter 4.

With the experiment detailed in **Chapter 4**, I sought to investigate whether superoxide is able to promote Fe solubility of lithogenic particles from a variety of geographic source regions, producing Fe(II) in the dissolution process. My interest in superoxide as an intermediate was spurred particularly by the discovery of widespread superoxide production by heterotrophic bacteria (Diaz et al., 2013), which opens up the possibility that "photochemistry-like" reactions, i.e. involving superoxide, may take place at all depths of the ocean. Such a process would not only be relevant for dust particles deposited in the ocean and subsequently sinking through the water column, but also for sedimentary particles from the shelf and shelf break that may be transported hundreds of kilometers in the subsurface (e.g., Lam and Bishop, 2008; Lam et al., 2006).

The deposition of aerosols is thought to be an important Fe supply mechanism for the HNLC subarctic Pacific Ocean (Jickells et al., 2005; Moore and Braucher, 2008), and several researchers have observed anomalously high phytoplankton biomass in this

region following the deposition of dust and ash (e.g., Bishop et al., 2002; Hamme et al., 2010). The observed phytoplankton response is usually ascribed to Fe fertilization from the respective aerosols. However, all aerosols may not be created equal. In **Chapter 5**, I report on an aerosol deposition event in the HNLC subarctic Pacific Ocean in May 2012 that did not appear to elicit a phytoplankton response. The aerosol likely stemmed from Siberian forest fires. While it resulted in elevated dFe and Fe(II) concentrations at depth, surface dFe concentrations and key biological parameters related to phytoplankton biomass and production did not show any sign of enhancement.

Chapter 2

Dissolved iron and iron(II) distributions beneath the pack ice in the East Antarctic (120°E) during the winter/spring transition

Schallenberg, C., van der Merwe, P., Chever, F., Cullen, J.T., Lannuzel, D., Bowie, A.R. (2015). Dissolved iron and iron(II) distributions beneath the pack ice in the East Antarctic (120°E) during the winter/spring transition. In press in *Deep-Sea Research II*.

2.1 Abstract

Distributions of dissolved iron (dFe) and its reduced form, Fe(II), to a depth of 1000 m were investigated under the seasonal pack ice off East Antarctica during the Sea Ice Physics and Ecosystem experiment (SIPEX-2) sea-ice voyage in September-October 2012. Concentrations of dFe were elevated up to five-fold relative to Southern Ocean background concentrations and were spatially variable. The mean dFe concentration was 0.44 ± 0.4 nM, with a range from 0.09 to 3.05 nM. Profiles of dFe were more variable within and among stations than were macronutrients, suggesting that coupling between these biologically-essential elements was weak at the time of the study. Brine rejection and drainage from sea ice are estimated to be the dominant contributors to elevated dFe concentrations in the mixed layer, but mass budget considerations

indicate that estimated dFe fluxes from brine input alone are insufficient to account for all observed dFe. Melting icebergs and shelf sediments are suspected to provide the additional dFe. Fe(II) was mostly below the detection limit but elevated at depth near the continental shelf, implying that benthic processes are a source of reduced Fe in bottom waters. The data indicate that dFe builds up under the seasonal sea-ice cover during winter and that reduction of Fe may be hampered in early spring by several factors such as lack of electron donors, low biological productivity and inadequate light below the sea ice. The accumulated dFe pool in the mixed layer is expected to contribute to the formation of the spring bloom as the ice retreats.

2.2 Introduction

The Southern Ocean is the most extensive high nutrient, low chlorophyll (HNLC) region on the planet, i.e. a region where insufficient supply of Fe to surface waters limits primary production (Boyd et al., 2000; de Baar et al., 1995; Martin, 1990). The lack of an adequate Fe supply directly impacts Earth's climate by limiting the efficiency of the biological carbon pump and, by extension, the ocean's ability to absorb atmospheric carbon dioxide (Martin, 1990; Sunda, 2010; Watson et al., 2000). Elucidating the biogeochemical cycling of Fe in the Southern Ocean is therefore a crucial step towards a better understanding of the connections and feedbacks between ocean processes and climate. Particular attention in this respect has been given to identifying Fe sources that are most quantitatively important to Southern Ocean biogeochemical budgets (e.g., de Jong et al., 2012; Lancelot et al., 2009; Tagliabue et al., 2014, 2009).

For an essential nutrient, the chemistry of Fe is distinctive insofar as it is not only sparingly soluble in seawater under prevailing environmental conditions, but is also subject to significant scavenging loss onto particle surfaces (Liu and Millero, 2002; Ye et al., 2011). As a result, it has a very short residence time in the oceans compared to macronutrients and some other trace elements, and dFe concentrations in surface waters can be in the picomolar range (Boyd and Ellwood, 2010). The vast majority (>99%) of dFe in the ocean is complexed by organic ligands (Boye et al., 2001; Gledhill and Buck, 2012; Gledhill and van den Berg, 1994; Rue and Bruland, 1995). These ligands play an important role in setting the solubility limit for Fe (Baker and Croot, 2010; Tagliabue et al., 2014; Thuróczy et al., 2012).

The bioavailability of the different forms of Fe in the ocean is a matter of ongoing

investigation (Shaked and Lis, 2012). For example, there is evidence that particulate Fe (pFe) is accessible to some phytoplankton (Rubin et al., 2011), and certain fractions of pFe can also release dissolved and soluble Fe over time (e.g., Schroth et al., 2009). Generally, however, dFe is assumed to be the primary pool from which phytoplankton draw, with inorganic Fe the preferred speciation but the organically-bound fraction also being accessible (Maldonado and Price, 1999; Maldonado et al., 2005). In particular, the reduced form of dFe, i.e Fe(II), is considered to be highly bioavailable. Fe(II) is more soluble in seawater than the oxidized form, and reduction of Fe has been shown to be an intermediate step in Fe uptake by various phytoplankton (e.g., Kranzler et al., 2011; Maldonado and Price, 2001; Shaked et al., 2005). In addition, photochemical reduction of organically-bound Fe decreases ligand binding strength, making complexed Fe more labile (Barbeau et al., 2001).

Fe(II), however, is thermodynamically unstable under oxic conditions and detectable steady-state concentrations of the reduced species necessitate constant production to balance biological uptake and oxidation, or that Fe(II) is protected from loss processes, for example through ligand stabilization (Croot et al., 2001; Roy et al., 2008). In the surface ocean, Fe reduction on cell surfaces and photochemical reactions involving chromophores are the most prominent pathways for Fe(II) production (Barbeau et al., 2001; Maldonado and Price, 2001; Rijkenberg et al., 2005). At depth, remineralization processes, hydrothermal vents and benthic fluxes from anoxic sediments are important sources of Fe(II) (Lohan and Bruland, 2008; Sarthou et al., 2011; Sedwick et al., 2014; Statham et al., 2005).

Large parts of the Southern Ocean are seasonally covered by sea ice (Comiso, 2010), which has important implications for the delivery of Fe. Sea ice is highly enriched in Fe relative to seawater, so melting of the ice in spring supplies Fe in both dissolved and particulate form to the surface ocean (e.g., Lannuzel et al., 2010; van der Merwe et al., 2011a,b; Vancoppenolle et al., 2013). In addition, melting of sea ice adds freshwater to the surface layer, enhancing stratification and thereby creating favourable conditions for the initiation of the spring bloom. Ice melting also injects dissolved and particulate organic material, such as exopolysaccharides produced by sea-ice algae and bacteria (Norman et al., 2011; van der Merwe et al., 2009). These have the potential to influence Fe bioavailability as they may act as ligands and/or electron donors for the photochemical reduction of Fe (Hassler et al., 2011a,b).

Seasonal sea ice also poses an obvious barrier to studying the water column below. For this reason, there are very few reports of Fe distribution under the ice, especially in

waters below the upper mixed layer. The data presented in this manuscript highlight the spatial variability in dFe concentrations below the Antarctic pack ice to a depth of 1000 m and allow me to contemplate the relevant Fe sources that set the stage for the spring bloom in the seasonally ice-covered Southern Ocean.

2.3 Materials and Methods

2.3.1 Study area

Sampling was undertaken during a multi-disciplinary sea-ice study, SIPEX-2, in September/October 2012 aboard RV Aurora Australis. The sampling region lies between 62 and 66°S and 118 and 122°E (Figure 2.1), an area off the East Antarctic shelf that is seasonally covered by sea ice. Seven stations were sampled, all with bottom depths $\geq$ 2000 m. Stations 0–6 are located offshore of the Antarctic continental shelf, while station 7 is located at the shelf break.

2.3.2 Sampling methods

All sampling and sample handling followed GEOTRACES recommendations (Cutter et al., 2010). An autonomous trace element-clean rosette system (TMR model 1018, General Oceanics) was deployed from the stern of the RV Aurora Australis. The system consists of a polyurethane powder-coated aluminum frame with sacrificial Mg anodes and is equipped with 12 $\times$ 10 L externally-closing Teflon^{TM}-lined Niskin-1010X bottles as well as an RBR temperature logger (TDR-2050). The TMR was ballasted with plastic-coated lead weights and attached with a stainless steel (316 grade) shackle to $\sim$2000 m of Dyneema^{TM} rope on a purpose-built winch dedicated to TMR deployments. This TMR system has been used successfully on previous research voyages and has been shown to be non-contaminating for trace elements (e.g., Bowie et al., 2009). The main CTD aboard RV Aurora Australis used SBE 9plus instrumentation from Sea-Bird Electronics.

Samples for dFe, Fe(II) and macronutrient analyses were filtered through acid-cleaned 0.2 μm cartridge filters (Pall Acropak) in a trace-metal clean laboratory under constant airflow from several ISO class 5 HEPA units. All plastic ware was acid-cleaned according to GEOTRACES protocols (Cutter et al., 2010) prior to use. Samples for dFe analysis were collected into 125 mL low-density polyethylene bottles,

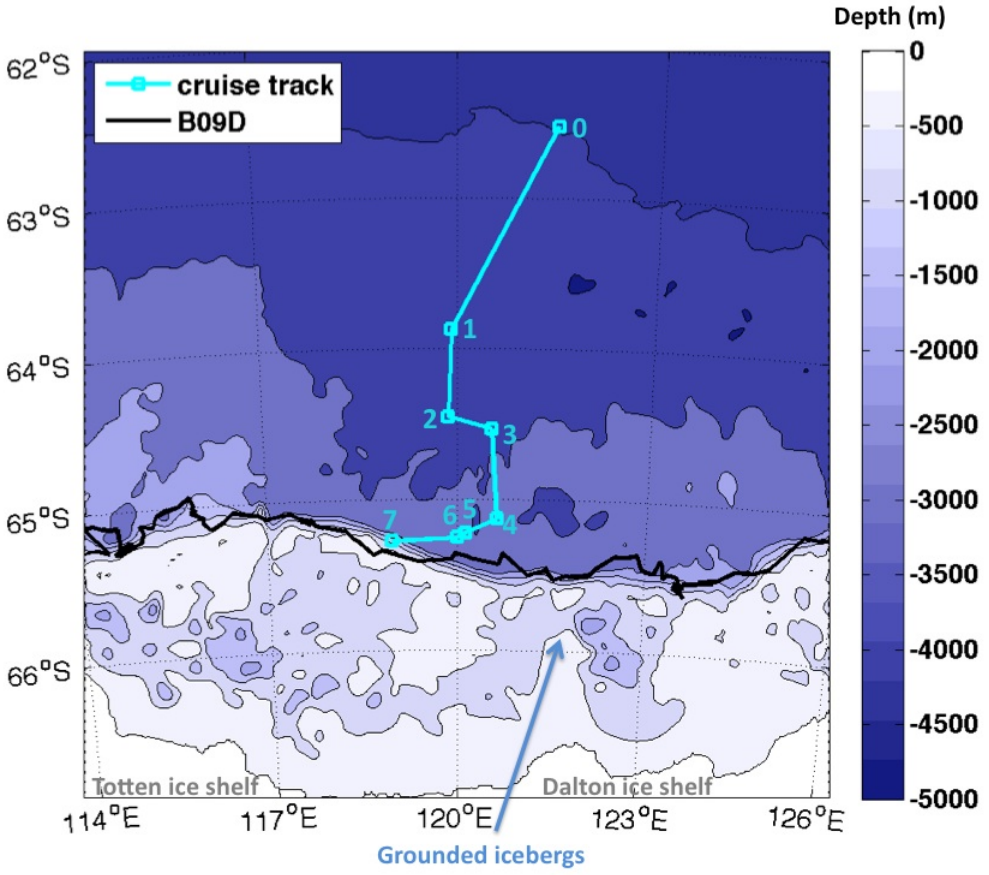

Figure 2.1: Map of station locations (cyan) with nearby coastal and shelf features as well as underlying bathymetry (ETOPO1). The track of iceberg B09D is also indicated (in black). Bathymetry contour levels are as follows: 0, 500, 1000, 1500, 2000, 3000, 4000 and 5000 m.

acidified to pH 1.7 with Seastar Baseline hydrochloric acid (HCl) within 12 hours of collection and stored at room temperature until analysis back in the shore-based laboratory. Macronutrient samples were stored at -20°C in 10 mL polypropylene tubes. Seawater for determination of Fe(II) was collected in 60 mL Teflon^{TM} bottles and analyzed immediately. Note that no Fe(II) measurements were undertaken at stations 0 and 1, and not all available depths were sampled for Fe(II) at the remaining stations due to logistical constraints.

2.3.3 Macronutrients

Samples for $Si(OH)_4$, PO_4^{3-} and NO_3^-+NO_2^- were analyzed at Analytical Service Tasmania (Hobart, Australia) within 6 months of sample collection. Dissolved inorganic nutrients were determined using standard colorimetric methodology as adapted for flow injection analysis using an auto-analyzer.

2.3.4 Dissolved Fe

Dissolved Fe in this study is operationally defined as the Fe fraction that passes through a 0.2 μm filter. A modified flow injection analysis (FIA) method was used to measure dFe that relies on the detection of Fe(III) with the chemiluminescent reagent luminol (de Jong et al., 1998; Obata et al., 1993). Samples and standards were treated with hydrogen peroxide (H_2O_2; final concentration = 10 μM) at least 1 hour prior to measurement to oxidize any Fe(II) that might be present (Lohan et al., 2006). The system buffers the samples in-line to pH = 4 before passing them for 3 minutes through a pre-concentration column packed with 8-hydroxyquinoline chelating resin (8-HQ). A solution of 0.3 M HCl (Seastar) then elutes Fe(III) from the resin and mixes with 0.8 M ammonium hydroxide (NH_4OH), 0.1 M H_2O_2 and 0.3 mM luminol containing 0.3 mM triethylenetetramine (TETA) and 0.02 M sodium carbonate (Na_2CO_3), yielding an optimum luminol chemiluminescence reaction pH of 9.5. The resulting solution is passed through a $\sim$5 m mixing coil maintained at 35°C before being pumped to the flow cell mounted in front of a photo-detector.

System blanks were 0.014 ± 0.004 nM, yielding a detection limit (3 $\times$ blank standard deviation) of 0.013 nM. Results for SAFe reference materials for Fe were in good agreement with consensus values (Table 2.1).

2.3.5 Fe(II)

Fe(II) was determined by luminol chemiluminescence detection following the approach of Hansard and Landing (2009) but without sample acidification. Sampling began within minutes after the first Niskin-X bottle (always from the surface) arrived in the clean container. Samples were analyzed within 2 minutes of filtration and were pumped simultaneously with the luminol reagent into a spiral flow cell made of flexible Tygon^{TM} tubing (ID = 0.7 mm) that was mounted in front of a photomultiplier tube (Hamamatsu H9319-01) in a custom-made light-tight box. Flow rates for luminol

Reference standard	# of analyses	Measured (nmol L^{-1})	Calculated (nmol kg^{-1})	Consensus value (nmol kg^{-1})
D2	6	0.90 ± 0.03	0.88 ± 0.03	0.933 ± 0.023
D1 (305)	6	0.69 ± 0.04	0.67 ± 0.04	0.67 ± 0.04
S	2	0.107 ± 0.002	0.105 ± 0.002	0.093 ± 0.008

Table 2.1: Results for analyses of SAFe reference materials, showing the respective means and standard deviations. For conversion to nmol kg^{-1}, seawater density was assumed to be 1.025 kg L^{-1}.

and sample were ∼4.5 mL/min. The photomultiplier tube was operated at 900 V with a 200 ms integration time. Photon counts were recorded using FloZF software (GlobalFIA) and were averaged over 10 second intervals with 5 replicates for each sample and standard. The relative standard deviation of these repeat measurements was between 1 and 3%.

The luminol recipe for 1 L reagent is as follows: 0.13 g luminol, 0.34 g Na_2CO_3, 40 mL concentrated NH_4OH and 10-12 mL concentrated HCl (Seastar). This results in 0.75 mM luminol with 3.2 mM Na_2CO_3. The pH of the reagent was adjusted to ∼10.0 with small amounts of NH_4OH and HCl. It was found that luminol sensitivity increases with age, so batches were prepared well in advance and used up to 3 months later.

Fe(II) calibration curves were obtained with Fe(II) standard additions in the range 0–100 pM. A 10 mM standard of ammonium iron(II) sulfate hexahydrate was prepared fresh in 0.1 M Seastar HCl and considered stable in the fridge for up to a month. From this stock solution, intermediate standards (50 μM and 50 nM) were prepared in 0.05 M Seastar HCl no more than 10 minutes prior to measurement. Standards were added to cooled (2–4°C) seawater that had been collected at earlier stations in the cruise and been left in the dark for >24 hours.

Previous investigators (e.g., Rose and Waite, 2001) have commented on the light-sensitivity of the luminol reagent, and it is therefore frequently stored in the dark. In my setup, the reagent was likewise stored in an amber HDPE bottle, but it was found that sensitivity is greatly increased if fluorescent light shines on the clear pump tubing during analysis, so a fluorescent lamp pointed at the pump tubing was an integral part of my system. Indeed, the signal enhancement is so strong that care

must be taken to shield the apparatus from ambient light fluctuations.

Fluorescent light also increases the background chemiluminescence signal of the luminol, so that a linear standard curve will have a non-zero intercept. This intercept was routinely subtracted from the measured photon counts for samples and standards. Blanks, i.e. aged seawater samples, were measured throughout the analysis to keep track of baseline fluctuations, but were not subtracted (mean = 0.17 ± 4 pM, n=22). Detection limits of the method (3 × standard deviation of the zero standard) were between <1 and 4.2 pM (mean = 2.4 ± 1.3 pM, n=5).

The method is very sensitive to the choice of seawater that is used for standard additions, i.e. the seawater matrix for standards needs to be matched carefully to samples. For this reason, relatively fresh seawater was used for standard additions. However, with the extremely low Fe(II) concentrations encountered during SIPEX-2, even this approach frequently yielded negative values, possibly due to differing sensitivities and/or not fully decayed Fe(II) in the standard seawater. It can be argued that the lowest concentration measured in a profile is likely very close to zero. Such an assumption allows us to shift profiles with negative concentrations into the positive range by subtracting the lowest measured value. Both concentrations, i.e. original and "adjusted", are reported and discussed in this manuscript. The largest adjustment (9.7 pM) was necessary at station 4, followed by station 2 with an adjustment of 8.1 pM. The data for the remaining stations were adjusted by <5 pM.

2.4 Results

2.4.1 Sea-ice conditions

All stations with the exception of station 0 were in the inner pack ice. Station 0 was in the marginal ice zone, where deformed first-year sea ice covered approximately 70% of the ocean. At all other stations, the pack ice covered 95–100% of the surface and was often heavily deformed.

The sea-ice thermodynamic properties, structure and iron content are described in Lannuzel et al. (2014). Briefly, dFe (<0.2 μm) in the ice was in the range 0.9 to 17.4 nM, and pFe concentrations reached up to 990 nM (at station 7). The ice exhibited mostly spring-like conditions, with brine volume fractions well above 5%. This indicates high ice porosity and brine channel connectivity, allowing for brine exchange with the water column below (Golden et al., 1998). Even though the sea

ice at station 4 is classified as transitional, i.e. between winter and spring, it was also permeable. Ice texture analysis highlights that the sea ice sampled during SIPEX-2 grew in thickness because of dynamic processes and snow ice formation, leading to a dominance of granular ice over columnar ice. This complex ice texture is mirrored by the heterogeneous distribution of biogeochemical tracers in the sea ice (macronutrients, chlorophyll *a*, POC, PON, DOC and iron). There are no sea-ice data for trace metals or sea-ice properties and structure from stations 0, 1 and 5.

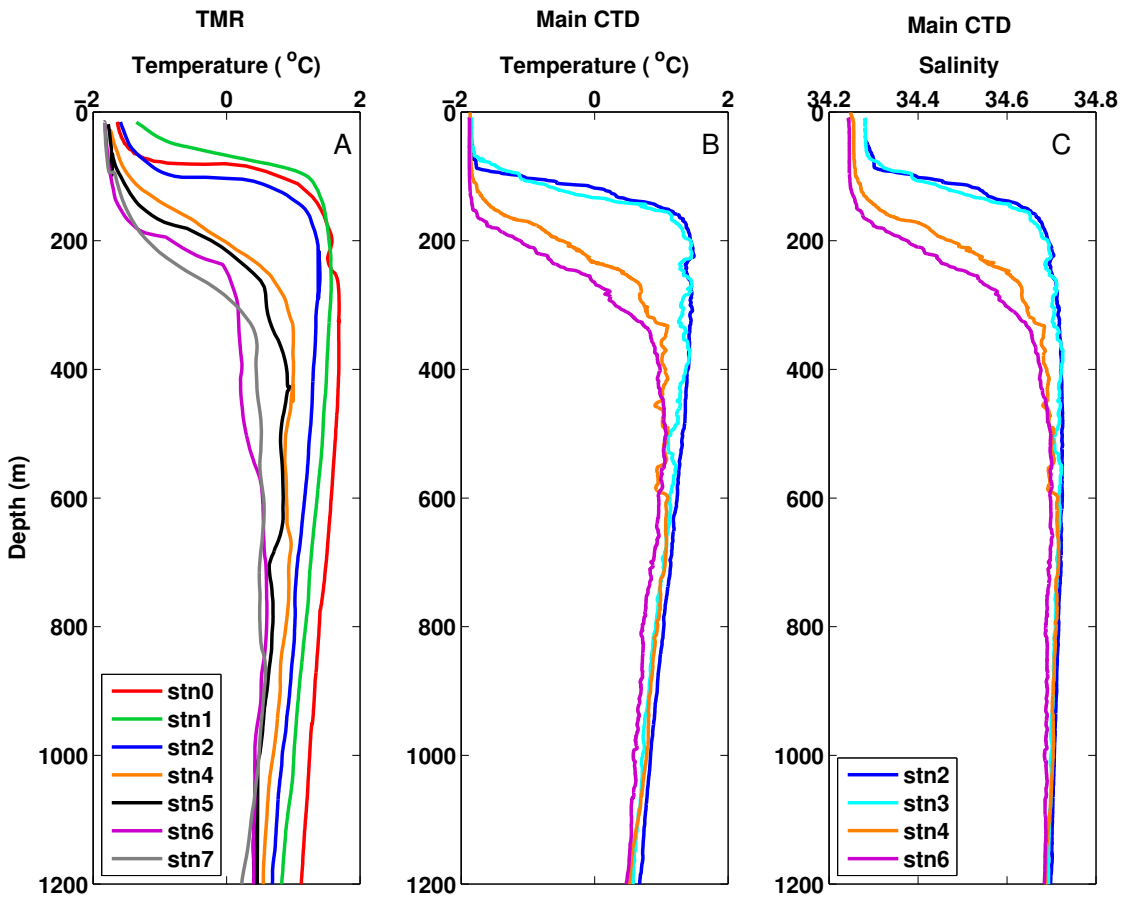

Figure 2.2: Temperature profiles from A) the TMR and B) the main CTD. The TMR temperature logger appears to have smoothed out the profiles relative to the more accurate CTD temperature probe. C) Salinity profiles from the main CTD corresponding to temperature profiles in B.

2.4.2 Water column physical properties

Temperature data from both the main CTD and the TMR are shown in Figure 2.2. The CTD temperature is more accurate and has a higher sampling rate; it can thus be used to vet the measurements from the logger deployed on the TMR. In addition, the CTD measures salinity. The temperature and salinity profiles from the main CTD show a surface winter mixed layer that generally deepens poleward from 90 m at station 2 to about 160 m at station 6 (Figure 2.2). Station 3 does not follow the trend exactly with a mixed layer depth of 70 m, but otherwise shows a very similar pattern to station 2. The surface layer is fresh and cold (salinity 34.25–34.29, temperature -1.85°C) relative to the deeper waters, and the temperature maximum is found around 200 m at the offshore stations and near 400–500 m closer to the Antarctic continent. The salinity of the mixed layer decreases towards the continent.

The TMR temperature profiles that were measured proximate to CTD deployments, both in space and time, agree reasonably well with the CTD profiles as far as the general shape is concerned. However, they appear "smoothed" compared to the CTD data. The "smoothing" effect is likely the result of different instrument response times and logging frequencies, with the TMR logger only recording data every 5 seconds and a response time of 3 seconds compared to a sampling frequency of 24 s^{-1} and a response time of 0.07 seconds on the CTD. Both CTD and TMR travelled at an average speed of 1 m s^{-1}. The CTD data are therefore more accurate, but the TMR data nonetheless capture the general shape of the profiles and confirm the deepening of the surface mixed layer towards the shelf.

The TS diagram for the 4 casts of the main CTD shows distinct differences in the intermediate water (∼150–800 m) between stations (Figure 2.3). Waters in this depth range tend to be warmer — and in the upper layers also fresher — farther offshore (stations 2 and 3) compared to waters closer to the continent (stations 4 and 6).

2.4.3 Macronutrients and chlorophyll *a*

The observed range of values for NO_3^-+NO_2^- , PO_4^{3-} and $Si(OH)_4$ (Figure 2.4, Table A.1), agrees well with expectations for the remote Southern Ocean (e.g., Ibisanmi et al., 2011; Klunder et al., 2011; Sedwick et al., 2008). $Si(OH)_4$ concentrations are lower in the mixed layer (∼60 μM) compared to deeper waters (100–120 μM) and the profiles reflect the deepening of the mixed layer poleward. NO_3^-+NO_2^- concentrations range from 30 to 33 μM, and PO_4^{3-} concentrations range from 2.2 to 2.4 μM with

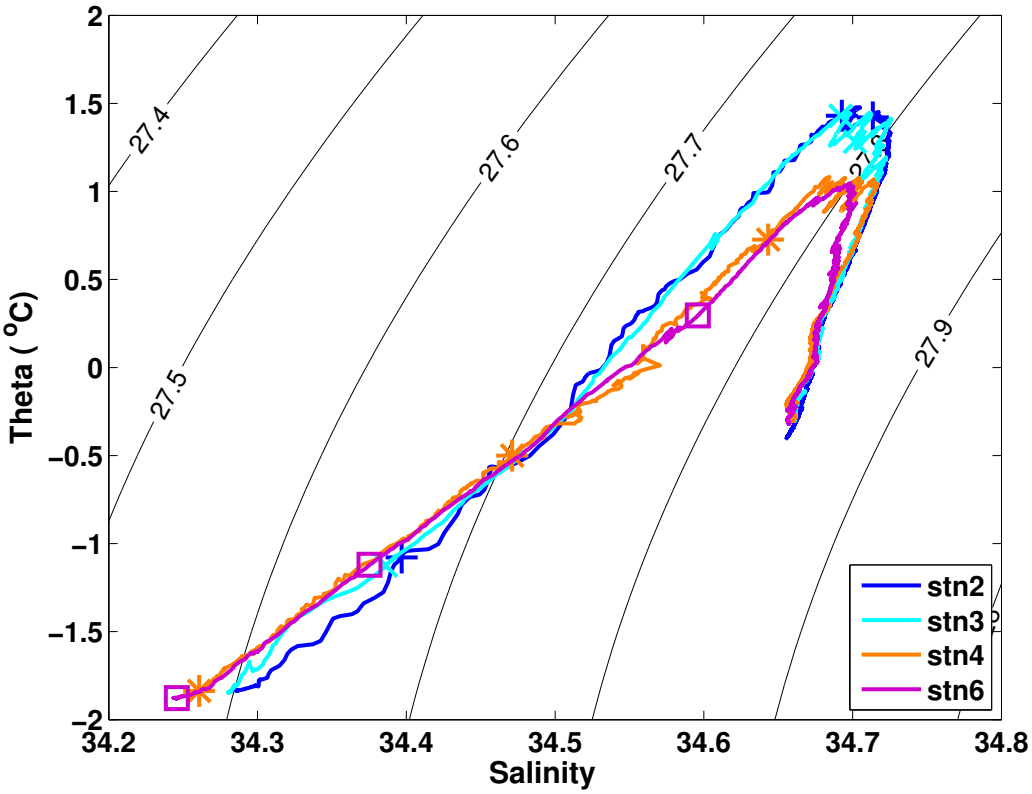

Figure 2.3: Temperature-salinity diagram for data from the main CTD. Symbols indicate the 100, 200 and 300 m marks.

the exception of station 7. Overall, the NO_3^-+NO_2^- and PO_4^{3-} profiles show very low variability with depth and between stations (note the scales on Figure 2.4), with a few exceptions. Firstly, the mixed layer PO_4^{3-} values at station 7 are considerably lower than at any other station. Secondly, the NO_3^-+NO_2^- profiles exhibit the highest variability between 100 and 300 m depth, with stations 0–2 showing sub-surface maxima that appear to coincide with the pycnocline.

The only chlorophyll *a* (chl *a*) profiles available are from the main rosette housing the CTD, and they all show very low chl *a* concentrations with the highest values (0.2–0.3 μg L^{-1}) in the top 50 m at station 6 (personal communication, Karen Westwood). At stations 3 and 4, chl *a* concentrations hover around 0.1 μg L^{-1}, and at station 2 they are between 0.1 and 0.2 μg L^{-1}.

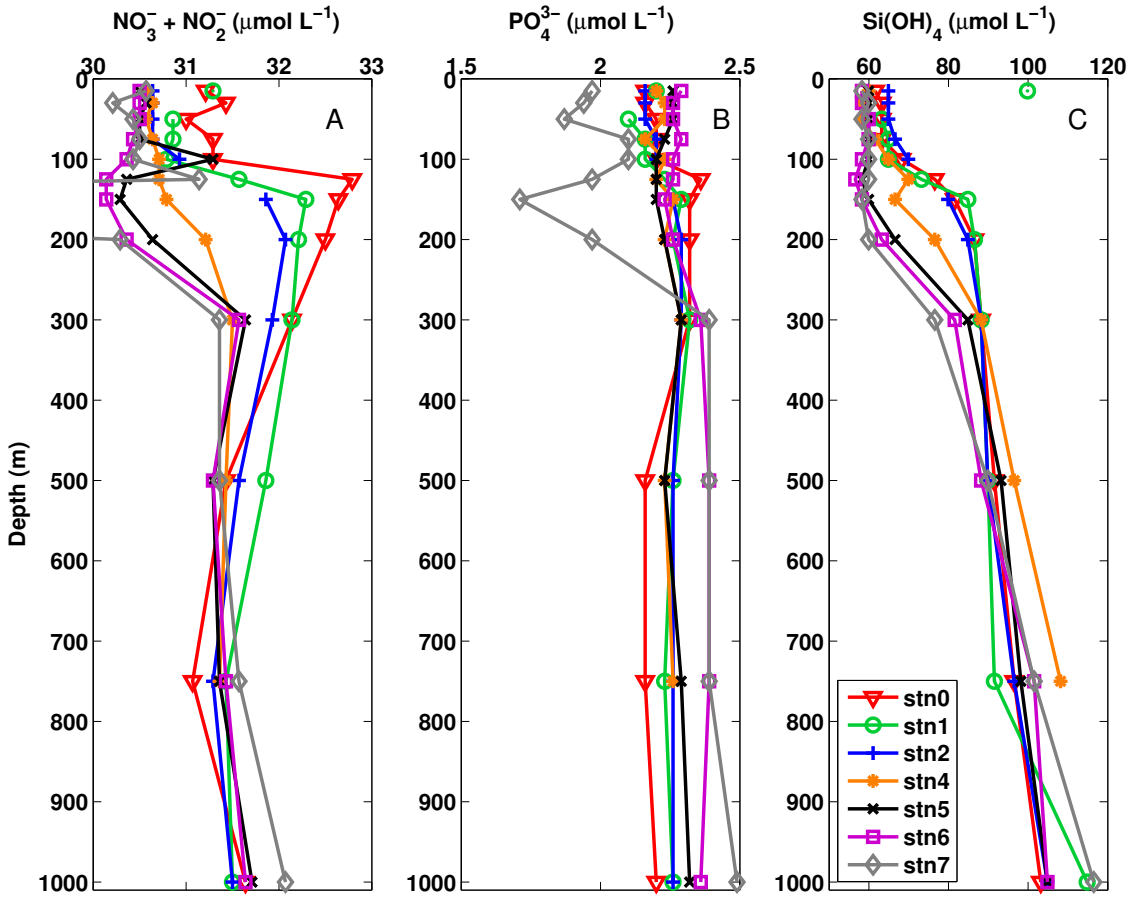

Figure 2.4: Macronutrient concentrations in the water column: A) Nitrate + nitrite, B) Phosphate, C) Silicic acid.

2.4.4 Dissolved Fe

The measured dFe concentrations are in the range 0.09 to 3.05 nM, with a mean of 0.44 ± 0.4 nM and a median of 0.34 nM (Figure 2.5, Table A.1). The dFe profiles show much higher variability both between stations and within profiles than is found in the macronutrient data (Figure 2.4). Mean dFe concentrations vary by up to a factor of 5 between stations (0.16 nM at station 5 vs. 0.81 nM at station 1), and for most of the profiles are higher than those reported for the remote Southern Ocean, which rarely exceed 0.4 nM at the depths sampled here (Bowie et al., 2009; Boye et al., 2001; Chever et al., 2010; Coale et al., 2005; de Jong et al., 2012; Ibisanmi et al., 2011; Klunder et al., 2011; Lannuzel et al., 2011; Moore and Braucher, 2008). Only station 5 resembles a "typical" Southern Ocean profile with low (<0.3 nM) dFe

concentrations throughout, lowest near the surface and slightly increasing with depth. The dFe profile from station 6 is similar (mean = 0.26 nM) but with slightly increased dFe values at depth, i.e. 0.57 nM at 1000 m.

Three of the seven profiles (stations 0, 2 and 4) exhibit maxima at the shallowest depth sampled (15 m), with concentrations 2 times higher than the next shallowest depth, and up to 4 times higher than subsurface minimum dFe concentrations (Figure 2.5). The dFe concentrations in these surface peaks range from 0.47 to 1.04 nM, compared to 0.17 nM at station 5. Given that these values were measured from the stern of the ship and after significant ice breaking, there is the obvious possibility of contamination. However, very low (<0.2 nM) dFe concentrations at 15 m were observed at other stations, such as stations 5 and 6, indicating that I was able to sample without contamination in these instances. I am therefore confident that elevated dFe concentrations measured at shallow depths are not the result of ship-derived contamination but are indicative of natural dFe inputs.

The dFe values for stations 1 and 7 are also elevated at 15 m compared to Southern Ocean background concentrations, but show less pronounced surface peaks, with dFe concentrations elevated throughout the mixed layer. As a whole, dFe appears to be most variable throughout the mixed layer or just below. This variability is especially apparent at station 1, where a sub-surface peak at 100–125 m shows dFe concentrations up to 3 nM.

There are localized maxima around 500 m in three non-consecutive profiles (i.e. from stations 1, 4 and 7; Figure 2.5), with all three profiles showing very similar concentrations (1.03 ± 0.02 nM). Note, however, that the depth resolution around these peaks is poor, i.e. the true "peaks" may lie anywhere between 300 and 750 m. These three profiles also have generally higher dFe concentrations at all depths compared to the other stations. In particular, the profile from station 7 stands out, with dFe concentrations elevated at all depths (range 0.62 to 1.04 nM). Therefore, dFe concentrations at station 7 are approximately 5 times higher than at station 5, which displays concentrations characteristic of the remote Southern Ocean (0.09 to 0.26 nM; Table A.1).

2.4.5 Fe(II)

While most of the Fe(II) measurements during SIPEX-2 were below the detection limit (Figure 2.6A, Table A.1), a few exceptions stand out. At stations 6 and 7,

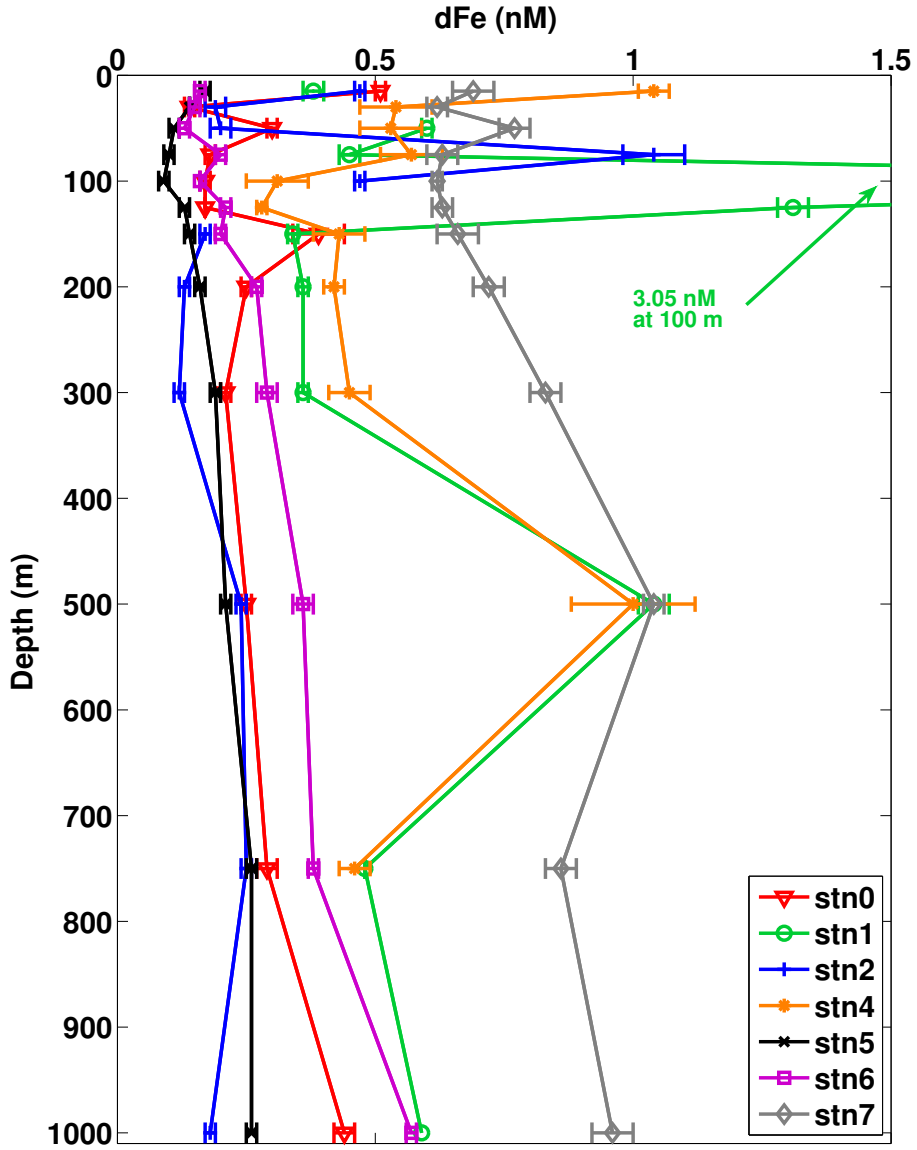

Figure 2.5: Dissolved Fe concentrations; error bars are equivalent to one standard deviation based on triplicate measurements of the same sample.

Fe(II) was clearly detectable at 1000 m, with (unadjusted) concentrations of 33 and 22 pM respectively. The profile from station 5 shows surface values close to 20 pM, decreasing with depth but above the detection limit down to 100 m. Finally, the Fe(II) measurements from station 7 show relatively low values throughout although frequently above the detection limit, with only the 1000 m sample clearly distinguished.

Even when "adjusting" the Fe(II) profiles to account for the possible problems with matrix matching of the seawater used for calibration (see Section 2.3.5 for details), most of the Fe(II) concentrations fall below 10 pM (Figure 2.6A), with the notable exceptions mentioned above. Considering the standard deviations on the measurements (mean = 1.4 pM; range 0.3–3.6 pM) and the detection limits of the method (<1–4.2 pM), the majority of these low concentrations cannot be distinguished from zero within error. The profiles displaying Fe(II) as a percentage of dFe further support this, with most values falling well below 5%, i.e. confirming that Fe(II) accounts for a very small fraction of dFe (Figure 2.6B).

2.5 Discussion

2.5.1 Physical setting and macronutrients

The temperature and salinity profiles (Figure 2.2) are consistent with fresh, cold Antarctic Surface Water (AASW) in the winter mixed layer overlying warmer and saltier Circumpolar Deep Water (CDW) (Orsi et al., 1995). The surface mixed layer deepened towards the continent, as was observed previously in this region for this time of year, likely the result of ice production in the nearby Dalton Iceberg Tongue polynya and also related to density gradients associated with the Antarctic Slope Current (ASC) (Williams et al., 2011). The CDW properties typically weaken poleward as cold Antarctic water is mixed into the water mass; hence it is referred to as modified Circumpolar Deep Water (mCDW) (Williams et al., 2011). This trend of increased modification of the CDW towards the continent is evident in the TS-diagram, specifically in the depth range ∼150–800 m, with southern waters (i.e. stations 4 and 6) considerably colder (Figure 2.3).

The progressive modification of the intermediate mCDW is also reflected in the NO_3^-+NO_2^- profiles and, to a lesser degree, in the PO_4^{3-} data (Figure 2.4). Further offshore (stations 0–2), NO_3^-+NO_2^- concentrations show a sub-surface maximum in

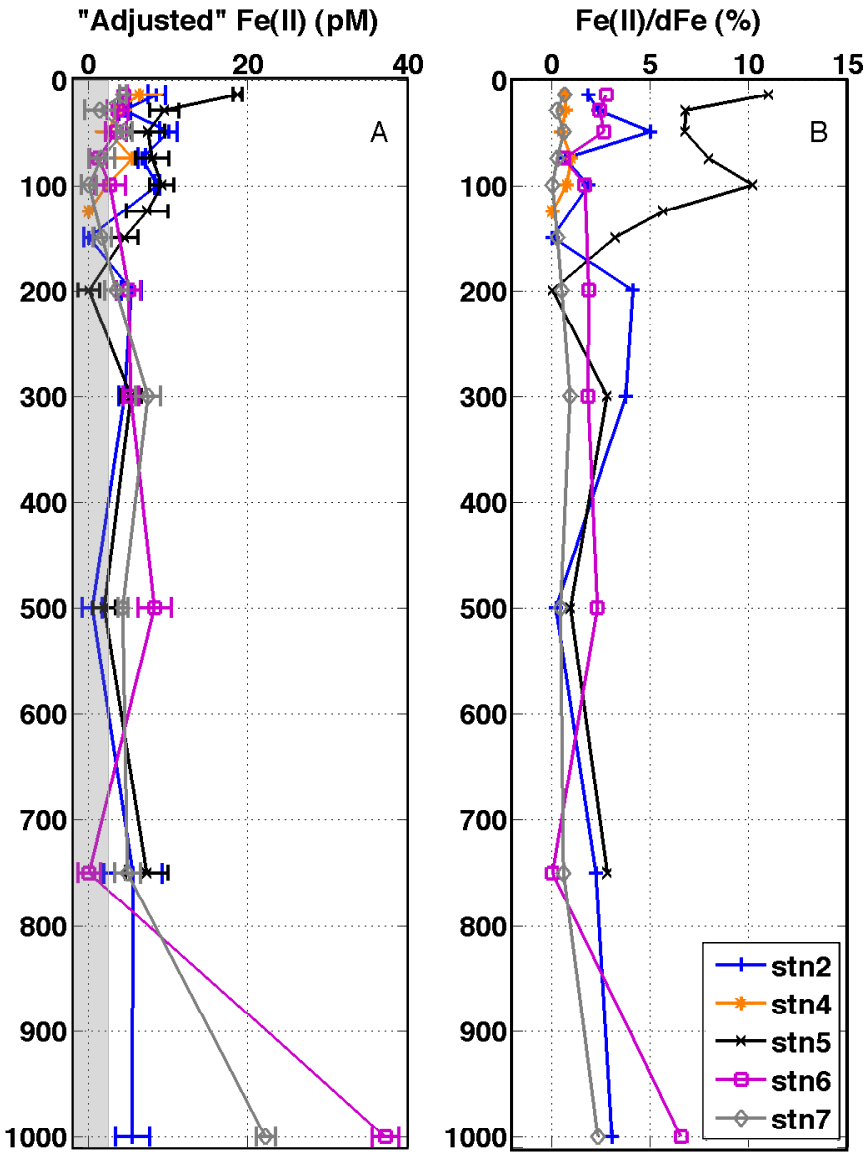

Figure 2.6: Fe(II) concentrations and Fe(II) percentage of dFe. A) Adjusted Fe(II), i.e. where the lowest (negative) concentration in each profile is assumed to be zero and concentrations of the whole profile are shifted accordingly (see Section 2.3.5). B) Fe(II) expressed as a percentage of dFe. The "adjusted" Fe(II) values were used for the calculation. Error bars in A) are equivalent to one standard deviation based on 5 replicate measurements of the same sample. The average detection limit, 2.4 pM, is indicated by grey shading; detection limits for individual casts were in the range <1 pM to 4.2 pM.

the pycnocline. This peak is most pronounced at station 0 and decreases in subsequent profiles, until it is only barely evident at station 4 and beyond. It appears that the stronger influence of the CDW farther offshore, which is also evident in the temperature maxima in Figure 2.2B, causes the sub-surface peak in NO_3^-+NO_2^- concentrations, as the CDW is characterized by high nutrient concentrations. Indeed, the data of Klunder et al. (2011) show a similar maximum in a "typical" NO_3^- profile from 53°S, i.e. in the southern branch of the Antarctic Circumpolar Current.

The $Si(OH)_4$ profiles, on the other hand, do not exhibit any local maxima (Figure 2.4). Instead, they show a continuous increase with depth, likely reflecting the deeper dissolution depth for $Si(OH)_4$ relative to remineralization of nitrogen. This is in agreement with what others have found for the Atlantic sector of the Southern Ocean (e.g., Klunder et al., 2011; Löscher et al., 1997). The steepest $Si(OH)_4$ concentration gradient is found in the pycnocline, and the shapes of the profiles reflect the deepening of the mixed layer poleward. The AASW supports photosynthesis in austral summer, leading to the drawdown of nutrients in this water mass (Sokolov and Rintoul, 2007; Westwood et al., 2010). At the end of summer, atmospheric cooling and brine rejection resulting from sea-ice formation drive the convection that shapes the winter mixed layer (Williams et al., 2011), replenishing nutrients. However, $Si(OH)_4$ concentrations in the mixed layer remain considerably lower than in the underlying mCDW. There is a poleward trend of decreasing $Si(OH)_4$ and NO_3^-+NO_2^- concentrations in the mixed layer, which might be caused by more intense drawdown of nutrients south of the shelf break during summer (Sokolov and Rintoul, 2007).

There is no clear indication that the seasonal drawdown of nutrients had begun during SIPEX-2. The only exception may be the PO_4^{3-} profile from station 7, with drawdown evident near the surface as well as between 150 and 200 m depth. This being the latest station in the cruise, it is possible that primary productivity had begun to pick up in surface waters, perhaps marking the beginning of a spring bloom. However, biological activity is unlikely to explain PO_4^{3-} drawdown between 150 and 200 m. The closest chl *a* data available, from station 6, show an increase relative to the earlier stations but do not indicate bloom conditions (personal communication, Karen Westwood). The cause for the low PO_4^{3-} values at station 7 therefore remains unresolved.

2.5.2 Chlorophyll *a*

Chlorophyll *a* concentrations measured during the cruise are all very low, as would be expected under the pack ice (Arrigo and van Dijken, 2011). The highest chl *a* concentrations were measured at station 6, which was the latest of the 4 stations where chl *a* data are available. This may reflect the progression of the season, with spring conditions starting to be established and facilitating primary production in the water column.

2.5.3 Dissolved Fe

To my knowledge, this dataset represents the first systematic investigation of spatial variability in dFe below the Antarctic pack ice to a depth of 1000 m. There is very high variability within and among profiles, with many observations well above Southern Ocean "background" concentrations, i.e. >0.4 nM (Figure 2.5, Table A.1). Similar spatial variability was observed by Measures and Vink (2001) on a spring cruise in the Pacific sector of the Antarctic Polar Frontal Zone, about 100 miles north of the ice edge. Though their dFe concentrations were generally lower than in this study, Measures and Vink also saw structure in dFe profiles within the mixed layer. They attribute much of the spatial variability to strong meandering of the fronts in that region.

None of the dFe depth profiles beneath Antarctic sea ice that are reported in the literature exhibit variability as high as was observed during SIPEX-2. For instance, Gerringa et al. (2012) show dFe profiles to a depth of 300 m from the ice-covered shelf in the Amundsen Sea. Their 10 profiles have a consistent shape, with a surface peak, followed by a sub-surface minimum, and then a monotonic increase with depth. The highest dFe concentration measured was <0.6 nM. Croot et al. (2004a) saw similar values and profile shapes near the ice edge along 6°E. However, Sedwick et al. (2000) observed considerable dFe variability in the upper water column under the sea ice in the Ross Sea, with average dFe concentrations around 1 nM, and de Jong et al. (2012) report one dFe profile from the marginal ice zone that also shows variability with depth (range 0.2–0.7 nM), not unlike some of the profiles in this study. SIPEX-2 was conducted several months earlier in the season than any of these studies, i.e. during a time when there was negligible biological production and persistent ice cover. I was thus able to observe the system at a time when dFe inputs from a variety of sources were revealed, as is evident in the high dFe variability, while uptake had not

yet begun.

Most studies investigating dFe concentrations in the water column below Antarctic sea ice have focused on the surface layer. For example, Lannuzel et al. (2008) report dFe concentrations of 0.7–1.7 nM for the upper 30 m of the water column under highly porous spring/summer sea ice in the Weddell Sea. The measurements by de Jong et al. (2012) from the same cruise are slightly lower for the upper mixed layer (0.6 nM) and increase monotonically with depth. At 1000 m, they found a value of 2.8 nM dFe (bottom depth 1386 m). In the East Antarctic during the winter-spring transition, dFe concentrations under the pack ice were in the range 0.14 to 4.5 nM (Lannuzel et al., 2007; van der Merwe et al., 2011a). These surface values are comparable to the dFe concentrations encountered in this survey (0.09–3.05 nM overall, 0.16–1.04 nM at 15 m).

Clearly, these findings implicate sea ice as a likely source of the observed dFe enrichment. In what follows, I will consider sea ice as well as other potential sources for the water column dFe enrichment observed in this study.

Pack ice

Antarctic sea ice and brine display greatly enhanced particulate and dissolved Fe concentrations compared to the underlying water column (de Jong et al., 2013; Lannuzel et al., 2008, 2007; van der Merwe et al., 2011a,b, 2009). The mechanisms leading to this enrichment are not fully understood, but it is believed that organic matter-associated Fe is preferentially incorporated into newly-forming sea ice, at least in part due to adsorption to frazil ice crystals. Processes such as convection and accumulation at the ice-water interface would then incorporate additional Fe during sea-ice growth (Lannuzel et al., 2010). While the Fe is largely retained in the sea ice over winter when the ice is too cold to be permeable, the situation changes in spring as warming opens up the brine channels. This increased permeability allows brine drainage into the water column below and Fe can thus be transferred from the sea ice to the water column (Lannuzel et al., 2010, 2007). Brine drainage releases dissolved Fe. When sea ice melts, the particulate Fe, which remained attached to the walls of the brine channels, is released into the seawater together with particulate organic carbon (Lannuzel et al., 2013; van der Merwe et al., 2011a,b).

Several Antarctic studies have attributed phytoplankton blooms in the vicinity of a seasonally-retreating ice edge to the release of dFe from melting sea ice (e.g., Croot

et al., 2004a; Sedwick and DiTullio, 1997; Shadwick et al., 2013; Westwood et al., 2010). Elevated biomass was not encountered in this study, but dFe concentrations in the water column under the ice, particularly near the surface, were considerably elevated, possibly because the seasonal biological uptake had not yet begun. There are several lines of evidence suggesting that the overlying sea ice was a likely source for at least part of this observed dFe enhancement.

For one, the upper 200 m of the water column showed the highest dFe concentrations and also the highest variability in dFe (Figure 2.5), consistent with sporadic input from the sea ice via brine exchange. As mentioned above and discussed in more detail by Lannuzel et al. (2014), the sea ice was highly porous during SIPEX-2, allowing for such an exchange. In sea ice, dFe and macronutrients are decoupled because they are incorporated into the ice from different sources (e.g., van der Merwe et al., 2009; Vancoppenolle et al., 2013). This decoupling was also observed in the water column in this study (all $r^2 < 0.1$ for correlations between macronutrients and dFe).

Three of the dFe profiles presented here show pronounced peaks near the surface, i.e. at 15 m (stations 0, 2 and 4). It is tempting to attribute these peaks to brine drainage and/or ice melt. There are no sea-ice Fe data available for station 0, but the ice at station 2 shows the lowest dFe concentrations in the bottom ice layer compared to all other ice stations in this study (Lannuzel et al., 2014), which might hint at recent dFe loss, for example from brine drainage. Similarly, station 4 shows the lowest dFe concentrations throughout the ice. Brine salinities for both stations are indicative of gravity driven brine drainage (Lannuzel et al., 2014). It is thus conceivable that dFe had very recently been released together with salts from the sea ice into the water at these stations. Indeed, surface dFe peaks appear to be common under sea ice (e.g., Gerringa et al., 2012). In addition, deployments of the TMR were usually the first thing to happen at a station in order to avoid contamination. I am thus confident that the 15 m enrichments observed stem from natural processes.

With some assumptions, it is possible to calculate a mixed layer dFe budget that can be compared to the sea-ice Fe inventory (Table 2.2). In the absence of comprehensive CTD data for all stations, the mixed layer depth is assumed to be 90 m for stations 0–2, 120 m for station 4 and 160 m for all remaining stations. These depths are the mixed layer depths at stations 2, 4 and 6 respectively (Figure 2.2B). The dFe depth distributions were linearly interpolated. The integrated mixed layer dFe inventories, with the exception of station 7, are within a factor 2 of estimates reported for the Pacific sector of the Antarctic Polar Frontal Zone in spring (Measures and Vink,

2001).

Assuming that station 5 represents background dFe concentrations characteristic of this region, one can subtract this station's integrated dFe value for the respective depth range from the inventory of the other stations to calculate the dFe surplus, i.e. dFe above background (Table 2.2).

It is difficult to estimate what fraction of the surplus dFe could have been supplied by the sea ice due to the fact that the ice was already porous during SIPEX-2 and therefore the Fe concentrations were likely not the true winter values, but rather represent what was left after some degree of brine drainage. Previous work has shown that the average dFe in winter pack ice in the East Antarctic is in the range 8–19 nM (Lannuzel et al., 2010). Assuming an average ice thickness of 1 m, this yields an inventory of 8–19 μmol m^{-2}. During SIPEX-2, only a fraction of this Fe would have entered the water column at the time of sampling, as the average dFe inventory in the pack ice was still 7.3 μmol m^{-2} (Lannuzel et al., 2014). Using the upper limit of 19 μmol m^{-2} and subtracting 7.3 μmol m^{-2} yields an inferred previous dFe input from the sea ice of 11.7 μmol m^{-2}, which is insufficient to account for the dFe surplus in the mixed layer at all but two stations (Table 2.2).

Stn no/ $\mathbf{z}_{int}$	**0** **(90 m)**	**1** **(90 m)**	**2** **(90 m)**	**4** **(120 m)**	**5** **(160 m)**	**6** **(160 m)**	**7** **(160 m)**
ML	25.1	54.0	44.0	67.8	19.8	27.8	104.9
200 m	54.0	172.0	73.3	99.4	25.8	37.5	132.8
500 m	123.0	348.0	121.8	287.9	83.3	130.5	397.3
1000 m	281.8	671.7	236.8	-	207.1	341.7	862.3
ML *EX*	13.8	42.7	32.7	53.5	0	8.0	85.1
200 m *EX*	28.2	146.2	47.5	73.6	0	11.7	107.0
500 m *EX*	39.7	264.7	38.5	204.6	0	47.2	314.0
1000 m *EX*	74.7	464.6	29.7	-	0	134.6	655.2

Table 2.2: Depth-integrated dFe inventories in the water column (μmol m^{-2}) for a range of integration depths (z_{int}); assumed mixed layer (ML) depths are indicated in brackets below the station numbers. "*EX*" denotes excess inventory above background, i.e. station 5.

However, pFe in pack ice can be up to 20 times enriched relative to the dFe fraction (van der Merwe et al., 2011a). This was also the case during SIPEX-2, where pFe in the sea ice represented on average 94% of the total Fe pool (Lannuzel et al., 2014). Depending on the fate of pFe in the water column, it could well have contributed to the dFe concentrations observed in the mixed layer, especially since 67% of the sea-ice pFe was biogenic and considered highly labile (Lannuzel et al., 2014). Assuming that pFe input from the sea ice was 10 times higher than the dFe input, between 2% and 62% of this pFe would need to dissolve in order to close the dFe budget for the mixed layer.

Drifting icebergs

SIPEX-2 saw the passage of a large tabular iceberg (B09D) in the vicinity of the ship. Stations 4–7 all lie in the proximity of the iceberg's wake, with station 7 being closest to the berg's track and occupied about 10 days after its passage. B09D is a remnant of iceberg B09, which initially broke off the Ross Ice Shelf in 1987. Its draft is not known, but can be estimated to be around 260 m, i.e. an average depth for icebergs calved from the Ross Ice Shelf (Dowdeswell and Bamber, 2007). Though passing icebergs may alter water column Fe distributions in their wake in several ways, e.g. by releasing both particulate and dissolved Fe (e.g., Lin et al., 2011; Löscher et al., 1997; Raiswell, 2011; Raiswell et al., 2008, 2006), it is not very probable that B09D contributed to the observed dFe peaks near 500 m, especially when considering that one of these peaks was observed at station 1, which was not proximal to the wake of the iceberg.

The temperature profile at station 7, though crude in its resolution, does not show any signs of deep mixing beyond the expected mixed layer depth (Figure 2.2). Therefore, attribution of the generally high dFe concentrations at station 7 to the passage of B09D is also unlikely, as one would expect to see homogenization of the water column beyond 200 m if significant iceberg-induced upwelling had occurred (Jenkins, 1999; Neshyba, 1977; Stephenson Jr. et al., 2011). It is thus more likely that the elevated dFe values at station 7 are the result of lateral input (see below).

Though B09D was the most prominent iceberg encountered on this cruise, there were also numerous smaller icebergs near the ship at any given time, and as early as station 0. The highest dFe concentration on the cruise was recorded at station 1 at 100 m (Figure 2.5), just below the mixed layer (Figure 2.2). The 125 m sample

at station 1 also shows highly-elevated dFe concentrations, providing evidence that the measured higher-than-average dFe values are real and not the result of bottle contamination. The temperature profile at station 1 shows the warmest temperatures in the 100–200 m range (Figure 2.2A), coincident with the observed dFe peak. It is not unusual for icebergs to have keel depths >100 m (Dowdeswell and Bamber, 2007), so basal melting of a nearby iceberg could have produced the observed dFe peak at station 1. Lin et al. (2011) found that dFe concentrations in the vicinity of icebergs in the Weddell Sea were in the range 1.2–2.9 nM, with the highest concentrations measured between 150 and 250 m depth. Similarly, de Jong et al. (2012) report a dFe enhancement of 0.3 nM above background levels at 250 m depth in the wake of an iceberg, coincident with the warm core of the CDW at the same depth. Given the temperature profile for station 1 in this study, it is thus conceivable that the observed dFe maximum was the result of basal melting of a nearby iceberg, but there are no salinity data available for this station to confirm the presence of melt water.

Shelf sources

The SIPEX-2 cruise track approached the Antarctic continent, with station 7 being closest to the Antarctic shelf (Figure 2.1). This station shows the highest water column dFe concentrations observed, with Fe levels well above background (e.g. station 5) to a depth of 1000 m (Figure 2.5). The temperature and nutrient profiles are indicative of stratification (Figures 2.2 and 2.4); deep mixing is therefore unlikely to explain the enhanced dFe. Rather, lateral advection from the shelf may have introduced Fe from sediments. The importance of continental margins and shelf sediments as sources of Fe has long been recognized, including for the Southern Ocean (e.g., de Jong et al., 2012; Elrod et al., 2004; Hatta et al., 2013; Lam and Bishop, 2008; Lam et al., 2006; Marsay et al., 2014; Moore and Braucher, 2008). Indeed, several modelling studies point to Fe fluxes from sediments as the most important external Fe input for the Southern Ocean in terms of both Fe budgets and carbon sequestration (Lancelot et al., 2009; Moore and Braucher, 2008; Tagliabue et al., 2014, 2009; Wadley et al., 2014).

The dFe concentrations at station 7 are elevated throughout the water column, to at least 1000 m depth. Station 6 shows a similar pattern, although the dFe concentrations are lower than at station 7. Considering stations 5–7 in isolation and focusing on depths >100 m, it is evident that there is a considerable increase in dFe

concentrations with decreasing distance from the shelf (Figures 2.1 and 2.5). Similar dFe enrichment at all depths was seen by de Jong et al. (2012; Figure 5) in a series of stations approaching the Antarctic continent, with dFe concentrations up to 0.7 nM at depth at a station hundreds of kilometres from the shelf, which they attribute to lateral transport of dFe-enriched shelf waters. The range of concentrations encountered at station 7 (0.62–1.04 nM) is higher, but this would be expected as this station is on the shelf break. The station 7 dFe concentrations are comparable — although at the high end — to dFe profiles reported from near the Pine Island Glacier (0.4–0.8 nM), which are also almost uniform with depth (Gerringa et al., 2012). While Gerringa et al. attribute about half of the increase above background concentrations to melting of the glacier, they ascribe the other half to sedimentary processes. Station 7 of this study is too far (∼200–250 km) from neighbouring ice shelves and glaciers to make these a probable dFe source, and it is likely that the nearby shelf was a dominant influence on Fe concentrations.

Shelf waters may become enriched in dFe as they travel across the shelf because of benthic efflux from the sediments (Marsay et al., 2014). Dense shelf water forms when brine rejection due to sea-ice formation increases the salinity of the underlying water column. The resulting shelf water can cross the shelf break if the bathymetry permits, and if sufficiently dense (>28.27 σ_θ), it will be transported down the continental slope to form Antarctic Bottom Water (AABW). Although Williams et al. (2011) found no evidence for the production of sufficiently dense shelf water for AABW formation in the region of the SIPEX-2 study area, shelf water with intermediate density could still cross the shelf break and partially descend the continental slope. These modified shelf waters would be in contact with shelf sediments before flowing down the slope, likely becoming enriched in dFe along the way. As these waters flow off the shelf, they are mixed into the westward flowing slope current and could thus have contributed to the uniformly high dFe concentrations measured at station 7.

Similarly, advection from shelf sediments may explain the conspicuous dFe maxima around 500 m that were observed in 3 of 7 profiles (Figure 2.5). The three maxima at 500 m (stations 1, 4 and 7) clearly stand out from the profiles and may invite speculation about a bottle contamination, since all three samples were taken from the same Niskin-X bottle. However, several factors dispel such an explanation. For one, the three dFe profiles exhibiting a maximum at 500 m were not from consecutive deployments, i.e. samples from the same Niskin-X bottle measured in between "peak" profiles show no elevated dFe. Secondly, it is striking that the three peak con-

centrations that were measured at 500 m agree very well in magnitude within their respective limits of error, i.e. 1.03±0.02 nM dFe. Such a coincidence is rather unlikely for a contamination but may be explained by the solubility limit of Fe as dictated by the availability of Fe-binding ligands. This sort of mechanism was suggested by Thuróczy et al. (2012) for the waters near Pine Island Glacier, where ligands were close to saturated, most likely due to constant dFe supply from melting of the glacier.

There is no Fe-ligand data from SIPEX-2, but Croot et al. (2004a), sampling near 56°S and 6°E, reported organic Fe-complexing ligand concentrations of 1.3 nM Fe equivalents at 400 m (n=1). Near the Kerguelen Archipelago, Gerringa et al. (2008) found mean Fe ligand concentrations from 400–600 m depth (n=23) to be 0.93 nM Fe equivalents. In the Atlantic sector of the Southern Ocean, mean Fe ligand concentrations in the same depth range (n=7) were 1.05 nM Fe equivalents (Thuróczy et al., 2011). Thus, the dFe concentrations measured in the peaks at 500 m agree well with the expected binding capacity of Fe ligands for that depth in the Southern Ocean, although for completeness it should be mentioned that two studies found considerably lower Fe-complexing ligand concentrations: Ibisanmi et al. (2011) measured 0.52–0.73 nM Fe equivalents at 500 m south of Tasmania, and Boye et al. (2001) report Fe ligand concentrations (at 400–600 m) ranging from 0.15 to 1.24 nM (mean=0.58 nM; n=6) in the Atlantic sector of the Southern Ocean.

It is possible that the Dalton Iceberg Tongue, which is proximal to the cruise track (∼60 km from station 4, ∼100 km from station 7), contributed to the elevated dFe concentrations at 500 m. This feature comprises numerous grounded icebergs, and the grounding depth is estimated around 500 m, consistent with observations of ice-gouge features in Antarctic sediments at water depths up to 500 m (Barnes and Lien, 1988). One could thus speculate that the observed dFe peaks at 500 m stem from either sediments that are disturbed by the keels of the icebergs, or from melting of the icebergs at the base, or both.

The role of circulation in distributing dFe

It is somewhat surprising that one of the observed dFe peaks at 500 m is found at station 1, about 170 km north of the shelf break. If the Fe enrichment does in fact originate from the shelf, it must have been transported 170 km north, for example by the generally westward flowing Antarctic Slope Current (ASC), which follows the shelf break in this region (Bindoff et al., 2000; Williams et al., 2011). The ASC

appears to feed a weak cyclonic gyre between 90 and 120°E, the return flow of which is estimated to be in the vicinity of station 1 (Bindoff et al., 2000; see Figure 11). Bindoff and colleagues also found evidence of two cold-core eddies or meanders in the region, which have the potential to transport waters away from the shelf break.

It is interesting to note that stations 1 and 4, which both exhibit dFe peaks at 500 m, have comparable dFe concentrations at all depths below 150 m. In fact, these are the highest deep dFe concentrations measured on SIPEX-2 — apart from station 7 — consistent with the associated water mass originating near the shelf. The dissimilar dFe concentrations in the surface layer might be explained by the influence of sea ice and icebergs as previously mentioned.

It may seem counterintuitive that stations 5 and 6, both near the shelf break, do not show any dFe enhancements at depth. The Antarctic Slope Front has been found to vary both in strength and position in this region (Bindoff et al., 2000), which may indicate similar variability in the ASC. The presence of meanders in the ASC as found by Bindoff et al. (2000) further supports the notion of variability. It is thus possible that the current prevented shelf waters from reaching stations 5 and 6, while allowing them to influence stations 4 and 7, and possibly even station 1.

Biological implications

The data described in this study, combined with the sea-ice Fe data from Lannuzel et al. (2014), allow an estimation of the fertilization potential of the available dFe at the end of winter. Lannuzel et al. (2014) have calculated that the melting sea ice could provide a total of 6 μmol m^{-2} dFe and 81 μmol m^{-2} biogenic pFe. Assuming that this Fe is injected into a mixed layer (ML) of 25 m depth (Strutton et al., 2000) and is added to an average background dFe concentration of 0.4 μmol m^{-3} (this study, see Table 2.2) yields total ML dFe concentrations of 0.64 μmol m^{-3} for dFe, and 3.64 μmol m^{-3} for dFe and biogenic pFe combined. With a C:Fe molar ratio of ∼70,000:1 for Southern Ocean phytoplankton (Twining and Baines, 2013), and integrating over the ML, this translates to 14 and 77 g C m^{-2}, respectively. Comparing this number to the annual primary production for the marginal ice zone in the Southwest Pacific sector of the Southern Ocean, which Arrigo et al. (2008) estimate at 41.1 g C m^{-2} $year^{-1}$, illustrates that the dFe inventory present under the sea ice in spring, combined with the dFe from melting sea ice, could support up to 34% of the annual primary production in this area. Assuming that part of the biogenic pFe contained in sea ice is also bioavailable,

up to 100% of the observed primary production could be supported. I acknowledge the large uncertainty associated with the numbers in this calculation, but the results highlight the importance of the sea-ice cover for building up an Fe reservoir within and underneath the ice that has a significant fertilization potential.

2.5.4 Fe(II)

The most striking aspect of the Fe(II) data is the almost complete absence of Fe(II) in the water column (Figure 2.6). While there are no other Fe(II) measurements from this far south to compare the data to, this result is consistent with the observations by Sarthou et al. (2011), who observed local minima in labile Fe(II) concentrations associated with winter waters in the South Atlantic and attributed these minima to the absence of biological activity. Most other Southern Ocean Fe(II) data are restricted to the surface and/or stem from artificial Fe enrichment experiments and are thus difficult to compare to this study (e.g., Bowie et al., 2002; Croot et al., 2001, 2008, 2007; Croot and Laan, 2002). While Fe(II) concentrations during Fe enrichment experiments may be as high as 1 nM (Croot et al., 2001; Croot and Laan, 2002), surface measurements from the unaltered Southern Ocean range from below the detection limit to 30 pM, in line with my results (Bowie et al., 2002). To my knowledge, there are no other Fe(II) data from below the seasonal sea ice in the Antarctic. However, an inspection of the known sources of Fe(II) may help explain the near-zero concentrations of Fe(II) in the presented dataset.

In the surface ocean, biological activity and photochemistry are thought to be the main drivers of Fe(II) production, while at depth remineralization processes — especially those associated with anoxic sediments — as well as hydrothermal inputs contribute Fe(II) (e.g., Barbeau et al., 2001; Croot et al., 2001; Lohan and Bruland, 2008; Maldonado and Price, 2001; Rijkenberg et al., 2005; Sarthou et al., 2011; Sedwick et al., 2014; Statham et al., 2005). There are no known hydrothermal vent systems in the study area, and the timing of the cruise – i.e. late winter/early spring — makes remineralization processes in the water column as well as biological activity in the surface waters improbable sources for Fe(II). Indeed, chl *a* concentrations were very low, indicating pre-bloom conditions.

This leaves photochemistry and sedimentary processes as possible sources for Fe(II). In the open ocean, the photochemical reduction of Fe is intrinsically linked to biological activity, as it requires the presence of electron donors such as photoreactive

Fe-ligands or chromophoric dissolved organic matter (CDOM), which are produced either actively or as a byproduct by marine microbes (Barbeau et al., 2001; Nelson et al., 1998, 2004; Rijkenberg et al., 2005; Rochelle-Newall and Fisher, 2002). Sea-ice melting and brine exchange can be an important source of CDOM for the seasonally ice-covered Southern Ocean (Kieber et al., 2009; Norman et al., 2011; Ortega-Retuerta et al., 2010a,b). During SIPEX-2, the sea ice exhibited high porosity and brine channel connectivity, allowing for brine exchange with the water column below (Lannuzel et al., 2014). Even though this could have contributed CDOM to the seawater, the ice and its snow cover reduced the amount of solar radiation reaching the underlying seawater; as a result, photochemical production of Fe(II) would have been minimal or absent, consistent with my measurements. The only exception is station 5, where Fe(II) was measurable in the surface waters to a depth of 100 m. Neither irradiance nor air temperatures (as recorded by the ship's underway system; data not shown) were anomalously high, but it cannot be ruled out that a CDOM pulse from the sea ice and/or biological activity enhanced Fe(II) production at this station.

The non-zero Fe(II) data at 1000 m at stations 6 and 7 are likely related to sedimentary processes on the continental shelf, as these two stations lie closest to the shelf break. Summertime phytoplankton blooms in surface waters above the shelf provide organic matter to the sediments, supporting benthic Fe(II) fluxes (Berelson et al., 2003; Lohan and Bruland, 2008). Isopycnal transport from the shelf could therefore explain the observed elevated Fe(II) at depth. Similarly, the measurable but low Fe(II) concentrations throughout the water column at station 7 may reflect a sedimentary influence at all depths, as discussed for dFe in section 2.5.3.

2.6 Conclusions

Dissolved Fe concentrations under the seasonal pack ice in the East Antarctic were found to be highly variable both vertically and horizontally, and were frequently elevated up to five-fold relative to Southern Ocean background concentrations. Multiple potential sources for this dFe enrichment were identified, including brine drainage from sea ice, melting of icebergs and benthic fluxes from shelf sediments. In the mixed layer, sea ice is expected to be the most important contributor to elevated dFe concentrations, but budget considerations indicate that projected dFe fluxes from the ice alone are insufficient to account for all observed excess dFe. Dissolution of particulates released from melting sea ice may account for the additional dFe observed in

seawater.

The spatial variability of dFe may arise from both sporadic influences, such as brine drainage and sea-ice melting, as well as long-range processes, such as transport of dFe from the shelf break to the open ocean. Near the shelf, sedimentary processes potentially influence dFe concentrations not only at depth but also throughout the water column as dense shelf water is mixed into the ASC. Variability in currents and fronts proximal to the shelf are thought to play an important role in creating the observed dFe patchiness.

Fe(II) concentrations were generally low and mostly below the detection limit, reflecting an absence of processes that generate Fe(II) during the study period. This indicates that Fe(II) production in the surface layer depends on sea-ice melt and/or biological activity in the water column as well as solar irradiance, i.e. that Fe(II) supply is predominantly seasonal. At depth, Fe(II) was found to be elevated at two stations near the shelf break. These Fe(II) enrichments likely originate from shelf sediments.

In summary, dFe from multiple sources appears to build up under the seasonal sea ice during winter and is expected to contribute to the formation of the spring bloom as the ice retreats in this sector of East Antarctica. Dissolved Fe enrichments from shelf sediments may be supplied to surface waters far from land through mixing and upwelling.

Chapter 3

Iron(II) variability in the northeast subarctic Pacific Ocean

Schallenberg, C., Davidson, A.B., Simpson, K.G., Miller, L.A., Cullen, J.T. (2015). Iron(II) variability in the northeast subarctic Pacific Ocean. In press in *Marine Chemistry*.

3.1 Abstract

Distributions of dissolved iron (<0.2 μm, dFe) and its reduced form, Fe(II), were measured during 3 cruises along Line P, a transect from the continental slope to the high nutrient, low chlorophyll (HNLC) northeast subarctic Pacific Ocean. Concentrations of Fe(II) ranged from below the detection limit (4.3 pM or less) to 330 pM, and dFe concentrations up to 3.6 nM. Maximum concentrations for both Fe(II) and dFe occurred in waters over the continental slope, with Fe(II) consistently increasing towards the bottom, consistent with Fe(II) supply from benthic sources on the continental slope. Low oxygen concentrations ($\sim$10 μM) and pH ($\sim$7.5) in the North Pacific oxygen deficient zone (ODZ) likely serve to stabilize Fe(II) and may contribute to enhanced dFe release from slope sediments via reductive dissolution. Concentration gradients along isopycnal surfaces indicate that Fe(II) is transported several hundred kilometers from the continental slope at depth, and there is evidence that episodic events may advect shelf-derived Fe(II) similar distances near the surface. Comparison of transport times and Fe(II) half-lives suggests that it is unlikely for pre-formed Fe(II) to be transported these distances, but that sedimentary particles advected off

the shelf and slope may constitute a continuous source of Fe(II) both at depth and near the surface. At the offshore stations, the Fe(II) time series reveals deep local maxima that are transient in time and space and are consistent with a sporadic Fe(II) source, such as remineralization of sinking particles.

3.2 Introduction

In about 40% of the surface ocean, primary production is limited by insufficient availability of the micronutrient iron (Fe), which is essential for cellular functions such as photosynthesis (Moore et al., 2002; Raven et al., 1999). Iron scarcity in remote parts of the global ocean results from its low solubility in oxygenated seawater combined with only sporadic and modest rates of supply (Duce and Tindale, 1991; Jickells et al., 2005; Liu and Millero, 2002). The impact of Fe limitation is to diminish the input to the biological carbon pump and, by extension, the ocean's ability to absorb carbon dioxide from the atmosphere (Martin, 1990; Sunda, 2010). Elucidating the supply mechanisms and biogeochemical cycling of Fe in the ocean is therefore a crucial step towards better understanding the links between marine biogeochemical processes and climate.

The remote northeast (NE) subarctic Pacific Ocean is a high nutrient, low chlorophyll (HNLC) region of the world ocean where Fe limits primary productivity (Boyd et al., 2004; Tsuda et al., 2005). Surface waters there receive Fe from intermittent sources such as atmospheric deposition (Bishop et al., 2002; Boyd et al., 1998; Crusius et al., 2011; Duce and Tindale, 1991; Hamme et al., 2010) and the penetration of mesoscale eddies generated near shore (Brown et al., 2012; Johnson et al., 2005; Lippiatt et al., 2011). In addition, Fe-enriched shelf waters may be advected offshore as a result of tidal currents and coastal downwelling, and as part of the ocean general circulation (Cullen et al., 2009; Lam and Bishop, 2008; Lam et al., 2006; Siedlecki et al., 2012). Indeed, continental shelves are increasingly recognized to play an important role in supplying Fe to the open ocean on a global scale (Elrod et al., 2004; Johnson et al., 1999), but the relative contribution of different sources to the global Fe budget is still poorly constrained (Raiswell and Canfield, 2012).

In the NE subarctic Pacific, an extensive oxygen deficient zone (ODZ) between 600 and 1400 m depth adds to the complexity of the system. The low ($\sim$10 μM) oxygen (O_2) waters in the core of the ODZ are in contact with sediments on the continental slope, creating conditions conducive to reductive Fe dissolution, as has been observed

in similar environments elsewhere (Homoky et al., 2012; Lohan and Bruland, 2008; Noffke et al., 2012; Severmann et al., 2010). Indeed, Nishioka et al. (2007) observed dFe (<0.22 μm) distribution patterns in the western subarctic Pacific that are consistent with such a sedimentary Fe source, even with oxygen concentrations about 5 times higher in the western subarctic Pacific than in my study area.

In addition to facilitating reductive dissolution of Fe from the sediments, the low O_2 concentrations in the ODZ are expected to stabilize Fe(II), the reduced form of dFe, in the water column. Fe(II) is more soluble in seawater than the oxidized form, and it may also be more bioavailable to phytoplankton and bacteria (e.g., Kranzler et al., 2011; Maldonado and Price, 2001; Shaked et al., 2005). However, Fe(II) is unstable in the presence of O_2, and its half-life is inversely proportional to the in situ O_2 concentration (Millero et al., 1987). Conditions in the ODZ, and their predicted change with continued de-oxygenation of the subsurface ocean (Whitney et al., 2007), are therefore expected to exert substantial influence on the supply and fate of dFe from sedimentary sources on the continental shelf and slope.

The data presented here comprise a time series of Fe(II) along a transect in the HNLC subarctic Pacific and allow an investigation into the temporal and spatial variability in Fe(II), with a particular view towards identifying Fe sources and the role of Fe(II) in supplying dFe to the subarctic NE Pacific.

3.3 Materials and Methods

3.3.1 Study area

Samples were collected during 3 cruises along the Line P transect in the northeast subarctic Pacific Ocean. The cruises took place aboard the CCGS John P. Tully in May/June 2012 (called the June 2012 cruise hereafter), August 2012 and August 2013. The sampling region lies between 48 and 50°N and 125 and 145°W (Figure 3.1) and comprises 26 CTD stations, 5 of which are sampled intensively to characterize water column chemistry. The transect covers the continental shelf and slope, but a majority of stations are oceanic, with bottom depths greater than 3000 m. Of the stations sampled for dFe and Fe(II), only P4 has a bottom depth of less than 3000 m, as it is located on the continental slope (bottom depth ∼1300 m).

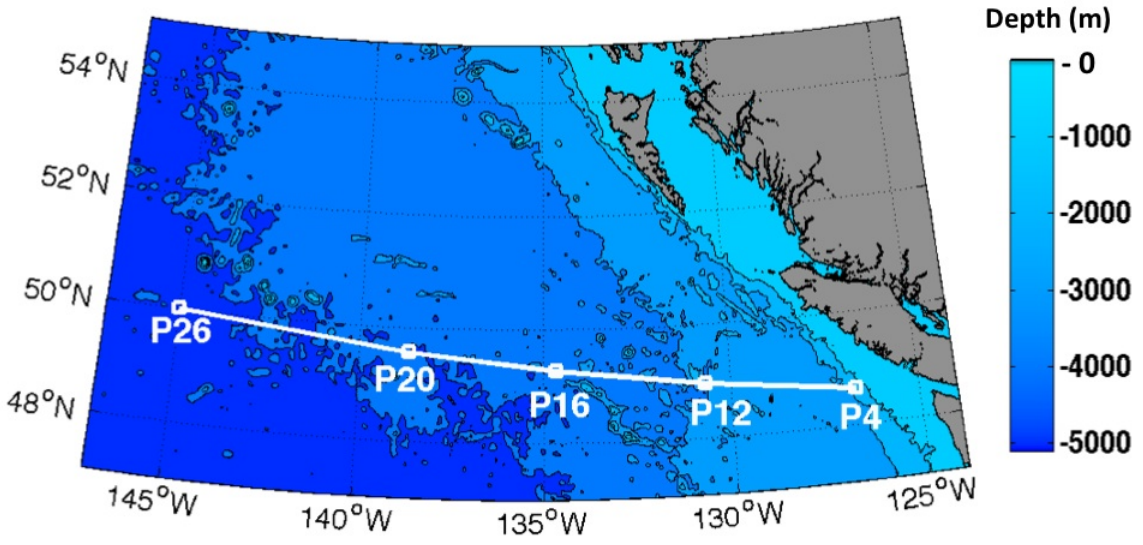

Figure 3.1: Map of the Line P transect in the subarctic NE Pacific. Major chemistry stations are indicated, and underlying bathymetry is contoured at 1000 m intervals.

3.3.2 Sampling methods

Seawater sampling and handling followed GEOTRACES recommendations (Cutter et al., 2010). During the June 2012 cruise, samples between 10 and 40 m at stations P4, P20 and P26 were collected with a Teflon^{TM} bellows pump, and at P16, samples from 10 to 75 m were collected during a separate (short) cast using Teflon^{TM}-lined Niskin-X bottles mounted on a Kevlar line (see Table 3.1 for an overview). All other samples on that cruise were collected with Teflon^{TM}-lined 12 L GO-FLO bottles (General Oceanics) mounted on a Kevlar line on the side of the ship and triggered with Teflon^{TM} messengers. On the two August cruises, a trace element clean rosette system (TMR) with 12 × 12 L Teflon^{TM}-lined GO-FLO bottles, modelled after Measures et al. (2008), was deployed from the stern of the CCGS John P. Tully.

Note that with the TMR, bottles are closed on the upcast and surface bottles are thus closed last, so that minimal time elapses between closing these bottles and sampling, i.e. 10–30 minutes. The situation is reversed with the Kevlar line, where bottles are triggered sequentially starting at the surface, and up to 2.5 h may pass before these bottles can be sampled, due to the time it takes for the Teflon messenger to reach the deeper bottles. See Table B.1 in Appendix B for a comparison between

		June 2012		August 2012		August 2013	
Stn	**Depths (m)**	**Sampling**	**Analysis**	**Sampling**	**Analysis**	**Sampling**	**Analysis**
P4	10–40	*Pump*	*Fe(II), dFe*	TMR	Fe(II)	*TMR*	*Fe(II), dFe*
	50–1200	*GO-FLOs*	*Fe(II), dFe*	TMR	Fe(II)	*TMR*	*Fe(II), dFe*
P12	10–2000	*GO-FLOs*	*Fe(II), dFe*	*TMR*	*Fe(II)*	*TMR*	*Fe(II), dFe*
P16	10–75	Niskin-X	Fe(II), dFe	-	-	TMR	Fe(II), dFe
	100–2000	GO-FLOs	Fe(II), dFe	-	-	TMR	Fe(II), dFe
P20	10–35	Pump	Fe(II), dFe	-	-	*TMR*	*Fe(II), dFe*
	75–2000	GO-FLOs	Fe(II), dFe	-	-	*TMR*	*Fe(II), dFe*
P26	10–35	*Pump*	*Fe(II)*	-	-	*TMR*	*Fe(II), dFe*
	50–2000	GO-FLOs	Fe(II), dFe	-	-	*TMR*	*Fe(II), dFe*

Table 3.1: Overview of sampling methods and analyses on the respective cruises. Italicized text indicates daytime sampling.

expected Fe(II) half-lives and time elapsed between closing of bottles and analysis. It is reasonable to assume that steady-state conditions are maintained in closed bottles from below the sunlit surface layer, i.e. Fe(II) production and loss terms are not altered in the bottle. During daylight hours in the photic zone, where photochemical production of Fe(II) is expected to be significant, closing of bottles may lead to a sampling bias towards lower Fe(II) concentrations. The strength of the bias depends on the Fe(II) half-life and the time that elapsed between bottle closing and sampling; however, the bias may be weakened or even negligible due to the presence of Fe(II)-stabilizing organic ligands (e.g., Roy et al., 2008).

GO-FLO samples for dFe and Fe(II) were filtered through 0.2 μm AcroPak^{TM} 500 filters (Pall) in a trace metal clean container, while samples from the pump were filtered with a 0.2 μm Opticap® capsule filter (Millipore) in a trace metal clean flow bench. All plasticware was extensively acid-cleaned according to GEOTRACES protocols (Cutter et al., 2010). Samples for dFe analysis were collected into 500 mL low-density polyethylene bottles, and acidified to pH 1.7 with Seastar Baseline hydrochloric acid (HCl) in the laboratory in Victoria, and stored at room temperature.

Seawater for Fe(II) determination was collected in 60 mL Teflon^{TM} bottles and analyzed immediately.

3.3.3 Dissolved Fe

Dissolved Fe (dFe) in this study is operationally defined as the Fe fraction that passes through a 0.2 μm filter. Note that dFe data are only available for the June 2012 and August 2013 cruises, and that they frequently have less depth resolution than the corresponding Fe(II) data.

Dissolved Fe was measured using a modified flow injection analysis (FIA) method that relies on detection of Fe(III) with the chemiluminescent reagent luminol (de Jong et al., 1998; Obata et al., 1993). Samples and standards were treated with hydrogen peroxide (H_2O_2; final concentration = 10 μM) at least 3 hours prior to measurement to oxidize any Fe(II) that might be present. This time frame is a departure from the 15 minutes recommended by Lohan et al. (2006), but preliminary studies in our laboratory showed that a longer reaction time is necessary to recover all Fe(III) when high natural concentrations (e.g., >1 nM) are present. The system buffers the samples in-line to pH = 4 with 0.12 M ammonium acetate before passing them for 2 minutes through a pre-concentration column packed with chelating iminodiacetic acid (IDA, Toyopearl, AF Chelate 650M). A solution of 0.1 M HCl (Seastar) then elutes Fe(III) from the resin and mixes with 0.96 M ammonium hydroxide (NH_4OH), 1.6 M H_2O_2 and 0.1 mM luminol containing 0.3 mM tetraethylenepentamine (TEPA) and 2.5 mM sodium hydroxide (NaOH), yielding an optimum luminol chemiluminescence reaction pH of 10. The resulting solution is passed through a ~5 m mixing coil maintained at 35°C before entering a spiral flow cell mounted in front of a photomultiplier tube (Hamamatsu HC 135-11). Flow rates for the respective solutions were as follows: 4.8 mL min^{-1} for sample, 0.9 mL min^{-1} for NH_4OH, H_2O_2, HCl and luminol, and 0.3 mL min^{-1} for the ammonium acetate buffer.

System blanks were 0.049 ± 0.024 nM (n = 12), yielding a detection limit (3 × blank standard deviation) of 0.07 nM. Results for SAFe reference materials for dFe were in good agreement with consensus values (Table 3.2).

3.3.4 Fe(II)

Fe(II) was determined by luminol chemiluminescence detection and the set-up of the system varied somewhat between cruises. Samples were not acidified and reported

Reference standard	# of analyses	Measured (nmol L^{-1})	Calculated (nmol kg^{-1})	Consensus value (nmol kg^{-1})
D2	10	0.95 ± 0.06	0.93 ± 0.06	0.933 ± 0.023
D1 (22)	4	0.69 ± 0.02	0.67 ± 0.02	0.67 ± 0.04
S	4	0.08 ± 0.01	0.08 ± 0.01	0.093 ± 0.008

Table 3.2: Results for dFe analyses of SAFe reference materials with 1 standard deviation. For conversion to nmol kg^{-1}, seawater density was assumed to be 1.025 kg L^{-1}.

values are not corrected for Fe(II) losses due to oxidation. During the 2012 cruises, I followed the approach of Hansard and Landing (2009), but did not acidify samples to prevent reduction of Fe(III) that might bias Fe(II) measurements. In their configuration, sample and luminol reagent are pumped simultaneously into a spiral flow cell made of flexible Tygon^{TM} tubing (ID = 0.7 mm) that is mounted in front of a photomultiplier tube (Hamamatsu H9319-01) in a custom-made light-tight box. Flow rates for luminol and sample were $\sim$4.5 mL min^{-1}. The photomultiplier tube was operated at 900 V with a 200 ms integration time. Photon counts were recorded using FloZF software (GlobalFIA, Fox Island, WA USA) and were averaged over 10-second intervals with 5 replicates for each sample and standard. The mean absolute standard deviation of these repeat measurements was 2.3 ± 2.5 pM.

During the 2013 cruise, an injection valve (Valco) was included in the set-up, similar to the system described by Croot and Laan (2002). Milli-Q was used as a carrier and was pumped at a flow rate of 6.5–7 mL min^{-1}, while luminol and sample were pumped at 4.5–5 mL min^{-1}. The injection loop had a volume of 1.2 mL. Peak height was determined after slight smoothing (3-point running mean) and subtraction of the baseline using FloZF software. The average of 4 replicate measurements was calculated for each sample, and the mean absolute standard deviation of these was 2.4 ± 0.4 pM. For a more detailed discussion of differences in procedures between cruises, see Appendix B.

Settings on the photomultiplier tube and reagents used were identical during all 3 cruises. Sampling always began within minutes after the first GO-FLO bottle (starting from the surface) arrived in the clean container (except at P4 during August 2012, where 30 minutes elapsed before the first sample was drawn), and samples were analyzed within 2 minutes of filtration. Pump samples were analyzed immediately

after filtration.

Details of calibration procedures and reagents are described in Schallenberg et al. (2015b). Briefly, 0.75 mM luminol containing 3.2 mM sodium carbonate (Na_2CO_3) was adjusted to pH 10.0 with small amounts of concentrated NH_4OH and HCl. A 10 mM standard of ammonium iron(II) sulfate hexahydrate was prepared fresh in 0.1 M Seastar HCl and considered stable in the fridge for up to a month. From this stock, intermediate standards (50 μM and 50 nM) were prepared in 0.05 M Seastar HCl no more than 10 minutes prior to measurement. Fe(II) calibration curves were obtained by adding Fe(II) standard (final concentration 0–400 pM) to cooled seawater (to match sample temperatures) that had been collected earlier at the same station (between 20 and 150 m depth) and had been left in the dark for >12 hours at ambient temperature to allow all Fe(II) to decay. Especially for stations near the coast, it is important to match standard seawater to samples, as negative values otherwise frequently result. This effect is most likely connected to varying concentrations of dissolved organic matter in the seawater, which can reduce the sensitivity of the luminol method (O'Sullivan et al., 1995). The analytical set-up was tested for its sensitivity to the presence of H_2O_2, and it was determined that the bias from up to 200 nM H_2O_2 is negligible, yielding a chemiluminescence signal that is below the detection limit of the analytical method for Fe(II).

The system was exposed to fluorescent light to increase luminol sensitivity, as described in Schallenberg et al. (2015b). However, the light also increases background chemiluminescence of the luminol, so that a standard curve will have a non-zero intercept. This is true even with an injection valve, as the background luminescence with seawater is higher than that with milli-Q, as has been previously observed (Croot and Laan, 2002). This intercept was routinely subtracted from the measured photon counts for samples and standards. Detection limits (3 $\times$ standard deviation of the zero standard) ranged from 1.9 ± 0.7 to 4.3 ± 1.8 pM between cruises (Table 3.3).

3.3.5 Fe(II) half-life calculation

Fe(II) half-lives were calculated based on the Fe(II) oxidation rate with O_2, following the approach of Millero et al. (1987). Briefly, the oxidation rate of Fe(II) with O_2 was estimated as a function of hydroxide (OH^-) concentration, temperature, ionic strength and O_2 concentration. While temperature and O_2 concentration were measured directly by sensors on the shipboard CTD package, ionic strength was calculated

Cruise	Detection limit ± 1 s.d. (pM)	# of measurements	Injection valve?
June 2012	1.9 ± 0.8	10	No
August 2012	2.6 ± 1.2	4	No
August 2013	4.3 ± 1.8	16	Yes

Table 3.3: Fe(II) detection limits for the respective cruises, determined as 3 × standard deviation (s.d.) of the zero standard.

from CTD salinity (Millero et al., 1987). The dissociation constant of water, K_w, was used to calculate OH^- concentrations from measured pH, and was corrected for ionic strength effects, temperature and pressure (Millero et al., 1987; Millero, 1995). The pH (total scale) was measured at sea on an Agilent 8543 spectrophotometer using a 3.0 mM solution of m-cresol purple (Dickson et al., 2007), with a precision of 0.003, based on duplicate measurements of replicate samples. The CO2SYS carbonate equilibrium program was used to adjust the pH to in situ temperature and pressure (Lewis and Wallace, 1998), as pH had been measured at 25°C in the shipboard laboratory. I used inputs of dissolved inorganic carbon (DIC) from a Line P cruise in June 2007, as no 2012 data are available at this time. However, the CO2SYS calculation is very insensitive to this input parameter.

The Fe(II) half-life ($t_{1/2}$) is inversely proportional to the Fe(II) oxidation rate, $k^{'}$, as follows:

$$t_{1/2} = ln(2)/k^{'} \tag{3.1}$$

The oxidation rate depends on a number of factors such as temperature, ionic strength and concentration of oxidants (see the Appendix B for details about estimating $k^{'}$). My calculation ignores the contribution of H_2O_2 to the oxidation of Fe(II) because H_2O_2 was not measured. The calculated Fe(II) half-lives are therefore likely overestimates (see Appendix B for a closer examination of how different estimates influence outcomes), especially where H_2O_2 concentrations and production rates are highest, e.g. near the ocean surface (Millero and Sotolongo, 1989; Yuan and Shiller, 2004) and in coastal waters (Vermilyea et al., 2010). Also note that only Fe(II) half-lives for the June 2012 cruise are shown, but the variability in environmental conditions is not expected to change Fe(II) half-lives significantly between cruises.

3.4 Results

3.4.1 Fe(II)

Fe(II) showed considerable variability within profiles and between cruises (Figures 3.2 and 3.3). The Fe(II) concentrations measured during the 3 cruises ranged from below the detection limit to >300 pM. At the 3 offshore stations (P16-P26), concentrations rarely exceeded 40 pM with the exception of P26 in June 2012 (Figure 3.2 A-C). The median of all measured Fe(II) concentrations at these 3 stations was 16 pM. Deep local maxima at the offshore stations varied between cruises and stations but tended to coincide with the upper reaches of the ODZ. Though depth resolution around local maxima was generally low, the profile from P12 in August 2013 shows a deep maximum that is supported by two measurements from different casts and different GO-FLO bottles (Figure 3.2D and Section B.3 in Appendix B), increasing confidence that deep local maxima are not the result of contamination.

Closer to the shelf at P4 and P12, higher Fe(II) concentrations were more prevalent, and for the most part, the profiles showed persistent patterns. At P12, Fe(II) concentrations generally increased with depth from the surface to about 1000 m and then decreased again deeper in the water column, with maximum values around 50 pM. However, the profile from June 2012 stands out with a striking feature in the upper 300 m: not only were the surface values exceptionally high (close to 90 pM), but there was also an Fe(II) peak at 150 m that showed similarly high Fe(II) concentrations. At P4, the general trend was that Fe(II) concentrations increased with depth. The highest Fe(II) concentrations for each cruise were always measured at P4 between 1000 and 1200 m, with concentrations well above 100 pM.

There is no clear trend in Fe(II) concentrations between cruises, but there was a much higher level of variability between stations during the June 2012 cruise than the August 2013 cruise (Figure 3.3). This is also reflected in the Fe(II) percentage of total dFe (Figure 3.4 A and B). In August 2013, the Fe(II) percentage at depth never exceeded 10% and showed little difference among profiles. However, numbers were consistently higher in surface waters, i.e. above 150 m. In June 2012, Fe(II) percentages were more variable among stations, but the general profile shape, with elevated values near the surface and lower Fe(II) percentages at depth, remained. In June 2012, P12 and P26 appeared to have an elevated Fe(II) fraction (of dFe) compared to the other stations. Interestingly, the station closest to shore (P4) does

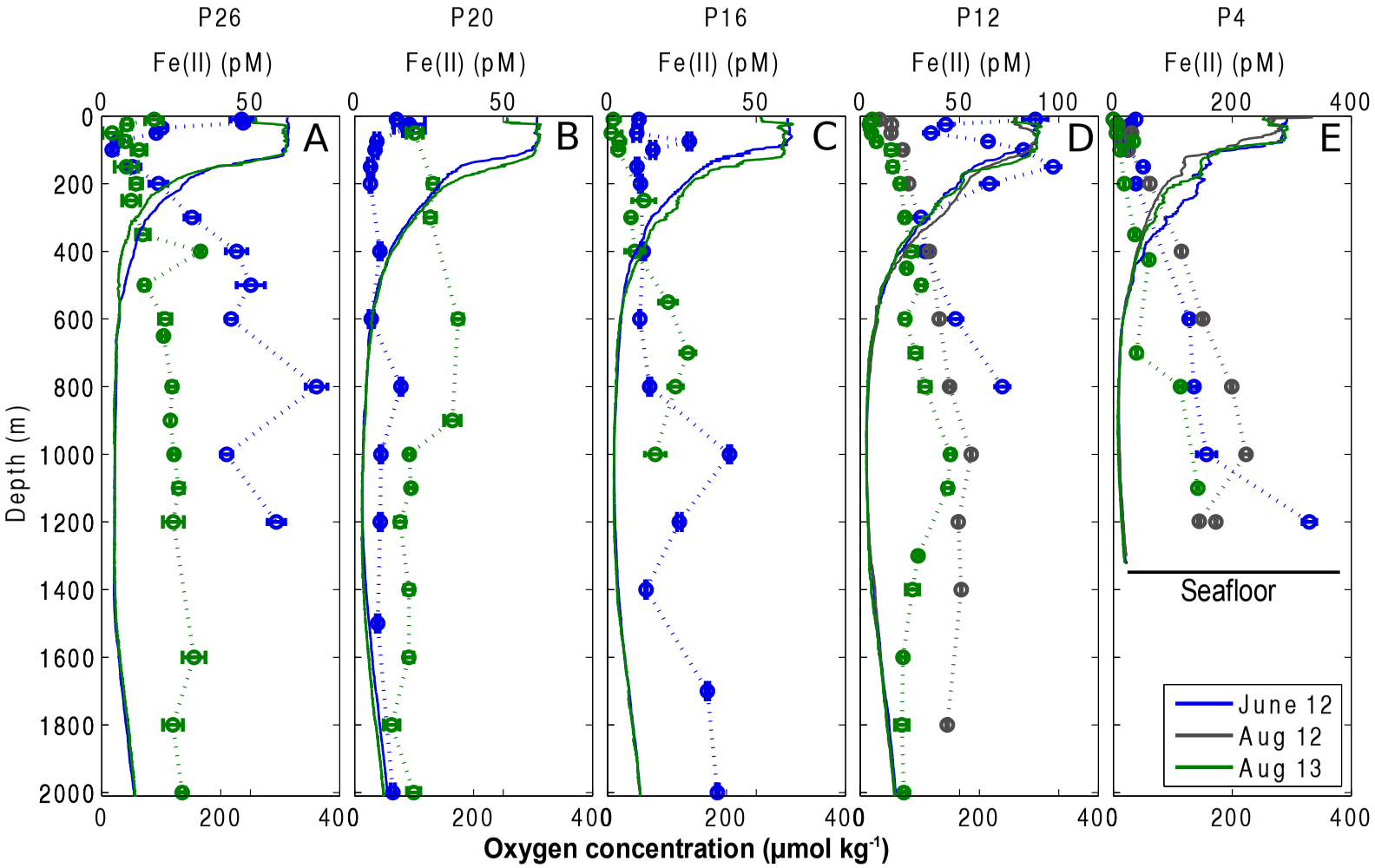

Figure 3.2: Fe(II) concentration depth profiles (pM) for each of the major stations along Line P, moving onshore from left to right (see Figure 3.1). Oxygen concentrations from the CTD oxygen sensor are displayed for reference (solid lines, bottom scale). Colours indicate different cruises: June 2012 (blue), August 2012 (grey) and August 2013 (green). Error bars are equivalent to one standard deviation from either replicate samples or replicate measurements (see Section B.2 in Appendix B for details). Note the different Fe(II) ranges on the x-axes for P4 and P12. The P26 profile for August 2013 is an adjusted composite of two casts (see Section B.3 in Appendix B for details).

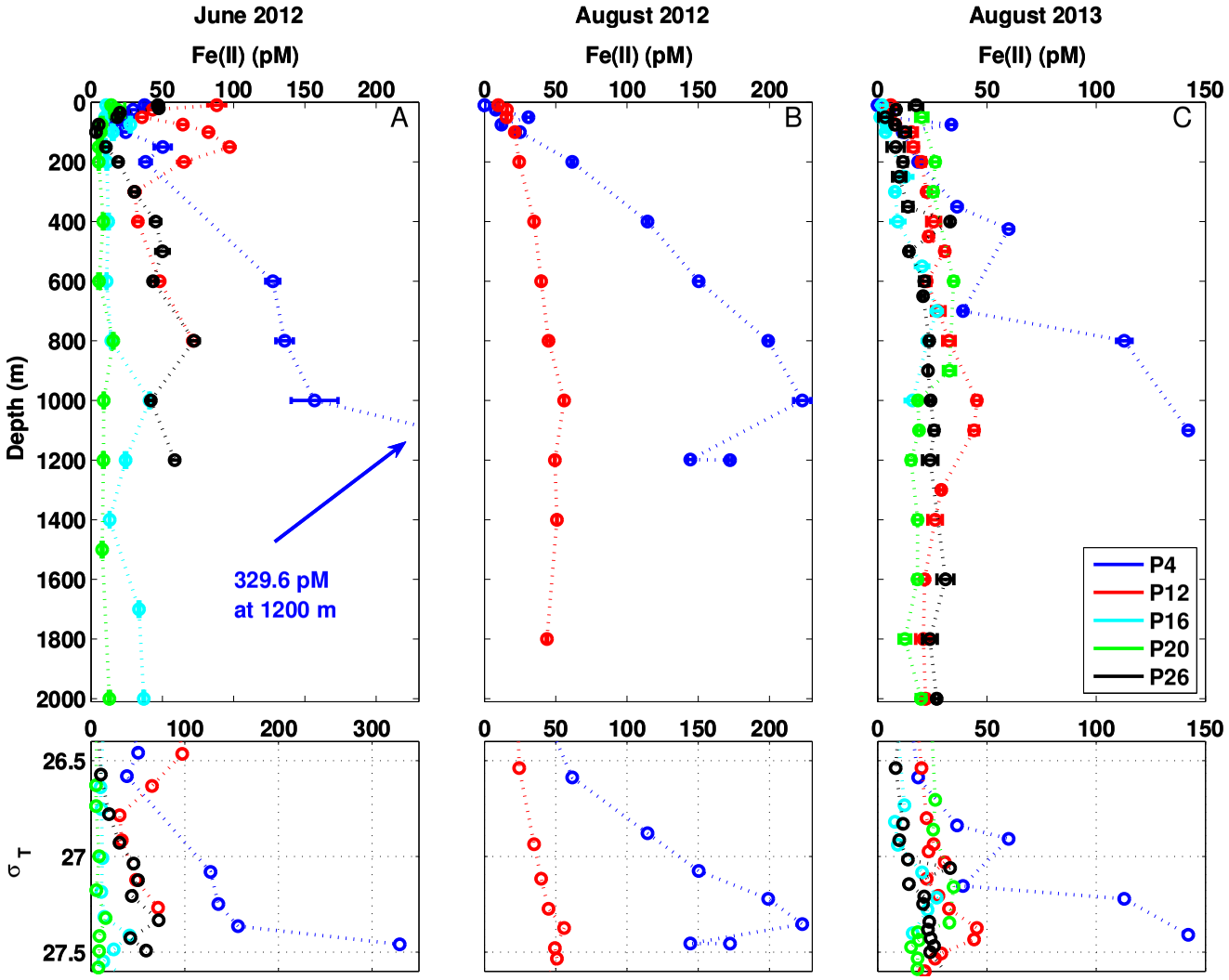

Figure 3.3: The same Fe(II) profiles as in Figure 3.2, but grouped by cruise, with colours indicating different stations. Error bars are equivalent to one standard deviation from either replicate samples or replicate measurements (see Section B.2 in Appendix B for details). Bottom panels show the same Fe(II) data, but with respect to density (σ_T) instead of depth (for depths >100 m only), and without error bars. Note the different Fe(II) ranges on the x-axes. The P26 profile for August 2013 is an adjusted composite of two casts (see Section B.3 in Appendix B for details).

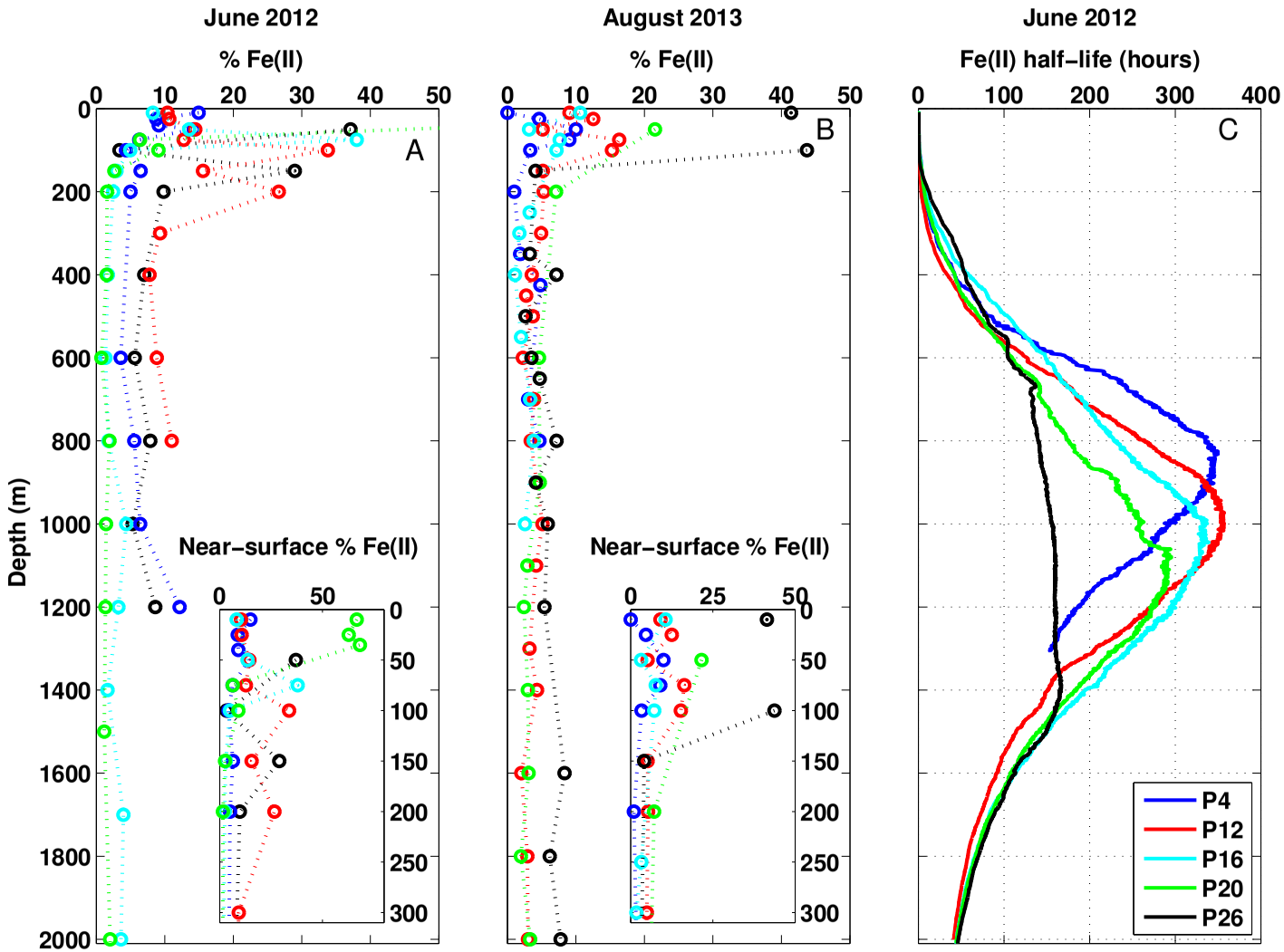

Figure 3.4: Fe(II) as a percentage of dFe for June 2012 (A) and August 2013 (B). Panel C shows calculated Fe(II) half-lives for June 2012 (see Sections 3.3.5 and B.4 for details). Half-lives at P26 are considerably shorter than at the other stations because oxygen concentrations are higher.

not stand out in terms of Fe(II) percentages on either cruise, even though absolute Fe(II) concentrations were highly elevated relative to stations farther offshore.

3.4.2 dFe

Dissolved Fe profiles for June 2012 and August 2013 are shown in Figure 3.5. As is the case for Fe(II), the highest concentrations were encountered at depth at P4, reaching >2 nM. At all other stations, dFe concentrations did not exceed 1 nM. In June 2012, the profiles showed high variability in the upper 200 m compared to August 2013, where surface concentrations were low for all stations (<0.2 nM) and increased with depth. Deeper in the water column, profile shapes and concentration ranges were more variable in August 2013 than in June 2012. For the latter, the 3 offshore stations (P16-P26) were in good agreement at depths greater than 200 m, showing a steady increase in dFe concentrations to a depth of 800–1000 m and a slight decrease below. Station P12 exhibited a similar trend but with generally lower concentrations, i.e. reaching only up to 0.65 nM compared to 0.92 nM at station P26. In August 2013, the deep dFe concentrations generally decreased from P12 to P26, with concentrations at P26 below 0.61 nM.

3.5 Discussion

The presented data are consistent with the known sources of dFe to coastal and open-ocean waters including river runoff, sediment resuspension, and reductive and non-reductive dissolution (Buck et al., 2007; Elrod et al., 2004; Homoky et al., 2013; Johnson et al., 1999; Lohan and Bruland, 2008). From the shelf, Fe-enriched waters can be transported offshore by anticylonic eddies (Brown et al., 2012; Johnson et al., 2005; Lippiatt et al., 2011) and cross-shelf transport, e.g. resulting from tidal currents (Cullen et al., 2009), downwelling events (Siedlecki et al., 2012) and advection related to the general circulation (Lam and Bishop, 2008; Lam et al., 2006). In addition, atmospheric deposition and hydrothermal vents may supply dFe to offshore waters (e.g., Bishop et al., 2002; Hamme et al., 2010; Tagliabue et al., 2010).

There is no evidence of mesoscale eddies for the three research expeditions, and the only known hydrothermal vent fields proximal to the study area, i.e. the Endeavour Hydrothermal Vents, are found more than 250 km distant from Line P and at a depth of ∼2250 m, which is deeper than our deepest measurements. Therefore, these

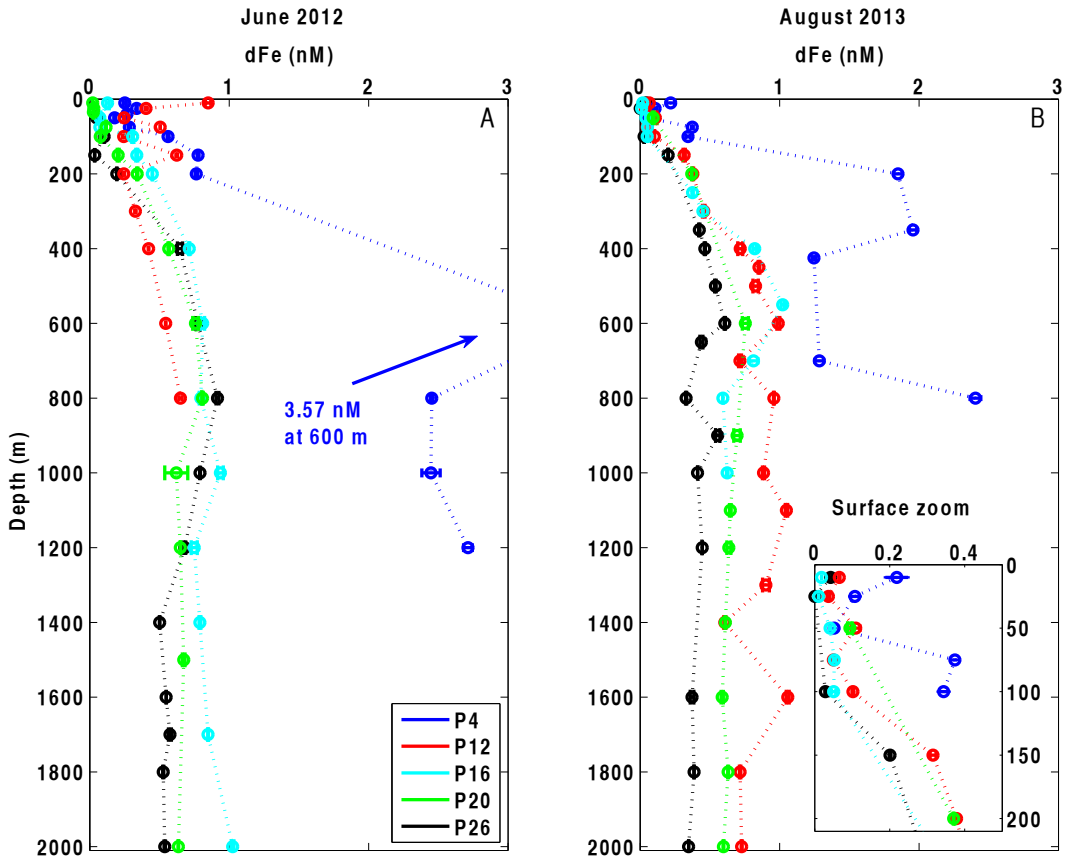

Figure 3.5: Dissolved Fe profiles (nM) for June 2012 (A) and August 2013 (B). Error bars are equivalent to one standard deviation from either replicate samples or replicate measurements.

potential sources of dFe are not considered to explain the distributions presented here. However, most other processes mentioned above are expected to influence the dFe and Fe(II) concentrations either directly or indirectly and will be discussed in more detail below.

3.5.1 Fe(II) on the continental slope

To my knowledge, the presented data comprise the first time series of Fe(II) in the subarctic Pacific Ocean. There are few studies from this oceanic region for comparison. Roy and Wells (2011), sampling on the continental shelf north of Vancouver Island in May 2007, found no detectable Fe(II). This contrasts with the continental slope station in my dataset, P4, which had the highest Fe(II) concentrations measured on all three cruises (Figure 3.2), one of which (June 2012) was during the same

season sampled by Roy and Wells. However, their measurements were restricted to the upper 180 m of the water column and likely did not encounter low-O_2 water. The low O_2 concentrations in deep waters at P4 (<10 μM, Figures 3.2 and 3.6) serve to stabilize Fe(II) by slowing its oxidation rate and prolonging its half-life (Figure 3.4C), thus enabling the accumulation of Fe(II).

In hypoxic (<65 μM O_2) shelf waters off the coast of Washington and Oregon, Lohan and Bruland (2008) found Fe(II) concentrations up to 19 nM in the bottom boundary layer (BBL) and attributed these to slow oxidation rates and increased Fe(II) flux from reducing sediments. For bottom waters off Peru containing <10 μM O_2, Hong and Kester (1986) reported Fe(II) concentrations up to 40 nM, decreasing markedly at 30–40 m above the seafloor. My deepest measurements for P4 are from 1200 m, which is >100 m above the seafloor and clearly above the BBL, based on beam attenuation. Therefore, I cannot directly compare my results to these literature data but contend that I see a marked Fe(II) increase with depth, consistent with the pattern observed by Hong and Kester (1986) in the main water column.

Maximum Fe(II) concentrations at P4 were up to 10 times higher than at the other stations, and the trend of steadily increasing concentrations with depth persisted through time (Figure 3.2E). The increasing Fe(II) concentrations are accompanied by decreasing O_2, and calculated half-lives for Fe(II) are maximal at about 800 m (Figure 3.4C). However, O_2 alone is insufficient to explain the observed Fe(II) patterns. For example, Fe(II) half-lives farther offshore, e.g. at P26, are only a factor 2 lower than at P4, whereas Fe(II) concentrations at P26 are up to 4 times lower (August 2013). This discrepancy illustrates an important distinction, namely that low O_2 concentrations are able to stabilize Fe(II) in the water column, but are unlikely to be responsible for producing Fe(II). This is further highlighted by the fact that there is no discernible relationship between calculated Fe(II) half-life and the observed Fe(II) fraction of dFe (Figure 3.4). Indeed, thermodynamic considerations (Morel and Hering, 1997) indicate that given the pH and O_2 concentrations prevalent in the ODZ of the subarctic Pacific Ocean, expected Fe(II) concentrations at equilibrium with the O_2/H_2O redox couple would be several orders of magnitude lower than were measured, implying that in situ processes must be maintaining Fe(II) levels in the picomolar range.

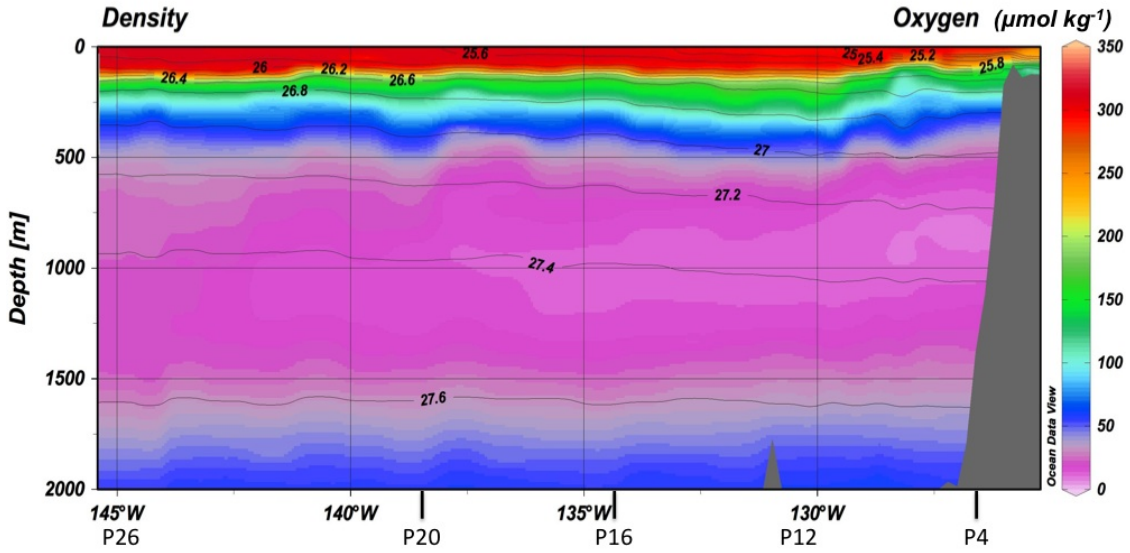

Figure 3.6: Cross-section along Line P of oxygen concentrations (μmol kg^{-1}; colours) and density distribution (σ_T, contours) for June 2012. Data interpolated from the shipboard CTD, with station spacing 1° longitude or better. Data courtesy of the Line P/Station P program run by the Institute of Ocean Sciences, Fisheries and Oceans Canada, Sidney, BC.

3.5.2 Fe(II) sources: Sediments

The Fe(II) data from P4 support a sedimentary source, such as particle re-suspension and reductive dissolution (Homoky et al., 2012; Hong and Kester, 1986; Lohan and Bruland, 2008; Severmann et al., 2010). Earlier studies have found increased concentrations of Fe-containing particles in the water column at P4 relative to the offshore stations, suggestive of a strong benthic influence (Lam et al., 2006; Nishioka et al., 2001).

Reductive dissolution has been observed repeatedly in environments where the sediment-water interface is poorly oxygenated (Homoky et al., 2012; Lohan and Bruland, 2008; Noffke et al., 2012; Severmann et al., 2010). Low O_2 concentrations at the sediment-water interface are found at P4 as well as stations closer to the shelf (Figure 3.6). These low O_2 concentrations not only stabilize Fe(II) in the BBL, but also enhance the diffusive Fe(II) flux from sediments, as the shallow O_2 penetration leads to reduced oxidative loss of Fe(II) in pore waters (Homoky et al., 2012; Lohan and Bruland, 2008; Severmann et al., 2010). The Fe(II) data for P4 (Figure 3.2) is thus consistent with reductive Fe release from the sediments.

The decreasing Fe(II) concentrations from the bottom towards the surface at P4 most likely reflect both upward mixing of Fe(II) from the BBL and transport along isopycnals intersecting with slope sediments closer to shore. With decreasing depth, the lateral distance from slope sediments increases, leading to longer transport times along isopycnals and therefore greater loss of Fe(II). In addition, increasing O_2 levels above the O_2 minimum around 900 m (Figure 3.6) will intensify oxidative loss of Fe(II) towards the surface.

3.5.3 dFe on the continental slope

The dFe concentrations at P4 are up to 3-fold higher than at the offshore stations, reaching >3 nM (Figure 3.5). Concentrations of similar magnitude, up to 5 nM, have been reported for stations on and near the shelf in the eastern and northern Gulf of Alaska (e.g., Cullen et al., 2009; Johnson et al., 2005; Lippiatt et al., 2010; Xiu et al., 2011). Earlier data along Line P similarly indicate that dFe concentrations in the range of 2 nM are not unusual at P4 (Nishioka et al., 2001). As discussed above for Fe(II), it is likely that the proximity to the slope as well as the low O_2 concentrations at depth contribute to the elevated dFe, consistent with a sedimentary — and reductive — source for dFe.

Freshwater sources such as the outflow from the Strait of Juan de Fuca may also contribute dFe to waters on the continental slope. Enhanced dFe input from freshwater systems entering the ocean has been observed for rivers along the west coast of the U.S. (Buck et al., 2007; Chase et al., 2005a). Chase et al. (2007) describe a mechanism for the supply of Fe involving river discharge in winter that supplies Fe to shelf sediments, followed by upwelling in summer that brings the Fe back to the surface, where it is available for primary production. In this scenario, the shelf acts as a "capacitor" for riverine Fe (Chase et al., 2007), and river discharge and upwelling act in tandem to bring Fe to the surface at a time when it can fuel primary production.

However, the situation in the Strait of Juan de Fuca differs in that the fluvial outflow is separated from the shelf by an enclosed coastal sea. As waters travel from river to ocean, estuarine circulation and intense tidal mixing increase their salt content, likely causing substantial loss of dFe to precipitation (Boyle et al., 1977), although dFe concentrations in the Strait of Juan de Fuca have not to my knowledge been measured. In addition, waters leaving the strait tend to flow northward along

the inner shelf in the Vancouver Island Coastal Current (Thomson et al., 1989), with little connection to the outer shelf. A portion of the Juan de Fuca outflow is also advected into the Juan de Fuca Eddy that is a regular feature at the mouth of the strait and contributes macronutrients to continental shelf waters via cross-shelf advection (MacFadyen et al., 2008). It is unclear, however, how much dFe could be deposited on the shelf and slope from this source.

During summer, coastal upwelling combined with wind mixing enhances the supply of macronutrients to surface waters on the Vancouver Island shelf (e.g., Crawford and Dewey, 1989). Even without a substantial riverine source supplying shelf sediments with Fe as described by Chase et al. (2007), it is likely that dFe associated with shelf sediments may reach surface waters over the shelf during upwelling events, as the shelf depth is generally $\leq$200 m (e.g., Whitney et al., 2005). Shelf waters are highly productive during summer (Crawford and Dewey, 1989; Hickey and Banas, 2008; Sackmann et al., 2004; Whitney et al., 2005), so remineralization in the sediments is a likely dFe source on the shelf (Elrod et al., 2004; Johnson et al., 1999). However, it is difficult to know how much of the upwelled dFe would reach P4 (which lies $\sim$50 km from the shelf break), as phytoplankton will quickly utilize Fe in the well-lit surface layer. In summary, the presented data do not allow me to weigh the relative contributions from different dFe sources on the continental slope, but profiles at P4 are consistent with supply from the sediments playing an important role.

3.5.4 Offshore dFe

Martin et al. (1989) reported the first dFe concentrations for Station P26 (Station Papa), ranging from <0.1 to 0.7 nM between the surface and 4000 m. More recent studies in the Gulf of Alaska have found concentrations of a similar range, with maximum values close to 1 nM at depth (Brown et al., 2012; Johnson et al., 2005; Roy and Wells, 2011; Xiu et al., 2011), in line with my observations for stations P12-P26 (Figure 3.5).

There is also evidence for considerable seasonal and year-to-year variability in dFe at P26. For example, Johnson et al. (2005) report dFe concentrations at P26 below 100 m depth that approach those seen in a Haida eddy but are not associated with eddy activity. They attribute the elevated dFe to increased upwelling of Alaska Gyre waters during a La Nina year (Johnson et al., 2005). Nishioka et al. (2001) also observed variability in dFe concentrations at P26 for different cruises and speculated

that this might reflect variable remineralization patterns. In addition, there is indirect evidence that sporadic atmospheric deposition may introduce biologically labile Fe to the subarctic NE Pacific, leading to increased primary production (Bishop et al., 2002; Boyd et al., 1998; Hamme et al., 2010). The cruise-to-cruise variability in the dFe data at the offshore stations is thus consistent with the temporal and spatial variability of Fe sources to the remote subarctic Pacific and the relatively short residence time of dFe in seawater.

3.5.5 Offshore Fe(II)

The range of Fe(II) concentrations at the offshore stations is similar to previous observations in this region. For example, Roy et al. (2008) report Fe(II) concentrations up to 50 pM in surface waters of the NE subarctic Pacific, though they did not detect any Fe(II) below 50 m. In another study, Roy and Wells (2011) did not detect any Fe(II) at all at station P26 during two cruises. This is in contrast to the data of Hansard et al. (2009) for a transect along 152°W from Tahiti to Alaska, where they found Fe(II) concentrations up to 60 pM. The two studies employed different methodologies, which could account for some of the differences. Hansard et al. (2009) acidified their samples to pH 6, which prolongs the Fe(II) half-life and may reduce some of the Fe(III) present, while Roy and Wells (2011) did not acidify. My samples were not acidified either, but my results (Figures 3.2-3.4) agree well with those of Hansard et al. (2009), both in terms of the observed range of concentrations and in the shapes of the profiles, with higher Fe(II) fractions near the surface (Hansard et al., 2009).

However, the actual Fe(II) concentrations (as opposed to the Fe(II) fraction of dFe) do not consistently show surface maxima in my data set (Figures 3.2 and 3.3). While there are some surface maxima in the Fe(II) data from June 2012 (Figure 3.3), such maxima are only barely evident in August. This might be a result of the different sampling methods used during the cruises, i.e. pumping from the surface waters in June 2012, and GO-FLOs on the TMR for the other cruises. It is likely that less Fe(II) would be lost to oxidation during pump sampling, with only 1–2 minutes passing between sampling and analysis, compared to 10–30 minutes between closing of surface GO-FLO bottles and analysis. Pump sampling was undertaken during both day and night, and surface maxima were not restricted to daytime sampling (e.g. P20, June 2012), so they are unlikely to result from exposure to sunlight during

the pumping process.

The surface maxima in Fe(II) percentage, as well as Fe(II) concentration, when they occurred (Figures 3.3 and 3.4), are suggestive of photochemical and biological Fe reduction in the well-lit layers of the water column (Hansard et al., 2009; Hong and Kester, 1986; Sarthou et al., 2011). Fe(II) maxima are evident near the surface during both day and nighttime sampling, consistent with the observations by Hansard et al. (2009) in the North Pacific. This indicates that Fe(II) is either being stabilized by ligands, as has been suggested by several authors (e.g., Croot et al., 2001; Roy et al., 2008), or that processes independent of solar radiation, such as Fe reduction at cell surfaces (Maldonado and Price, 2001; Shaked et al., 2005), play an important role.

As a whole, the Fe(II) concentrations reported here are considerably lower than what has been observed in ODZs in other parts of the world. In the ODZ of the eastern tropical North Pacific, for example, Hopkinson and Barbeau (2007) measured maximum Fe(II) concentrations around 0.12–0.15 nM at O_2 concentrations <5 μM. In the Arabian Sea, Moffett et al. (2007) observed Fe(II) concentrations >0.5 nM at the O_2 minimum, accounting for up to 50% of dFe. Oxygen concentrations in the Arabian Sea ODZ can be <1 μM, while in the NE subarctic Pacific the lowest O_2 concentrations are around 10 μM (excluding P4, where O_2 was as low as 7 μM). This may explain at least in part why Fe(II) concentrations and Fe(II) fractions were considerably lower than were reported in these other studies. However, a later research campaign in the Arabian Sea found maximum Fe(II) concentrations around 0.3 nM at similar O_2 and dFe concentrations as the earlier study by Moffett et al. (2007), suggesting that Fe(II) varies with factors other than O_2 and dFe (Kondo and Moffett, 2013).

3.5.6 Offshore transport of slope-derived dFe and Fe(II)

The beam transmittance data for P4 from all three cruises showed decreased transmittance near the seafloor, consistent with particle re-suspension near the sediment-water interface. Particle re-suspension is frequently assumed to be a source of dFe, and shelf sediment signatures have been detected hundreds of kilometres offshore in various locations (e.g., de Jong et al., 2012; Johnson et al., 1999; Nishioka et al., 2007; Shigemitsu et al., 2013). With respect to the NE Pacific, previous studies have found highly elevated concentrations of particulate and labile Fe at P4 (Lam et al., 2006; Nishioka et al., 2001), consistent with offshore transport of shelf- and slope-derived

waters.

The deep Fe(II) maxima evident around 1000 m at P4 and P12 (Figure 3.2) are suggestive of offshore transport of slope-derived Fe(II). Indeed, the high Fe(II) concentrations appear on similar density surfaces (Figure 3.3), supporting the interpretation that they are linked by along isopycnal transport. To verify whether such transport is realistic, I calculated Fe(II) half-lives for the June 2012 cruise, following the approach of Millero et al. (1987). As shown in Figure 3.4, maximum half-lives close to 350 h are found in the ODZ at station P4. This should be considered an upper limit because oxidation by agents other than O_2, e.g. H_2O_2, was not taken into consideration. As well, calculated half-lives are highly sensitive to the choice of model (see Appendix B for details), and should therefore be regarded as approximations only.

The distance between P4 and P12 is ∼300 km, and Fe(II) concentrations decrease from ∼180 to ∼45 pM at the depth of the local maxima, which translates into 2 half-lives, i.e. ∼700 hours. Isopycnal transport would thus have to be on the order 0.4 km h^{-1} or 0.12 m s^{-1} for Fe(II) to be transported from P4 to P12. This is about an order of magnitude higher than the upper end of estimated velocities for offshore transport from the continental slope in a model simulating dFe transport in eastern boundary upwelling systems, such as the Vancouver Island shelf (Siedlecki et al., 2012). It is therefore unlikely for pre-formed Fe(II) to be transported along isopycnals from P4 to P12, but transport of sedimentary particles may provide a continuous supply of Fe(II), as will be discussed below.

The concentration profiles do not suggest that the deep Fe(II) signature from the continental slope persists offshore beyond P12. Even though the June 2012 data show Fe(II) maxima in the ODZ at P16-P26, these maxima do not lie on the same density surfaces (Figure 3.3). While it is possible that different isopycnal surfaces intersect with shelf sediments at different times due to up- and downwelling near the coast, there is no clear trend of decreasing Fe(II) concentrations with distance from the continental slope as would be expected if the Fe(II) maxima were slope-derived. It is also conspicuous that the offshore data from August 2013 show no clearly defined Fe(II) maxima on the density surfaces in question. It is therefore highly unlikely that the localized Fe(II) maxima at stations P16-26 are derived from the continental slope.

Interestingly, the dFe data do not indicate offshore transport of deep waters beyond P4 (Figure 3.5). In June 2012, dFe at P12 below 200 m is lower than at any other station, disrupting any coherent onshore-offshore gradient. The data from August 2013 may indicate a dFe gradient below 400 m depth, from P4 to P26, but this

pattern is absent in the June 2012 data.

3.5.7 Fe(II) sources: Remineralization

Local maxima in Fe(II) concentrations in offshore waters are transient and tend to coincide with the upper reaches of the ODZ (e.g. P16, August 2013, 700 m, and P26, June 2012, 800 m, Figure 3.2), rather than with the lowest O_2 concentrations or longest Fe(II) half-lives (Figures 3.2 and 3.4), and the positions of local maxima differ between cruises and stations. This is consistent with an Fe(II) source that is transient and possibly seasonal, such as remineralization of sinking particles, as has been suggested previously for Fe(II) in ODZs distant from the continental shelf and slope (Hopkinson and Barbeau, 2007; Kondo and Moffett, 2013; Moffett et al., 2007).

Assuming a power function to describe the decrease in particle flux with depth (Martin et al., 1987), the rate of remineralization should be highest in the upper region of the ODZ where the particle flux is highest. Consequently, this is where local maxima in Fe(II) would be expected if Fe(II) production were a result of remineralization of sinking particles. Evidence for this scenario comes not only from my data, but also from the study by Moffett et al. (2007) in the ODZ of the Arabian Sea. They found that the local Fe(II) maximum was associated with the secondary nitrite maximum and that deeper in the ODZ, where O_2 concentrations were still low but a nitrite maximum was absent, there was no Fe(II) maximum (Moffett et al., 2007). Discussing this observation, these authors point to a pronounced nepheloid layer that coincided with the secondary nitrite maximum and likely consists of bacteria, suggesting that the Fe(II) maximum at the same depth may be connected to in situ remineralization associated with denitrification (Moffett et al., 2007). Revisiting the Arabian Sea 5 years later, Kondo and Moffett (2013) came to a similar conclusion, observing that local Fe(II) maxima are a persistent feature (as are the nitrite maxima), although their magnitude may vary seasonally with primary productivity in the overlying water column. A possible connection between denitrification and Fe(II) production is further supported by the discovery that marine anammox bacteria of the genus *Scalindua* are able to reduce Fe(III) as well as Mn(IV), providing a possible link between fixed nitrogen loss processes and Fe(II) production (van de Vossenberg et al., 2008).

The Arabian Sea is a major contributor to global water column denitrification (DeVries et al., 2012), as is the eastern tropical North Pacific, where Hopkinson and

Barbeau (2007) measured elevated Fe(II) in the ODZ. However, O_2 concentrations in the ODZ of the subarctic NE Pacific are not considered low enough to support widespread denitrification, which could explain the lower Fe(II) concentrations observed in this study. But it is possible that denitrification in micro-environments associated with settling particles contributes to the Fe(II) measured in the NE Pacific (Wright et al., 2012).

3.5.8 Fe(II) sources: Eolian dust

Buck et al. (2013) investigated the redox speciation of dFe resulting from deposition of eolian material in the marine environment and found that up to 26% of the soluble iron was in the reduced form. In addition to this study, there is indirect evidence that eolian input may be a source of Fe(II). Firstly, the Arabian Sea, where Moffett et al. (2007) found high Fe(II) in the ODZ towards the end of the monsoon season, receives considerable eolian dust input during the SW monsoon (Measures, 1999). A study in the same area but outside the monsoon season reported lower Fe(II) concentrations, and the authors discuss the possibility that the difference may be — at least in part — attributable to less dust deposition during the inter-monsoon period (Kondo and Moffett, 2013). Secondly, Hopwood et al. (2014) recently reported detection of Fe(II) released from glacial flours in a laboratory study, indicative of active redox cycling on the particles.

The remote subarctic North Pacific is subject to sporadic eolian deposition from a variety of sources, such as dust from Asia (Bishop et al., 2002), glacial flour from coastal Alaska (Crusius et al., 2011), and volcanic ash from the Aleutian Islands (Hamme et al., 2010). Atmospheric particle input could therefore have contributed to the observed Fe(II) concentrations in the NE subarctic Pacific, consistent with the transient nature of local Fe(II) maxima. The Fe(II) data from June 2012 show considerably higher variability than those from August 2013, with especially elevated Fe(II) concentrations at P26 (Figures 3.2 and 3.3). Dust storms from Asia are most likely to reach the remote NE Pacific in spring and early summer (Uematsu et al., 1983), so the high Fe(II) concentrations at P26 in June 2012 may be related to the settling of particles following an aerosol deposition event (see Chapter 5). The observed Fe(II) gradient is consistent with a constant rate of Fe(II) production, yielding higher Fe(II) concentrations at depth, where Fe(II) half-lives are longer (Figure 3.4C).

3.5.9 Fe(II) sources: Do particles have a role to play?

The Fe(II) profile from P12, June 2012, stands out with its pronounced maximum in the 100–200 m depth range (Figures 3.2D and 3.3A). This maximum persists in the Fe(II) percentage data (Figure 3.4) and is also evident in the dFe profiles (Figure 3.5), though less pronounced. The depth of this feature coincides with the depth where Lam et al. (2006) previously observed high concentrations of acid-leachable particulate Fe at P4, and it coincides with a warm temperature anomaly centered at 180 m that extends from the continental slope to P12 (data not shown). This anomaly is indicative of a subsurface intrusion of near-shore waters, which are influenced by the warm and salty California Undercurrent (Klymak et al., 2015), into the offshore domain. Thus, the observed maximum in Fe(II) (and dFe) concentrations may very well be located in waters that were very recently advected off the continental shelf and upper slope and that contain high concentrations of Fe-bearing particulates. Such a scenario highlights the importance of episodic events for the offshore transport of shelf-derived Fe.

The data suggest that particles in the subsurface may represent a persistent source of Fe(II). The subsurface Fe(II) maximum is found in waters with higher O_2, warmer temperatures and higher pH than prevail in the ODZ, shortening the expected Fe(II) half-life to less than 5 h. For 100 pM Fe(II) to reach P12 from the shelf, very high advective velocities and Fe(II) source concentrations are therefore required. Though I cannot rule out this possibility, largely because Fe(II) concentrations on the Vancouver Island shelf are poorly known, I propose that advected particles themselves may also be a source of Fe(II). While particles can effectively scavenge dFe, particularly in environments where dFe concentrations are high, such as the BBL (e.g., Homoky et al., 2012), a multitude of studies have concluded that offshore transport of particulates may also provide a resource for continued dFe release in the ocean interior (Chase et al., 2005b; Cullen et al., 2009; Lam and Bishop, 2008; Lam et al., 2006; Planquette et al., 2011). Freshly scavenged Fe is likely more labile than "aged" sedimentary particles themselves; suspended particles from the BBL may therefore act as a shuttle for labile Fe from the shelf and slope to the ocean interior (Homoky et al., 2012).

Lam et al. (2006) found that subsurface particles advected off the BC continental shelf were highly diverse in their Fe speciation, indicating a heterogeneous source that may include freshly scavenged material. Reduction could play a role in the Fe dissolution process, e.g. mediated by microorganisms associated with the particles (Canfield,

1988; Weber et al., 2006), providing a continuous Fe(II) source from particles. In addition, the speciation of particles off Vancouver Island may include a considerable Fe(II) fraction, as was observed for the western north Pacific (Lam et al., 2012). Lam et al. (2012) argue that the speciation of particulate Fe found in the water column reflects the type of margin adjacent to the study area, with active continental margins a source of Fe(II)-containing particles. The North Pacific is rimmed by active continental margins in both the east and the west.

There is no evidence of increased beam attenuation at P12, so I have no direct evidence of the presence of particles at the depth of the Fe(II) maximum, but beam transmittance at 650 nm is not sensitive to particles <1 μm in diameter (Sullivan et al., 2005). Therefore fine particles, e.g. resulting from the oxidation of sediment-derived Fe(II) in the oxygenated water column, would be missed by the transmissometer.

An alternative explanation for the elevated Fe(II) concentrations in the subsurface at P12 in June 2012 could be the sinking and remineralization of an earlier phytoplankton bloom. Cell lysis of a declining bloom might have caused the high dFe concentrations at the surface (Figure 3.5). Consistent with a post-bloom scenario, P12 features the lowest chlorophyll *a* concentrations measured on the June 2012 cruise ($<$0.4 mg m^{-3}). However, the macronutrient data show no sign of elevated remineralization in the 100–200 m depth range (not shown), i.e. there is no increase in macronutrient concentrations along with the elevated Fe(II) concentrations.

In conclusion, the question of whether suspended particles constitute a source of Fe(II) cannot be adequately resolved with the presented data. However, the data can be interpreted to support this suggestion as follows: It has already been established that the water column at P4 is enriched with acid-labile particles (Lam et al., 2006; Nishioka et al., 2001) relative to other stations, and P4 is also consistently the station with the highest Fe(II) concentrations (Figure 3.2). The anomalously high Fe(II) concentrations in the subsurface at P12 in June 2012 may be attributed to advection of particle-rich waters off the shelf and slope, as discussed above. Similarly, particles transported offshore along isopycnals may be primarily responsible for the deep local Fe(II) enhancement that extends from P4 to P12. Finally, the high Fe(II) concentrations and Fe(II) percentages at depth at P26 in June 2012 could be explained by eolian dust deposition (see Chapter 5). Clearly, the hypothesis that particles may constitute a source of Fe(II) deserves further investigation.

3.6 Conclusions

I have presented Fe(II) time series data along a transect in the NE subarctic Pacific. The observed patterns are consistent with a benthic source for Fe(II) and dFe on the continental slope. The benthic Fe(II) signal is detectable several hundred kilometres offshore at depths around 1000 m.

Concentrations of Fe(II) at the offshore stations exhibit high variability between cruises and with depth, emphasizing the dynamic nature of Fe(II) sources. There is no simple relationship between Fe(II) and O_2 concentrations or Fe(II) half-lives, highlighting the importance of sporadic and variable processes that produce Fe(II). These likely include remineralization of organic material, i.e. associated with sinking particles and aggregates, and may be connected to denitrification. In addition, sedimentary particles and the dissolution of aerosols may be potential sources of Fe(II).

There is evidence that episodic events, such as subsurface intrusions of near-shore waters into the offshore domain, may substantially elevate subsurface Fe(II) concentrations hundreds of kilometres offshore. The relatively shallow depth of the Fe(II) enrichment may make it available to phytoplankton in surface waters during deep mixing and upwelling. Such episodic events could thus provide a hitherto unrecognized Fe-source for the HNLC subarctic Pacific.

The presented data suggest that sediments on the continental slope constitute an important dFe source for the NE subarctic Pacific, and that low O_2 concentrations at depth serve to stabilize Fe(II). This indicates that the continued de-oxygenation of the ODZ in the NE subarctic Pacific (Whitney et al., 2007) may enhance Fe release from slope sediments, as was proposed by Homoky et al. (2012). While this may be true for the near future, Scholz et al. (2014) recently argued for a narrow "sweet spot" in O_2 concentrations where Fe-release from sediments is at a maximum and beyond which, i.e. at lower O_2 concentrations, precipitation of Fe sulphides occurs.

Chapter 4

Presence of superoxide enhances Fe solubility of dust in seawater

To be submitted to *Environmental Science & Technology*.

4.1 Abstract

The solubility of aerosol-associated iron (Fe) deposited to surface waters is a primary factor controlling open ocean Fe concentrations. A variety of leaching schemes have been employed to quantify and parameterize the Fe solubility of minerals, dusts and aerosols under a multitude of environmental conditions, but little work has been dedicated to the investigation of superoxide (O_2^-), a reductant with the potential to dissolve particulate Fe. An experiment with four different dust sources was conducted in artificial seawater (ASW), employing the superoxide thermal source SOTS-1 to generate steady-state O_2^- concentrations in the range of tens of picomolar. These O_2^- concentrations were sufficient to yield concentrations of dissolved Fe(II) similar in magnitude to those produced in light treatments compared to dark controls with the same dusts. Given the potential for ubiquitous production of O_2^- by heterotrophic bacteria throughout the ocean water column, these results indicate that Fe dissolution of dusts and aerosols via reduction by O_2^- below the euphotic zone could be as significant a process as photochemical reactions in the upper ocean, and represent a source of dissolved Fe at all depths of the ocean.

4.2 Introduction

The availability of iron (Fe) controls primary production in 40% of the surface ocean (Moore et al., 2002). By altering the efficiency of the biological carbon pump, temporal and spatial variability in Fe supply on millennial time scales may play an important role in modulating atmospheric carbon dioxide concentrations (Martin, 1990; Sigman and Boyle, 2000). Of particular interest in this context is the supply of Fe by atmospheric deposition (Jickells et al., 2005), and the Fe solubility of aerosols has therefore been the focus of numerous studies (e.g., Aguilar-Islas et al., 2010; Buck et al., 2006; Schroth et al., 2009; Sholkovitz et al., 2012). Common experimental designs include investigations of how temperature, pH, light levels and the presence of complexing ligands, among other factors, impact aerosol-associated Fe solubility in seawater (e.g., Borer et al., 2005; Fu et al., 2010). However, superoxide (O_2^-), a reactive oxygen species and potential reductant of particulate Fe, has received limited attention.

Superoxide is a reactive intermediate in the redox cycle between water and oxygen, and has been measured at picomolar to nanomolar concentrations in the surface ocean (Hansard et al., 2010; Rose et al., 2008; Rusak et al., 2011). It is implicated in the redox cycling of several trace metals such as Fe, copper (Cu) and manganese (Mn) in the ocean, and is of particular interest because it can act as both oxidant and reductant (Heller and Croot, 2010b; Learman et al., 2011; Rose, 2012; Rose and Waite, 2006; Voelker et al., 2000; Zafiriou et al., 1998):

$$M^{n+} + O_2^- + 2H^+ \rightarrow M^{(n+1)+} + H_2O_2 \tag{4.1}$$

$$M^{(n+1)+} + O_2^- \rightarrow M^{n+} + O_2 \tag{4.2}$$

The question of whether O_2^- increases the solubility and bioavailability of Fe is still disputed and is likely dependent on multiple factors, including the presence and strength of Fe complexing ligands (Rose, 2012; Rose and Waite, 2005). The ambient concentrations of Cu and dissolved organic matter (DOM) are also expected to exert an influence because they are both major sinks for O_2^- in the ocean (Goldstone and Voelker, 2000; Heller and Croot, 2011, 2010b; Voelker et al., 2000; Zafiriou et al., 1998).

The primary sources of O_2^- in the ocean include biological production by phytoplankton, corals and bacteria, as well as photochemical reactions (Diaz et al., 2013;

Kustka et al., 2005; Marshall et al., 2005; Micinski et al., 1993; Rose et al., 2010, 2005; Saragosti et al., 2010). Superoxide is assumed to be an intermediate in photochemical reactions at the ocean surface that can lead to the reduction of Fe (Fan, 2008; Miller et al., 1995; Powers and Miller, 2014). In the few studies investigating O_2^- in the ocean, concentrations were usually found to be highest in the well-lit surface layer (e.g., Hansard et al., 2010; Rusak et al., 2011), but it is worth keeping in mind that the fast decay of this reactive oxygen species makes it challenging to measure at deeper depths.

Only recently has it been discovered that O_2^- is produced by ubiquitous heterotrophic bacteria that are not restricted to the surface ocean (Diaz et al., 2013), opening the possibility that O_2^- may participate in redox reactions in the deep as well as the surface ocean. This may be of special interest with respect to the dissolution of particulate Fe such as is contained in dusts and aerosols. To date, it has been assumed that the oceanic processing and dissolution of atmospheric dust occurs primarily in the sunlit surface layer (e.g., Baker and Croot, 2010). However, if O_2^- can enhance Fe solubility of dusts, and if O_2^- is present in sufficient quantities in the deep ocean, then it is possible that a significant fraction of particulate Fe dissolution may occur below the sunlit surface layer but at depths shallow enough to serve as an Fe source to the surface during winter mixing events. Such a scenario would have important consequences for the Fe cycle in the ocean, especially as it pertains to the addition of dissolved Fe from atmospheric dust.

The presented experiment was designed to test whether O_2^- is able to promote Fe solubility of dusts from a variety of source regions, with a particular view towards the possibility that significant O_2^- production by bacteria may occur at all depths in the ocean and possibly in aggregates and biofilms associated with dust particles. The slowly decaying superoxide thermal source SOTS-1 was employed to generate near-constant steady-state concentrations of O_2^- over a time period of $\sim$24 hours (Heller and Croot, 2010a). For reference, the Fe solubility resulting from exposure to O_2^- was compared to Fe solubility resulting from exposure to sunlight, including ultraviolet (UV) radiation. Iron solubility, in this case, refers to the production of Fe(II) as measured spectrophotometrically after coordination with ferrozine. This reagent forms a strong complex with Fe(II), thus mimicking Fe(II) removal from the solution such as would be expected in the ocean due to Fe-uptake by biota, or due to complexation by naturally occurring ligands (Gledhill and Buck, 2012). It is acknowledged that the presence of strong organic ligands can promote surface

dissolution processes (e.g., Borer et al., 2005; Kraemer, 2004); this effect is not the focus of this study, and the influence of ferrozine in the presented experiments is accounted for by following Fe dissolution in the dark.

4.3 Methods

4.3.1 Reagents

A 10-mg batch of the superoxide thermal source SOTS-1 (Cayman Chemicals) was dissolved in 12 mL dimethylsulfoxide (DMSO) and refrozen in 1 mL aliquots at −80°C until used. Similarly, 15 kU of superoxide dismutase (SOD) from bovine erythrocites (Sigma-Aldrich) were dissolved in 11 mL ultra-high purity H_2O (Millipore Element, milli-Q) and refrozen in 1 mL aliquots at −20°C until used. Ferrozine reagent (3-(2-Pyridyl)-5,6-diphenyl-1,2,4-triazine-4',4"-disulfonic acid sodium salt; Fluka) was made fresh in milli-Q for each experiment at 20 mM concentration.

For Fe(II) calibrations, a 10 mM standard of ammonium iron(II) sulfate hexahydrate was prepared in 0.1 M Seastar Baseline hydrochloric acid (HCl) and considered stable at 4°C for up to a month. From this stock solution, a 10 μM intermediate standard was prepared fresh for each calibration in 0.05 M Seastar HCl.

The chemiluminescent reagent MCLA (6-(4-Methoxyphenyl)-2-methyl-3,7-dihydroimidazo[1,2-a]pyrazin-3(7H)-one hydrochloride; Sigma) was dissolved in milli-Q upon receipt and frozen at −80°C in 1-mL aliquots containing 2.0 and 2.5 mM MCLA each. These were thawed individually and diluted in 1 L milli-Q to yield 2.5 or 4 μM MCLA reagent. The reagent also contained 0.05 M sodium acetate and was adjusted to pH 6 with concentrated Seastar HCl. It was stored at 4°C when not in use and not used beyond 1 week of age.

4.3.2 Dusts

The experiment was run with four dusts from different source regions: China, Arizona, Australia and Alaska. The materials from China (CJ-1) and Arizona (PTI ID: 10368 BK) are standardized test dusts and their respective composition and particle size distribution has been described in detail elsewhere (Hwang and Ro, 2006; Nishikawa et al., 2000; Shelley et al., 2015). The dust from Alaska is a sample of previously airborne material and was collected in the vicinity of several retreating

Source region/ Characteristic	Alaska	Arizona (PTI ID 10368BK)	Australia	China (CJ-1)
Particle size distribution	n.d.	0-3 μm [4]	36% <125 μm 64% >125 μm and <425 μm	median ~1.5 μm, bulk <10 μm [1]
Weight% Fe	4.6-5 [5]	3.2-3.4 [3]	n.d.	4 [1] 2.94 ± 0.09 [2]
Weight% Fe_2O_3	n.d.	n.d.	<0.4, i.e. det.lim. of XRD method [8]	5.3 [1]
% Fe(II) in all Fe species [5]	72-79	n.d.	n.d.	33
Presence of clay?	yes [5]	possibly [6]	likely [7]	n.d.
Cumulative % Fe solubility [5]	1.9-3.2	n.d.	n.d.	0.54
Other	Possible presence of weathering products from volcanic ash [5]		Red-brown color; 84% silicon dioxide; presence of an X-ray amorphous phase is suggested, possibly consisting of nanoscale goethite and/or hematite [8]	Mostly aluminosilicate, silicon dioxide and calcium carbonate [1]

Source:
1 - Hwang and Ro, 2006
2 - Nishikawa et al., 2000
3 - Shelley et al., 2015
4 - Supplied by PTI
5 - Schroth et al., 2009; for Glacial material very similar in origin to our sample
6 - Fu et al., 2010; for Arizona test dust of unknown ID but from the same supplier
7 - Personal communication, Patrick De Deckker
8 - Results of XRD analysis at the Electron Microbeam/X-ray Diffraction Facility at the University of British Columbia, Canada

Table 4.1: Summary of qualitative properties of dust types used in this study. Note that properties are not determined (n.d.) for all dusts.

glaciers in the Copper River watershed. It is expected to be similar in composition to the glacial flour described by Schroth et al. (2009) (John Crusius, personal communication). The sample from Australia was collected from the ground in western central South Australia, near Lake Gairdner, in an area characterized by wind-driven erosion (Patrick De Deckker, personal communication) that is one of the possible source areas for dust storms that reach as far as Sydney, Australia. This is the only sample that was sieved in the lab; all other samples were used as received. For a summary of key physical and chemical characteristics of each dust, see Table 4.1.

The respective dust concentrations for the experiments were selected so as to yield a detectable Fe(II) signal. Dust concentrations tested were as follows, where the respective numbers refer to mg dust L^{-1}: Alaska40, Alaska120, Arizona140, Arizona200, Australia400 and China400. These dust concentrations are much higher than environmental concentrations that would result from a deposition event in the ocean (a few mg L^{-1}, depending on mixed layer depth), but they may be applicable to conditions in an aggregate of dust particles. Furthermore, dust concentrations based on weight ignore the influence of particle size distributions and the resulting surface areas, which may have a large influence on Fe solubility. Factors such as atmospheric processing, the presence of microbial communities, organic content and the age of samples are also expected to influence Fe solubility (Baker and Croot, 2010; Fujii et al., 2006; Sholkovitz et al., 2012), but are not addressed in this study. The rationale for choosing different dusts was not to compare the dusts directly, but to test whether treatment effects, i.e. exposure to superoxide and light, led to common trends in Fe solubility across a spectrum of dusts from different source regions. The differences in concentration and surface area between dusts are therefore not a concern in these experiments.

4.3.3 Experimental set-up for dust dissolution experiments with superoxide

All dust dissolution experiments were run in artificial seawater (ASW), with contaminant metals removed by ion exchange (Chelex-100) following Price et al. (1989). The ASW was microwave-sterilized according to the recommendations by Keller et al. (1988).

The experimental set-up included the following treatments:

- dark + 0.5 μM SOTS-1 (SOTS×1)

- dark + 2 μM SOTS-1 (SOTS×4)
- dark + 6 μM SOTS-1 (SOTS×12)
- dark
- light
- light + 3 kU SOD (only 1.5 kU in Alaska40)

Dark treatments (including SOTS-1 treatments, as these were also kept in the dark) were kept in 60 mL Teflon^{TM} bottles for the duration of the experiments, and light treatments were kept in 5.0 mil Norton® FEP film bags that are transparent to UV-A radiation (320-390 nm) (Welch Fluorocarbon). All equipment was extensively acid-cleaned prior to use, following GEOTRACES recommendations (Cutter et al., 2010). Experiments lasted 25-28 h because O_2^- production from SOTS-1 was expected to be reasonably constant during this time period but would begin to fall off more steeply as time progressed. All treatments were run in triplicate. Teflon bags and bottles were placed on shaker tables, and sub-samples were frequently drawn with a 5 mL plastic syringe and attached Tygon tubing in order to measure Fe(II) concentrations throughout the experiment. The temperature in the laboratory was on average 21.5°C (range 19-23°C). Because the light treatments relied on daylight (they were exposed to sunlight through a large 3rd-floor window), they were subject to a day-night cycle (∼8 h dark, ∼16 h light) rather than constant light. Also, window glass does not filter out UVA radiation (320-400 nm) but does block radiation of wavelengths <320 nm. The only exception to this light treatment was the experiment with Alaska40, which was illuminated with an OSRAM Ultra Vitalux® 300W bulb that emits UVA and UVB radiation of 13.6 and 3.0 W respectively, along with visible light. Due to the high wattage, the lamp also slightly heated the samples (∼29°C for the light treatments, ∼26°C for the dark treatments). Blank treatments (i.e. without dust added) were run twice for each treatment and were run in triplicate each time.

4.3.4 Procedure for dust dissolution experiments with superoxide

For each dust dissolution experiment, ASW volumes of 60 mL (dark treatments) and 100 mL (light treatments) were measured out and ferrozine was added to yield a final

concentration of 100 μM. Then SOTS-1 and SOD were added to the respective desired final concentrations and a dust "sludge" was prepared in 25 mL ASW. The sludge had dust concentrations ranging from 4.8 to 48 g L^{-1} and was placed on a stir table. Within minutes from preparation of the sludge, dust additions (500 and 835 μL) were made to the prepared Teflon^{TM} bottles and FEP film bags in a randomized order, with all additions finished within ~20 minutes.

4.3.5 Measurement apparatus and calibration for Fe(II) in dust dissolution experiments with superoxide

Fe(II) was measured using ferrozine, which forms a magenta complex with Fe(II) that has an absorbance peak at 562 nm (Stookey, 1970). Absorbance measurements were made using an Ocean Optics spectrophotometer (USB2000) and Ocean Optics halogen light source (HL-2000-FHSA). Subsamples from the treatments were filtered through a 0.2 μm Supor® Acrodisc® syringe filter (Pall) and injected into a liquid waveguide capillary cell (250 cm length, World Precision Instruments). Standards were prepared in ASW by adding aliquots of the intermediate Fe(II) standard. In order to keep the procedures consistent between standards and samples, standards were also injected into the waveguide through a 0.2 μm Supor® Acrodisc® syringe filter.

To account for baseline drift, absorbance at 700 nm was routinely subtracted from measurements. This gave blank values for the method (ASW + ferrozine) of -0.17 ± 0.65 nM (n=820). Calibrations were very consistent throughout the experiment (slopes ranged from 0.0059 to 0.0065 nM^{-1}), with $r^2 \geq 0.998$. The detection limit was 1.9 nM Fe(II) (3 $\times$ standard deviation of the blank).

4.3.6 Ancillary experiment: Superoxide decay with and without dust

In order to constrain expected O_2^- steady-state concentrations resulting from SOTS-1 decay, it is necessary to measure O_2^- decay in the respective treatments (Heller and Croot, 2010a). Superoxide decay was measured in ASW, in dust solutions prepared in ASW, and on SOTS-1 at 2 and 6 μM concentrations in ASW. The SOTS-1 solutions had been prepared months earlier in order to allow for all O_2^- produced by SOTS-1 to decay; the goal was to examine how the presence of SOTS-1 and potential

contaminants associated with it would affect O_2^- decay. Dust solutions had been prepared ∼3 hours before measurements began. All solutions were kept in previously acid-cleaned 60 and 30 mL Teflon^{TM} bottles.

The chemiluminescent reagent MCLA was employed for our O_2^- decay measurements, following the approach of Heller and Croot (2010c). Briefly, MCLA (2.5 μM) and sample were mixed in a hand-coiled flow cell made from Tygon tubing and mounted in front of a photomultiplier tube (PMT; Hamamatsu H9319-01) in a custom-made light-tight box, and the PMT signal (200 ms integration time) was recorded with FloZF software (GlobalFIA, Fox Island, WA USA). A peristaltic pump pulled both sample and MCLA through the flow cell at the respective flow rates of 5 and 2.5 mL min^{-1} to reduce dead time in the system (Heller and Croot, 2010c). A 150 μm mesh prevented dust particles from entering the flow cell.

Superoxide was made fresh for each decay experiment by adding ∼10 mg potassium superoxide (KO_2) to 0.1 M NaOH in a 10-cm Quartz cuvette, while absorbance was followed at the wavelengths 230, 240, 250 and 260 nm in order to estimate superoxide concentration in the solution as described by Heller and Croot (2010c). From the O_2^- cocktail, an addition was made to the sample under stirring and while both sample and MCLA were drawn into the flow cell. The signal from before the O_2^- addition yields the MCLA baseline that is ultimately subtracted from the decay signal, as it is the result of the auto-oxidation of MCLA at the experimental pH (Fujimori et al., 1993).

For ASW and SOTS-1 solutions, the O_2^- additions were such that the O_2^- concentration in the sample was ∼70 nM at the beginning of decay. For the dust solutions, the additions were considerably higher (∼1.7 μM) because the decay was so fast that there was no decay signal detectable at lower O_2^- concentrations, even though travel time between sample bottle and flow cell was no more than ∼6 seconds.

The first-order O_2^- decay constant, k_{obs}, was estimated with a least-squares linear fit on the log-transformed data (see Figure 4.1 for examples). For ASW and SOTS-1 solutions, the fits were performed on the initial 60 seconds of decay data, while for the dust solutions only the first 4 seconds of decay were found to be linear and appropriate for the fitting routine.

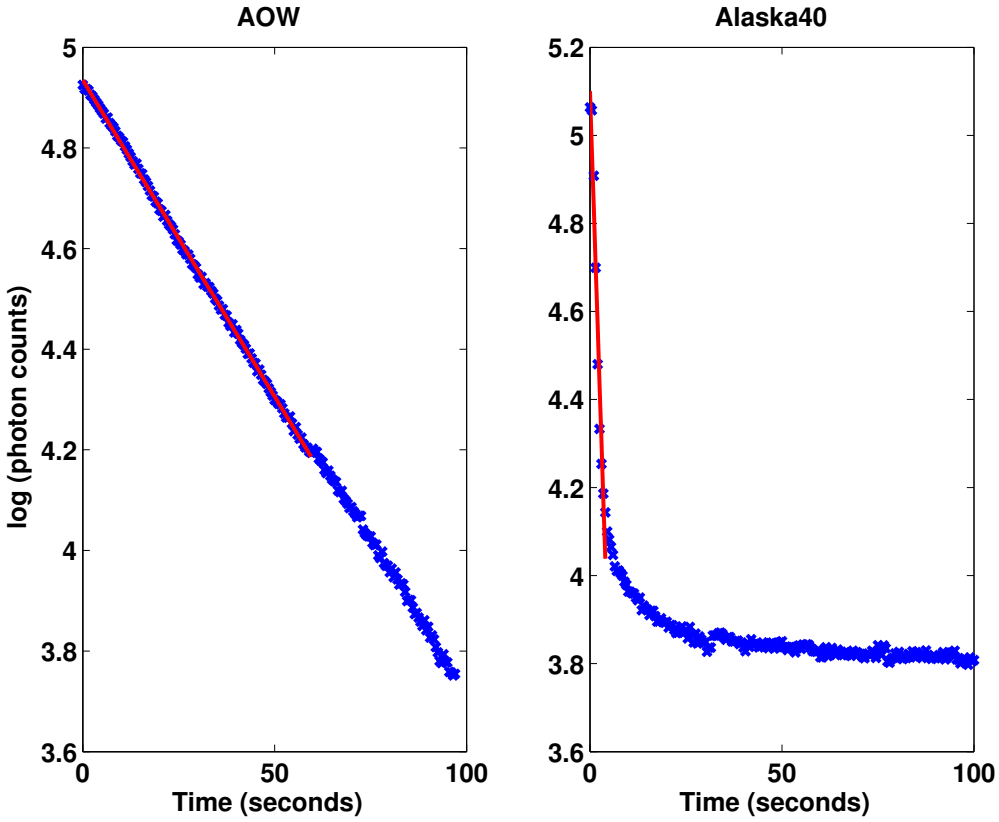

Figure 4.1: Examples from superoxide decay experiments: AOW on the left, and Alaska40 on the right. Log-transformed data are shown in blue, and linear fits to the initial decay data are shown in red.

4.3.7 Ancillary experiment: Superoxide steady-state concentrations from SOTS-1 decay

In order to test the steady-state O_2^- concentrations resulting from SOTS-1 decay, an experiment was performed where SOTS-1 was added at two concentrations (2.5 and 25 μM) to 0.2 μm filtered seawater collected previously under trace-metal clean conditions in the subarctic northeast Pacific Ocean. Over a 5-hour period, O_2^- was repeatedly measured in the two SOTS-1 solutions with MCLA (4 μM), using the same set-up as described above. The measurements were calibrated with O_2^- additions from a decaying O_2^- cocktail that had been prepared by adding ~10 mg KO_2 to 1 mM NaOH containing 7.5 μM DTPA (diethylene triamine pentaacetic acid, Sigma). The O_2^- decay was followed by measuring absorbance at 240 nm (where O_2^- has an absorbance peak), and O_2^- concentration at any given time was estimated based on

the following equation:

$$A_t = b(\varepsilon_{H_2O_2}[\mathrm{H_2O_2}]_t + \varepsilon_{O_2^-}[\mathrm{O_2^-}]_t) \tag{4.3}$$

where A_t is the absorbance measured at 240 nm at time t in seconds; b is the path-length in cm, $[\mathrm{H_2O_2}]_t$ and $[\mathrm{O_2^-}]_t$ are the concentrations of $\mathrm{H_2O_2}$ and $\mathrm{O_2^-}$ at time t; and $\varepsilon_{H_2O_2}$ and $\varepsilon_{O_2^-}$ are the respective effective extinction coefficients at 240 nm ($\varepsilon_{H_2O_2}$ = 45 $\mathrm{mol^{-1}\ cm^{-1}}$ at pH 10, calculated after Morgan et al. (1988); $\varepsilon_{O_2^-}$ = 2345 $\mathrm{mol^{-1}\ cm^{-1}}$, Bielski et al. (1985)). $\mathrm{H_2O_2}$ is a product that is formed with a 1 to 0.5 molar stoichiometry when $\mathrm{O_2^-}$ decays via uncatalyzed dismutation (Zafiriou, 1990):

$$2\mathrm{O_2^-} + 2\mathrm{H^+} \rightarrow \mathrm{H_2O_2} + \mathrm{O_2} \tag{4.4}$$

The addition of DTPA to the cocktail served to bind any trace elements that might have been present (Heller and Croot, 2010c), so that $\mathrm{O_2^-}$ decay proceeded in solution predominantly via disproportionation. It was thus possible to estimate $[O_2^-]_t$ at any given time with a least-squares fit to the decay data using the following relationships:

$$[\mathrm{O_2^-}]_t = \frac{1}{\frac{1}{[\mathrm{O_2^-}]_0} + k_D t} \tag{4.5}$$

and

$$[\mathrm{H_2O_2}]_t = [\mathrm{H_2O_2}]_0 + 0.5([\mathrm{O_2^-}]_0 - [\mathrm{O_2^-}]_t) \tag{4.6}$$

where k_D is the decay constant for $\mathrm{O_2^-}$ dismutation and $[\mathrm{O_2^-}]_0$ and $[\mathrm{H_2O_2}]_0$ are the initial concentrations of $\mathrm{O_2^-}$ and $\mathrm{H_2O_2}$ respectively.

An intermediate $\mathrm{O_2^-}$ standard was prepared by making an addition from the decaying $\mathrm{O_2^-}$ cocktail to 0.2 M NaOH containing 7.5 μM DTPA, following the approach of Hansard et al. (2010). At the high pH (>12) and given the relatively low $\mathrm{O_2^-}$ concentration in the intermediate standard ($\sim$1 μM), this standard is stable for >30 minutes. A calibration curve was generated by making additions from the intermediate standard to seawater, following the protocol of Rusak et al. (2011). The calibration was linear as has been observed previously (e.g., Diaz et al., 2013; Hansard et al., 2010; Heller and Croot, 2010c; Rusak et al., 2011) and was forced through the origin, yielding $r^2 = 0.97$ for $\mathrm{O_2^-}$ concentrations up to 6 nM.

4.4 Results and Discussion

The dust dissolution experiment brought some unexpected results, especially with respect to the observed superoxide concentrations and treatment blanks. The data and their implications are therefore presented in the order needed to understand and interpret the main results.

4.4.1 Superoxide decay constants from ancillary experiments

The estimated decay constants, k_{obs}, for the three different dust solutions were not significantly different from one another (1-way ANOVA, p >0.05, see Table 4.2). Likewise, the ASW and (decayed) SOTS-1 solutions showed very similar k_{obs}, with the differences not statistically significant (Table 4.2). The decay constants were therefore combined into two groups: +dust and −dust, where the k_{obs} is the mean for the respective group (Table 4.2).

Sample	k_{obs} (s^{-1})	**Number of obs.**	**Group** k_{obs} (s^{-1})	**Statistics (1-way ANOVA)**
ASW	0.012 ± 0.001	4	0.012 ± 0.002	F = 2.86 p = 0.09
ASW + 2 μM SOTS-1	0.012 ± 0.003	6		
ASW + 6 μM SOTS-1	0.010 ± 0.001	6		
ASW + Alaska40	0.257 ± 0.023	3	0.254 ± 0.018	F = 0.04 p = 0.96
ASW + China400	0.252 ± 0.020	3		
ASW + Arizona140	0.254 ± 0.020	3		

Table 4.2: Results of O_2^- decay experiments. Decay constants are reported with one standard deviation and are grouped together based on the results of statistical analysis (1-way ANOVA), indicating that the means are not statistically different from each other within groups.

A comparison of the mean decay constants in the two groups shows that the addition of dust increases k_{obs} by more than a factor 20 relative to the −dust treatments. However, the similarity of decay constants for the different dust solutions is peculiar and suggests that the observed k_{obs} is likely at the very margin of what the experimental set-up, i.e. with the given flow rates and travel time in the system, can measure.

This notion is corroborated by the fact that the amount of O_2^- added to these solutions had to be considerably increased in order to measure a signal at all (see Section 4.3.6). The observed k_{obs} in the +dust treatments are therefore considered a lower limit, and the increase in k_{obs} by a factor 20 in the +dust treatments relative to the −dust group is thus a very conservative estimate.

4.4.2 Superoxide steady-state concentrations from SOTS-1 decay

As is evident in Figure 4.2, the superoxide steady-state concentrations observed in the respective SOTS-1 treatments do not scale with the same 10:1 ratio as the SOTS-1 concentrations. Rather, they scale with a roughly 3.3:1 ratio over the duration of the experiment. In order to test whether the second-order disproportionation of O_2^- could be responsible for the observed discrepancy, the expected steady-state O_2^- concentrations were modelled including both first- and second-order decay for O_2^-. The numerical model was set up based on the following equation:

$$\frac{d[O_2^-]}{dt} = \mathrm{PR} - 2k_D[O_2^-]^2 - k_{obs}[O_2^-] \tag{4.7}$$

where PR is the production rate of O_2^- from SOTS-1 (Heller and Croot, 2010c):

$$\mathrm{PR} = 0.4k[\mathrm{SOTS}]_0 e^{-kt} \tag{4.8}$$

with the SOTS-1 decay constant at 25°C, $k = 2 \times 10^{-5}$ s^{-1}, from Heller and Croot (2010c). The constant for O_2^- disproportionation, k_D, was set at 5×10^4 M^{-1} s^{-1}, calculated for pH = 8 after Zafiriou (1990), and k_{obs} was set at 0.02 s^{-1}, an experimental value from decay experiments with seawater. The results displayed in Figure 4.3A clearly show that the second-order disproportionation of O_2^- is unlikely to explain the discrepancy between SOTS-1 concentration ratios and the observed steady-state O_2^- ratio under the experimental conditions.

The model was expanded further to include a catalytic superoxide decay term that scales linearly with the SOTS-1 concentration. The catalytic reaction between inorganic copper (Cu) and O_2^- serves as an example (Zafiriou et al., 1998), where the Cu concentration (as a linear function of SOTS-1) can be tuned to yield a ratio between steady-state O_2^- at the respective SOTS-1 concentrations that is closer to

observations, i.e. 3.3:1. The results are shown in Figure 4.3B and C, indicating that a contamination in SOTS-1 that can catalyze O_2^- decay could be responsible for the observed discrepancy between steady-state O_2^- and the respective SOTS-1 concentrations. The nature of the contamination is unknown, but an inorganic Cu concentration on the order 0.6–6 nM (for SOTS-1 concentrations of 2.5 and 25 μM respectively) would be sufficient to yield the observed results (assuming $k_{cat} = 10^9$ M^{-1} s^{-1}; Zafiriou et al. (1998)). It can thus be concluded, based on the observed steady-state O_2^- concentrations, that the SOTS-1 likely contains a contamination that not only lowers O_2^- concentrations in the experiment, but also lowers the O_2^- ratio between different SOTS-1 treatments.

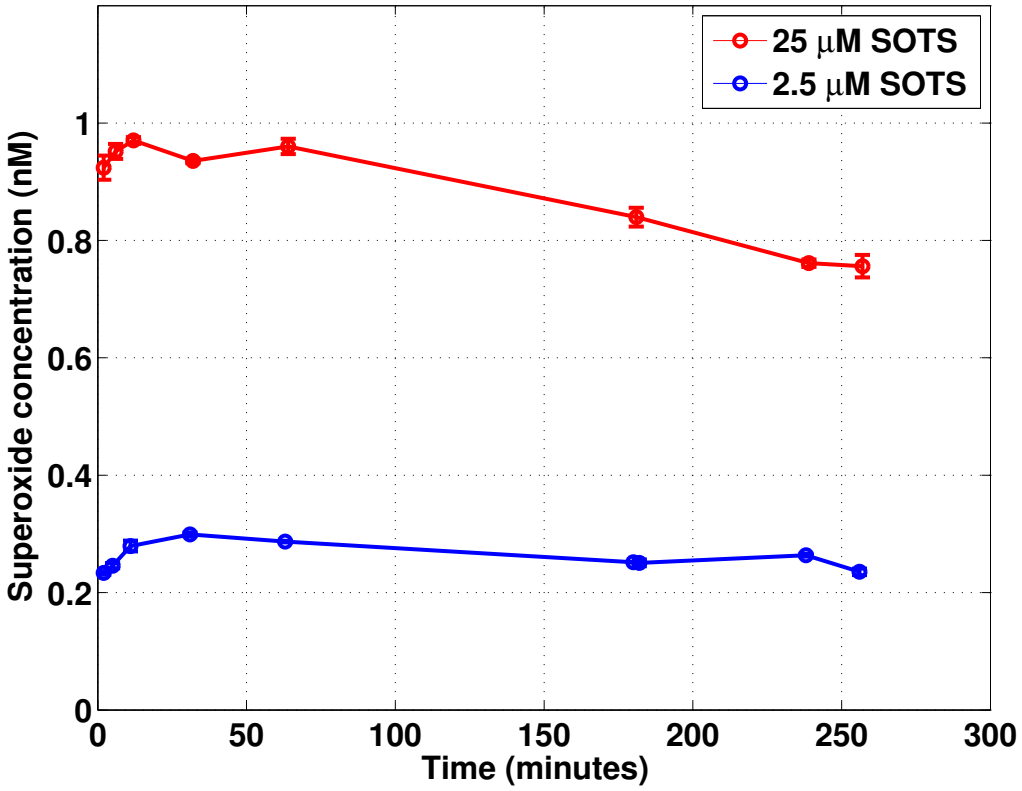

Figure 4.2: Superoxide steady-state concentrations (nM) in seawater over >4 hours for initial SOTS-1 concentrations of 25 (red) and 2.5 μM (blue). Error bars correspond to one standard deviation from triplicate measurements.

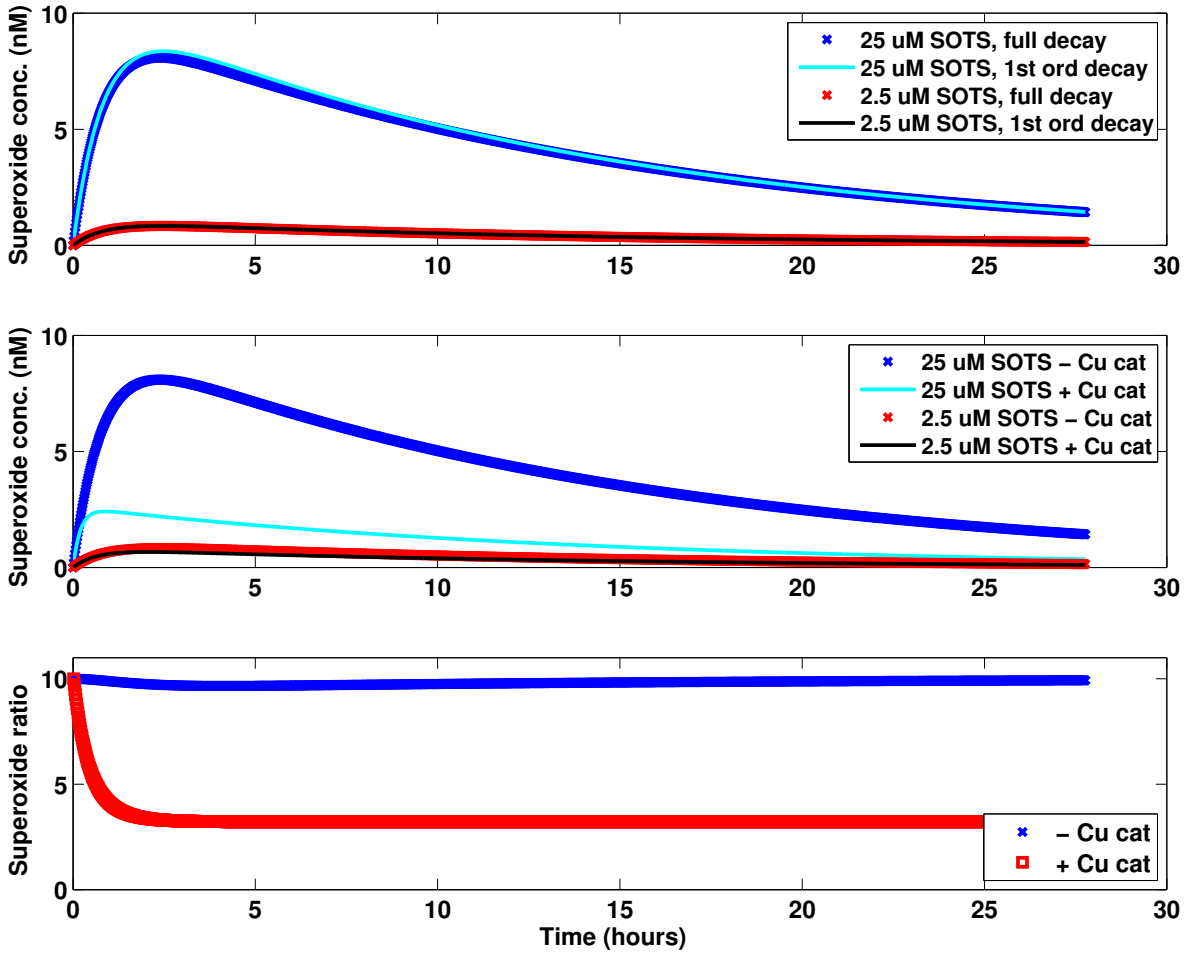

Figure 4.3: Results from the numerical model for O_2^- steady-state concentrations in seawater; see text for details of the model and its motivation. Panel A compares the predicted O_2^- for 25 and 2.5 μM SOTS-1 concentrations in two scenarios: 1) Only 1st-order decay of O_2^- is taken into account (cyan and black lines; for 25 and 2.5 μM SOTS-1, respectively); 2) Both 1st-order decay and the disproportionation of O_2^- are being considered (blue and red crosses). Panel B compares the model results for scenarios with (+Cu cat) and without (-Cu cat) catalytical O_2^- decay as a linear function of SOTS-1 concentration (see text for details). The red and blue lines are the same as in Panel A, with corresponding O_2^- concentrations for the "+Cu cat" scenarios in cyan (25 μM SOTS-1) and black (2.5 μM SOTS-1). Panel C shows the ratios between O_2^- concentrations for the two SOTS-1 concentrations, i.e. 25 μM SOTS-1 / 2.5 μM SOTS-1. The blue line indicates the ratio for the scenario without catalytic O_2^- decay (i.e. the ratio between the blue and red lines in panels A and B), and the red line corresponds to the scenario with catalytic O_2^- decay (the cyan and black lines in panel B).

4.4.3 Treatment blanks in dust dissolution experiments

The Fe(II) concentrations after >24 hours for the treatment blanks from the O_2^- experiment are shown in Figure 4.4. Each treatment blank was measured twice (each time in triplicate), and there was excellent agreement between replicates indicating that the blank was reproducible. Treatment blanks for the three SOTS-1 concentrations are, in some cases, higher than the Fe(II) that was measured for the respective treatments containing dust as well as SOTS-1. Contamination of the SOTS-1 reagent itself is the most likely source of the blank, although contamination levels did not scale directly with SOTS-1 concentrations: While SOTS-1 was added in the ratio 12:4:1, the Fe(II) blank for the respective treatments has the approximate ratio 3:1.5:1 (16.2:7.9:5.4 nM). I posit that the relative ratio of the Fe(II) blanks between SOTS-1 treatments is related to the steady-state O_2^- concentrations in the respective treatments, rather than the SOTS-1 concentration in solution. Note that the deviation from the O_2^- stoichiometry measured in the O_2^- steady-state experiment in seawater, i.e. 3.3:1 for a SOTS-1 ratio of 10:1 (see section 4.4.2 above), may be due to different SOTS-1 batches having different levels of contamination. The same SOTS-1 batch was used for all the dust dissolution experiments, but a different batch was used for the measurements of steady-state O_2^- concentrations in section 4.4.2.

The bulk of the Fe(II) measured in the SOTS-1 blanks stems most likely from the SOTS-1 itself rather than from the ASW because the blanks for ASW without SOTS-1 are considerably lower than those for the SOTS-1 blanks, even with light exposure (Figure 4.4). It is possible that the Fe is either in the particulate phase or coordinated with SOTS-1 functional groups, as the SOTS-1 molecule contains a deprotonated carboxylate group at the pH of the experiments that is present both prior to and after SOTS-1 decay (Heller and Croot, 2010a; Ingold et al., 1997). Carboxylate functional groups play an important role in the formation of ferric complexes (e.g., Butler and Theisen, 2010; Vraspir and Butler, 2009). In addition, SOTS-1 molar concentrations are between 90 and 370 times greater than the respective Fe(II) concentrations measured in the blank; such high molar ratios between SOTS-1 and Fe further favour Fe complexation. I am unaware of any published stability constants that describe the complexation of Fe(III) by SOTS-1.

A particulate Fe contamination or complexation of the Fe contamination is consistent with the observation that the decay constants for ASW with and without SOTS-1 are statistically indistinguishable (Table 4.2), implying that the Fe associ-

ated with SOTS-1 does not significantly enhance O_2^- decay. Organic complexation of Fe has been found to considerably slow the reduction of Fe by O_2^- (Rose and Waite, 2005), and particulate Fe, especially when aged, is likewise not very reactive with O_2^- (Fujii et al., 2006). It is also possible that the Fe contamination precipitated from the solution after SOTS-1 had decayed, as nanomolar concentrations of Fe are well above the solubility limit for Fe(III) in ASW; precipitation might render the Fe inert to O_2^-, thus explaining the slow O_2^- decay rates (Fujii et al., 2006).

There is one more indicator suggesting that the Fe contamination is not present as dissolved inorganic Fe(III): The Fe(II) measured for each SOTS-1 blank appears to be a function of the steady-state O_2^- concentration rather than the SOTS-1 concentration. If only inorganic Fe(III) were present, one would expect the Fe(II) concentrations in the respective blanks to scale directly with the contamination, and therefore with the SOTS-1 concentration, because the presence of the ferrozine complex can promote the spontaneous production of Fe(II) by biasing the redox equilibrium between the Fe redox species. This "spontaneous" pathway of Fe reduction is inhibited when Fe(III) is complexed by a strong organic ligand, or when the Fe is present in the particulate phase. However, Fe(II) production from particulate or organically complexed Fe(III) can be promoted by a reductant such as O_2^-, yielding Fe(II) concentrations that scale with the reductant rather than Fe(III) concentrations, as was observed in the experiment. It is therefore highly likely that the Fe contamination present in SOTS-1 is either organically complexed or in the particulate phase or a mixture of both, and the Fe(II) measured in the blanks results from this Fe contamination being reduced by O_2^-.

These details regarding the Fe contamination have important implications for the blank subtraction. The observation that the Fe(II) concentrations in the SOTS-1 treatment blanks scale with the steady-state O_2^- concentrations indicates that the blank that should be subtracted from the respective +dust treatments containing SOTS-1 ought to be corrected for the expected O_2^- concentrations. The measured O_2^- decay constants (k_{obs}, see section 4.4.1 above) for +dust treatments are more than 20 times higher than for −dust treatments, implying that the steady-state O_2^- concentrations in the +dust treatments are at least 20 times lower than in the −dust treatments, i.e. the SOTS-1 blanks. The measured Fe(II) concentrations in the respective SOTS-1 blanks were therefore divided by 20 to calculate a conservative blank that was ultimately subtracted from the experimental +dust data. See Figure 4.5 for a compilation of the "adjusted" blanks that were subtracted from the experimental

data for the respective treatments.

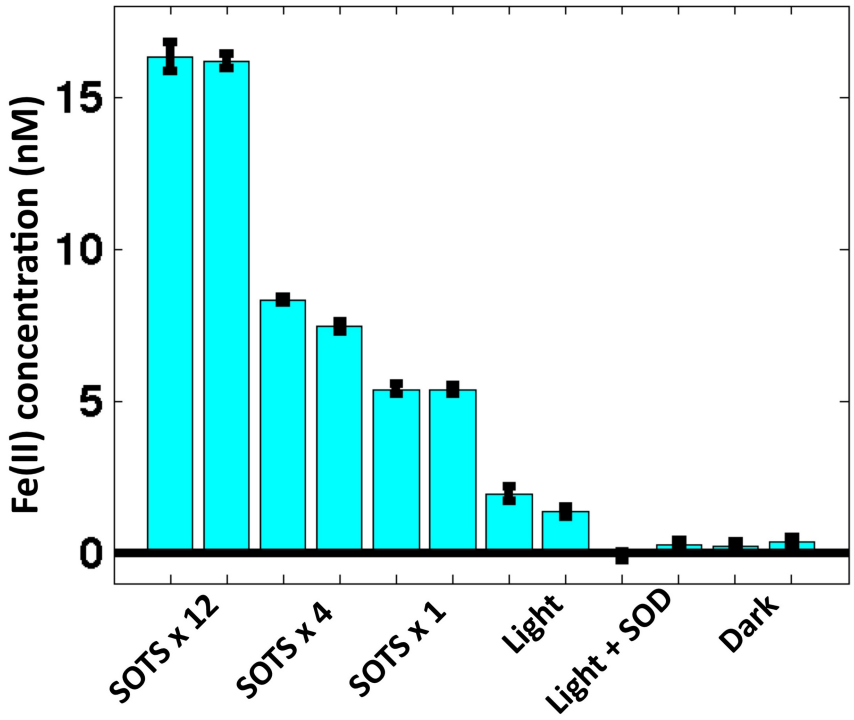

Figure 4.4: Fe(II) concentrations (nM) after >24 h, i.e. at the end of dust dissolution experiments, for the treatment blanks from the O_2^- experiment. The blank for each treatment was measured twice (hence 2 bars) and was measured in triplicate each time. Error bars correspond to the standard deviation from the triplicate measurements.

4.4.4 Validity of measured Fe(II) concentrations in dust dissolution experiments

The Fe(II) concentrations at the end of the dust dissolution experiments after blank correction are shown in Figure 4.6, and the ratios of Fe(II) concentrations in the three SOTS-1 treatments are listed in Table 4.3. Assuming a O_2^- ratio in the respective SOTS-1 treatments of approximately 3:1.5:1 as indicated by their respective blanks (see section 4.4.3 above), it is evident that the Fe(II) concentrations from most dust treatments approximately follow that ratio, indicating that Fe(II) relates to the concentration of O_2^-. The only exception is the China400 experiment, where Fe(II) ratios exceed those of the expected steady-state O_2^-, but in the majority of experiments,

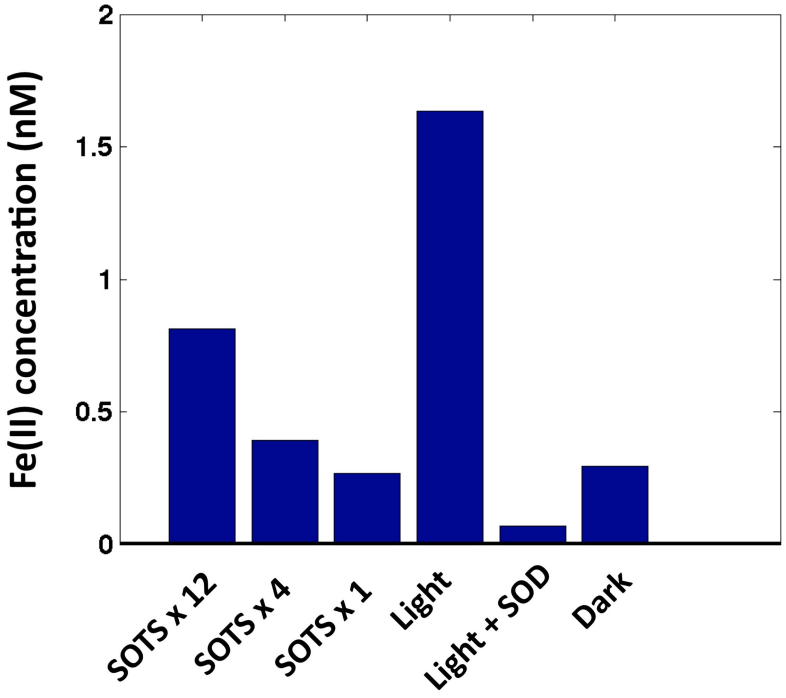

Figure 4.5: "Adjusted" Fe(II) concentrations (nM) for the treatment blanks from the O_2^- experiment as subtracted from the experimental endpoints. All treatment blanks comprise the mean of the 2 blanks shown in Figure 4.4; in addition, the SOTS-1 blanks were divided by 20 to account for the lower O_2^- concentrations in the +dust treatments compared to the −dust treatments, i.e. the blanks. See text for details.

Fe(II) is found in a ratio that reflects O_2^- concentrations.

Since it is assumed that Fe(II) concentrations in the SOTS-1 blanks are also a function of O_2^-, it follows naturally that the Fe(II) ratio in the +dust treatments very closely resembles the Fe(II) ratio in the SOTS-1 blanks. In addition to the reasoning outlined above for the blank subtraction, there are two more arguments indicating that the reported Fe(II) concentrations in the experiment do indeed stem from the dust substrate and not from SOTS-1.

Firstly, the Fe(II) concentrations measured in the light treatments are of a similar order as those in the high and medium SOTS-1 treatments, implying that there is a significant proportion of "labile" Fe in the dust that is accessible to a reductive mechanism involving photochemical reactions. Regardless of whether or not O_2^- is an intermediate in these reactions, it is reasonable to assume that this "labile" Fe would also be susceptible to reduction by O_2^-. The blank for the light treatments is

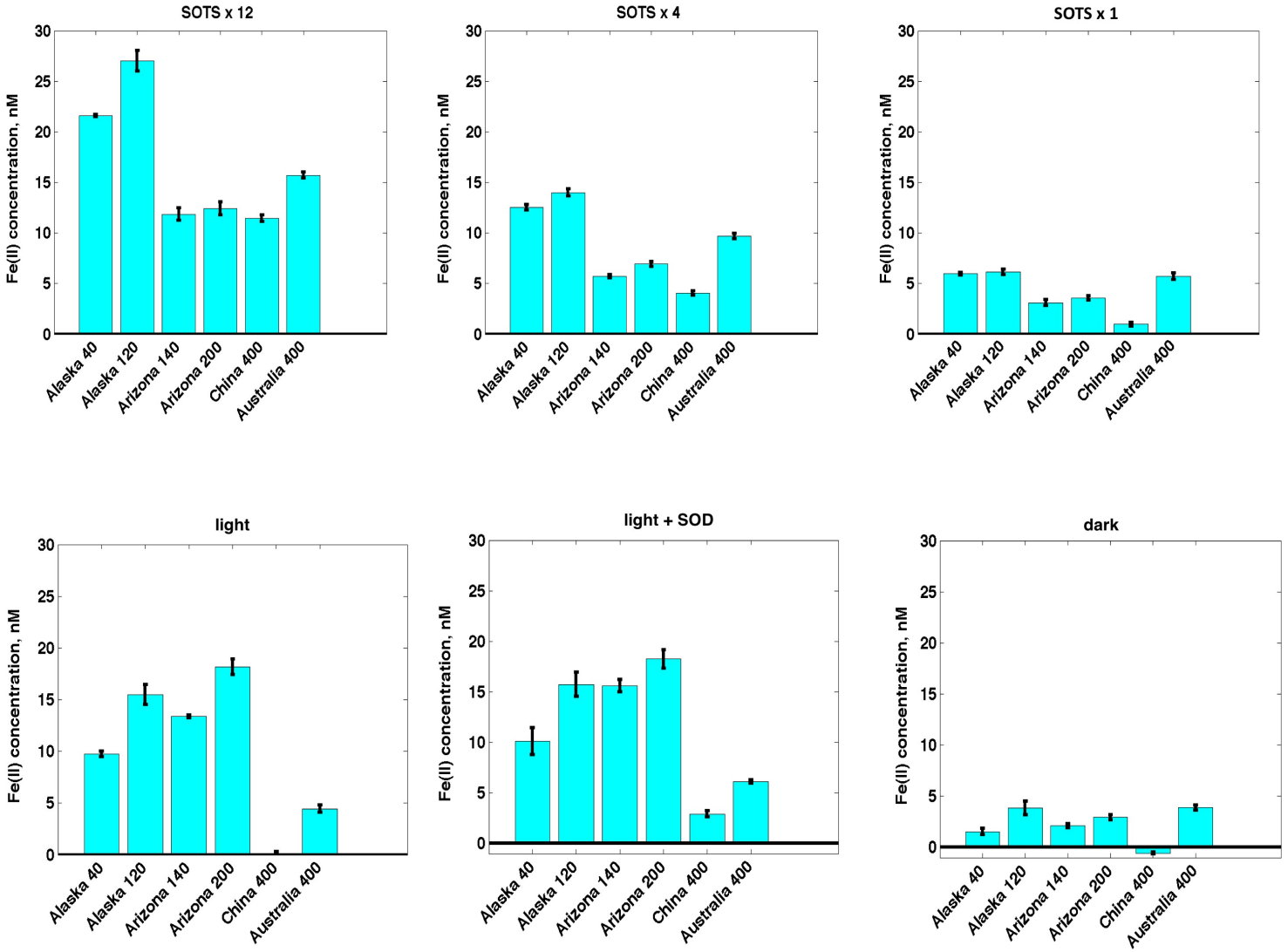

Figure 4.6: Comparison of Fe(II) concentrations after >24 h, i.e. at the end of dust dissolution experiments, for the respective treatments and dusts, after subtraction of treatment blanks (see Figure 4.5). Top panels show results for the 3 SOTS-1 concentrations, from high to low (6, 2 and 0.5 μM, respectively), and bottom panels display the results for light, light+SOD, and dark treatments, respectively.

Dust	**SOTS-1 × 12**	**SOTS-1 × 4**	**SOTS-1 × 1**
Alaska40	3.6	2.1	1
Alaska120	4.4	2.3	1
Arizona140	3.8	1.9	1
Arizona200	3.5	1.9	1
China400	11.8	4.2	1
Australia400	2.7	1.7	1

Table 4.3: Ratios of Fe(II) concentrations at the end of dust dissolution experiments and after blank subtraction for the respective dusts and concentrations, all normalized to the Fe(II) concentration of the lowest SOTS-1 treatment.

unambiguous and has been subtracted from the endpoints displayed in Figure 4.6, so there is no reason to doubt that the measured Fe(II) in these treatments does indeed stem from the respective dusts.

Secondly, Fe(II) evolution over the >24 h of the experiments (see Figures 4.7 and 4.8 for examples) shows differences between dusts that would not be expected if the measured Fe(II) were simply a function of the SOTS-1 contamination. Considering the combined weight of the arguments presented here, I am therefore confident that the Fe(II) concentrations shown in Figure 4.6 come from the dusts rather than from artifacts associated with experimental blanks.

4.4.5 Dust dissolution experiment: Influence of superoxide

The Fe(II) concentrations at the respective endpoints of the experiment (Figure 4.6) indicate that O_2^- is able to mobilize Fe(II) from a variety of dust sources. There is a clear dose effect of O_2^-, with higher O_2^- concentrations always yielding higher Fe(II). For all dusts and dust concentrations tested, the three SOTS-1 levels always resulted in Fe(II) concentrations that were significantly different from one another (1-way ANOVA for each dust and dust concentration at the α =0.05 level). In addition, the ratios between the respective Fe(II) concentrations for the different SOTS-1 treatments approximately follow the expected O_2^- ratios (Table 4.3) for all but one dust (China400), indicating that the Fe source, the dust, was not limiting. Even for the China400 experiment, there clearly is a dose-response for the different

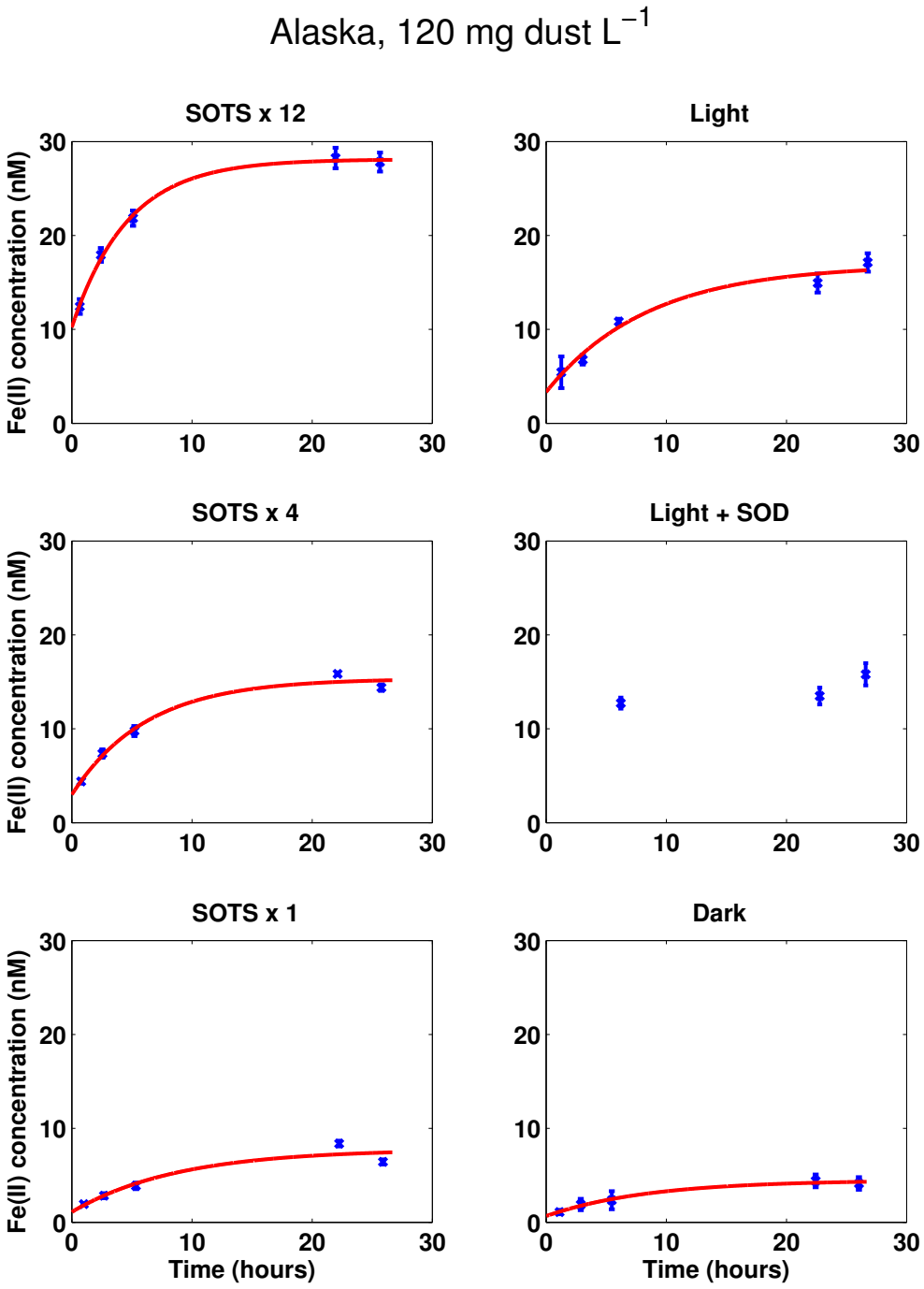

Figure 4.7: Example of time course data (not blank-corrected) for the experiment with glacial dust from Alaska at a concentration of 120 mg L^{-1}. Blue crosses represent individual data points from triplicate measurements, with error bars corresponding to one standard deviation; red lines indicate best least-squares fits of a 3-parameter model of the form $\mathrm{Fe}(t) = \mathrm{Fe}_0 + \mathrm{Fe}_{\max}\ (1 - e^{-kt})$, where Fe_0 is the initial Fe(II) at time $t = 0$, $\mathrm{Fe}_{\max}$ is the maximum Fe(II) attained, and k is the thermal decay constant for SOTS-1 at the temperature of the experiment (Heller and Croot, 2011).

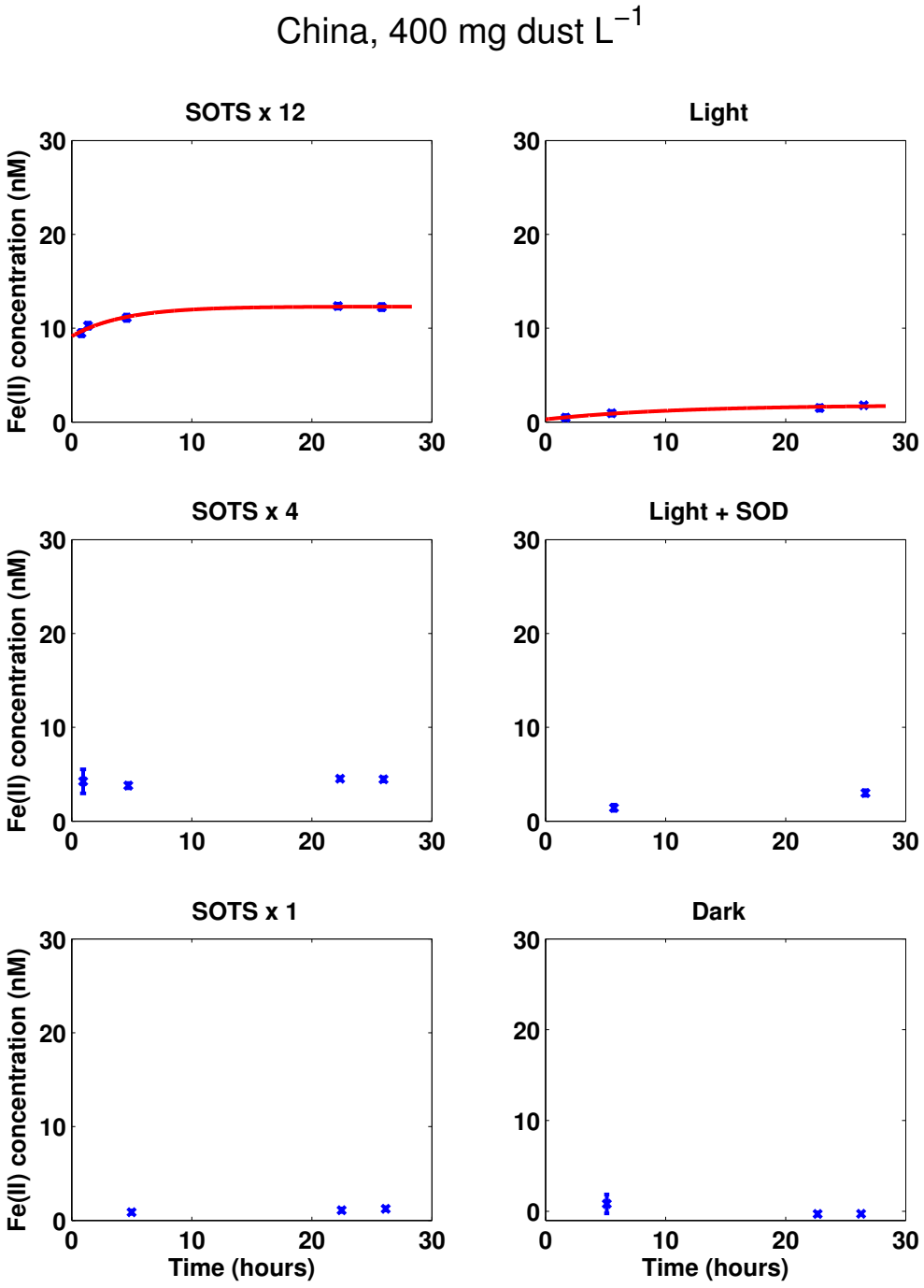

Figure 4.8: As in Figure 4.7, but with dust from China at a concentration of 400 mg L^{-1}.

SOTS-1 treatments, but it is exaggerated relative to the expected O_2^- concentrations, i.e. the Fe(II) ratios are higher than the O_2^- ratios (Table 4.3). It can thus be concluded that O_2^- is able to mobilize Fe(II) from all the dusts tested.

4.4.6 Dust dissolution experiment: Influence of light

All dusts except China400 and Australia400 exhibited statistically significant differences between the light and dark treatments at the α =0.05 level (Figure 4.6), indicating that photochemical reactions can play an important role in the redox cycling of Fe contained in mineral particles, as has been observed previously (Chen and Siefert, 2003; Fu et al., 2010). As the dark treatments show, very little Fe(II) is transferred from dust to the ocean in the absence of a reducing mechanism over the course of 24 hours. In fact, it is possible that the ferrozine reagent is responsible for the observed Fe(II) yield in the dark treatments, as the presence of this strong ligand can promote the reduction of Fe(III).

The light+SOD treatment always showed higher Fe(II) than the corresponding light treatment, though the difference is small and is statistically significant (at the α =0.05 level) only 50% of the time. While it is counter-intuitive that the suppression of O_2^-, as is expected with the addition of SOD, should enhance the reduction of Fe from dust sources, there are several potential explanations for this result. Firstly, it is possible that the SOD molecule suffered UV damage in the light and was therefore less effective. Secondly, the SOD molecule may behave as an electron donor and allow for reduction of Fe(III) in the light. Finally, O_2^- can also oxidize Fe(II). It is thus possible that the presence of O_2^- may have lowered the Fe(II) yield in the light treatments relative to SOD+light.

It is intriguing that there is not always a statistical difference between the light and light+SOD treatment, as this finding may imply that O_2^- is not — at least not in all instances and settings — an important intermediate in the light-induced mobilization of Fe(II) from dust. This raises the question about an alternative electron donor, with dissolved organic matter the most likely candidate. The ferrozine molecule, for instance, contains several aromatic rings and is therefore a possible electron donor. In addition, the ASW may have contained organics that had leaked from the Chelex-100 column during removal of trace metals. In the surface ocean, photochemical reactions involving strong organic ligands have been shown to reduce complexed Fe(III) (Barbeau et al., 2001), and chromophoric dissolved organic matter (CDOM) is not

only ubiquitous, but is noteworthy because of the numerous photochemical reactions it can undergo (Sharpless and Blough, 2014). If indeed organic molecules played a role in the reduction of dust-derived Fe in the experiment, it is therefore feasible that similar reactions could take place in the ocean.

The results for dust China400 further support the notion that the photochemical reactions leading to the release of Fe(II) do not necessarily rely on O_2^- as an intermediate. This dust showed a strong response to O_2^- as is evident in the SOTS-1 treatments (Figure 4.6), but no measurable Fe(II) was released in the light or dark treatments. However, Fe(II) was released in the light+SOD treatments, suggesting that the mechanism releasing Fe(II) in the presence of SOD is significantly different from the one with light exposure alone.

4.4.7 Comparison with other dust dissolution studies

An array of leaching methodologies has been applied to address the question of Fe aerosol solubility (e.g., Aguilar-Islas et al., 2010; Buck et al., 2006; Schroth et al., 2009), but very few studies have investigated the potential of O_2^- as a solubilizing agent. Studying aerosol dissolution in surface waters of the tropical Atlantic, Heller and Croot (2011) came to the conclusion that reactions with O_2^- did not play a significant role. Even though they observed a similar Fe(II) release in dust dissolution experiments with SOTS-1 as was seen in this study, the authors contend that O_2^- reactions with Cu organic complexes and dissolved organic matter are the main sink for O_2^- in the ocean, and that the encounter rate between O_2^- and aerosol particles would be low. However, this argument may not be applicable to aggregates and particle-associated biofilms that may be populated by O_2^--producing bacteria, as discussed below.

It is difficult to compare the results of this study to those of other dust dissolution experiments because I have limited information on the dust mineralogy, Fe composition and speciation (see Table 4.1), and I did not work with homogenous materials in terms of particle size and surface area. For the same reason it is challenging — and not the purpose of this study — to make direct comparisons between the different dusts investigated. However, a few points can be made.

Previous work has shown that Fe speciation and mineralogy in aerosols determine Fe solubility (e.g., Journet et al., 2008; Schroth et al., 2009) and that atmospheric processing, including the presence of non-lithogenic "combustion" aerosols, further

impact Fe solubility (Chen et al., 2012; Fu et al., 2014; Paris et al., 2010; Shi et al., 2011; Sholkovitz et al., 2012). Minerals that predominantly contain reduced Fe tend to show higher Fe solubility than those containing Fe in the oxidized state (Schroth et al., 2009); this general trend is also observed in this data set, where the glacial flour from Alaska, which is expected to contain the highest proportion of reduced Fe, shows the highest Fe(II) yields in the SOTS-1 treatments, even though the dust concentrations are lower than for any other dust (Figure 4.6). However, this trend relative to other dusts is less pronounced in the light and dark treatments. As discussed above, the absolute O_2^- concentrations in the respective SOTS-1 treatments were probably not uniform among dusts due to different dust compositions and concentrations, yielding differing O_2^- decay rates. The high Fe(II) yield in the SOTS-1 experiments with Alaska glacial flour can therefore not unequivocally be attributed to dust mineralogy but may also be a result of higher O_2^- concentrations relative to the other dusts.

4.5 Implications

The ability of O_2^- to induce the reduction and dissolution of Fe from particulate sources such as mineral aerosols has important implications for the Fe cycle in the ocean. Given the recent discovery of widespread O_2^- production by heterotrophic bacteria that are found throughout the ocean interior (Diaz et al., 2013), it opens the possibility of significant redox cycling of aerosol-associated Fe at all depths in the ocean. Such redox cycling may enhance Fe dissolution from aerosols relative to previous estimates, and it could also impact the bio-availability of the dissolved Fe, as Fe(II) is assumed to be the more biologically accessible form (e.g., Shaked et al., 2005). The presented data show that Fe(II) production strongly depends on the steady-state O_2^- concentration, which prompts the question how the O_2^- levels in the experiments compare to environmental concentrations.

The O_2^- steady-state concentrations in the dust dissolution experiment are estimated to be on the order of tens of picomoles L^{-1} based on the following observations: The O_2^- steady-state concentrations with 2.5 μM SOTS-1 are $\sim$300 pM in seawater (Figure 4.2). Superoxide decay in the solutions containing dust is about 20 times faster than in the absence of dust (see above), so it is a reasonable assumption that O_2^- steady-state concentrations in the 2 μM SOTS-1 treatment are 15 pM or less. Assuming a O_2^- ratio of 1:1.5:3 in the respective SOTS-1 treatments of 0.5, 2 and 6 μM (see above) thus yields maximum O_2^- concentrations of 10, 15 and 30 pM.

These concentrations are on the lower end of those observed in the ocean. For instance, Rose et al. (2008) measured O_2^- steady-state concentrations in the equatorial Pacific that ranged from below the detection limit to 167 pM. Interestingly, they found evidence of a "particle-associated and nonphotochemically generated source of superoxide" (Rose et al., 2008), including localized O_2^- maxima at depth. These observations are consistent with a biological source of O_2^- that does not depend on photochemistry, as was observed by Diaz et al. (2013) in a study on heterotrophic bacteria. In the Gulf of Alaska, Hansard et al. (2010) measured O_2^- concentrations up to 600 pM, and Rusak et al. (2011) found O_2^- concentrations east of New Zealand that reached tens of nanomoles at the depth of the chlorophyll maximum.

The study by Diaz et al. (2013) not only showed that O_2^- production is ubiquitous among heterotrophic bacteria, but also provided O_2^- production rates per cell, with a median of 1.2 amol O_2^- cell^{-1} h^{-1}. Extrapolating to average cell densities in the ocean of 10^5–10^6 cells mL^{-1} (Diaz et al., 2013) and assuming a typical pseudo-first order O_2^- decay rate of 2×10^{-3} s^{-1} (Rose et al., 2008) predicts steady-state O_2^- concentrations of ∼50 pM. The O_2^- concentrations employed in the experiments are thus in the realistic range, and at the lower end, of observed and predicted environmental concentrations. However, it is worth mentioning that the presence of dust particles would decrease steady-state O_2^- concentrations by increasing O_2^- decay rates, and it can't be assumed that the additional decay is solely due to Fe(II) production, as other dust constituents may also react with O_2^-. This being said, the conditions in aggregates and biofilms, where bacteria cells are packed much more densely than in the open ocean, may promote substantially higher local O_2^- concentrations. Indeed, Ohnemus and Lam (2015) recently demonstrated that lithogenic particles in the mixed layer are rapidly packaged into aggregates. The results of this study, indicating that O_2^- has the ability to induce the reduction and dissolution of Fe from particulate mineral sources, are therefore expected to be most relevant for such aggregates.

Further studies will have to determine whether ageing and processing of particles, for example in the sunlit surface layers of the ocean, alters their Fe solubility. Fujii et al. (2006) found that the O_2^--mediated production of Fe(II) from amorphous ferric oxyhydroxide (AFO) decreased with ageing of the AFO. A similar effect might be expected for atmospheric aerosols, especially if a labile Fe pool is exhausted.

4.6 Conclusions

The presented experiment aimed to investigate whether O_2^- was able to promote Fe dissolution and reduction of dust particles from a variety of sources and of different mineralogy. The results indicate that O_2^- at and even below concentrations that are expected to occur in the marine environment is able to enhance Fe dissolution from all dusts tested. The resulting Fe(II) concentrations are comparable to — and at times exceed — the Fe(II) yield from photochemical reactions on a time scale of 24 hours, indicating that the contribution of O_2^- to Fe dissolution from aerosols in the marine environment may be of similar magnitude as that of photochemical reactions. In particular, the discovery of widespread O_2^- production by ubiquitous heterotrophic bacteria (Diaz et al., 2013) opens the possibility that significant Fe dissolution from aerosols is not restricted to the well-lit surface layer of the ocean, but may occur at all depths. However, future work is necessary to evaluate how the ageing of particles in the atmosphere and surface layer of the ocean affects O_2^--mediated Fe solubility.

Chapter 5

Lack of a detectable phytoplankton response to an aerosol deposition event in the HNLC subarctic Pacific Ocean

To be submitted to *Geophysical Research Letters*.

5.1 Abstract

Deposition of atmospheric aerosols to the surface ocean is considered an important supply mechanism of biologically available iron (Fe) to remote ocean regions. Much research has focused on the spatial and temporal variability in aerosol deposition, and on the Fe solubility of different types of aerosols. However, information on the response of open-ocean phytoplankton to aerosol deposition remains sparse. Evaluating multiple lines of evidence from the high nutrient, low chlorophyll (HNLC) subarctic Pacific Ocean, I present evidence that the deposition of aerosols from Siberian forest fires in May 2012 did not result in elevated surface dissolved iron (dFe) concentrations, and did not elicit a detectable response in the phytoplankton community. Dissolved Fe concentrations showed the strongest enhancement in the subsurface oxygen deficient zone (ODZ), where oxygen concentrations <50 μmol kg^{-1} are prevalent. In contrast, dFe concentrations in the upper 200 m of the water column were at or below historic background levels. These observations are consistent with a short residence

time of aerosol particles in surface waters and possible dFe loss in the upper water column due to particle scavenging. Aerosol toxicity could also have contributed to the lack of a detectable phytoplankton response to the aerosol deposition event. The presented data suggest that the impact of aerosol deposition events on surface ocean biology depends strongly on the chemical composition of the aerosols and on their fate in the water column.

5.2 Introduction

Insufficient availability of the micronutrient iron (Fe) limits primary production in about 40% of the surface ocean (Moore et al., 2002). High nutrient, low chlorophyll (HNLC) areas result where the low solubility of Fe in seawater and low rates of Fe supply conspire to limit the growth of marine phytoplankton (Jickells et al., 2005; Liu and Millero, 2002; Martin et al., 1989). Fe limitation in HNLC regions reduces the efficiency of the biological carbon pump, thus diminishing the ocean's ability to absorb carbon dioxide from the atmosphere (Martin, 1990; Sunda, 2010).

The remote waters of the HNLC northeast Pacific Ocean receive Fe from intermittent sources such as atmospheric deposition (Crusius et al., 2011; Duce and Tindale, 1991) and the penetration of mesoscale eddies generated near shore (Brown et al., 2012; Johnson et al., 2005; Lippiatt et al., 2011). Fe addition from these sporadic sources enhances phytoplankton biomass and primary production in affected areas (Bishop et al., 2002; Boyd et al., 1998; Hamme et al., 2010; Xiu et al., 2014).

Much of the research into the potential impact of aerosol deposition events on oceanic biota has focused on the solubility of Fe in aerosols (e.g., Schroth et al., 2009; Sedwick et al., 2007; Sholkovitz et al., 2012). Combining this information with data on regional dust fluxes and assumed or measured Fe content of aerosols, it is possible to estimate the contribution of atmospheric deposition to dissolved Fe (dFe) concentrations in the global ocean (e.g., Duce and Tindale, 1991; Moore and Braucher, 2008; Tagliabue et al., 2009). In the subarctic North Pacific Ocean, atmospheric Fe supply from dust deposition is estimated to contribute 0.01–0.03 mmol Fe m^{-2} y^{-1}, comparable to the Fe input from sediments on the continental margins (Moore and Braucher, 2008). The majority of dust reaching this oceanic region is thought to originate from Asia, particularly the arid regions of China (Uematsu et al., 1983; Yuan and Zhang, 2006).

Aerosols from forest fires in Russia may also play an important role in contributing

soluble Fe to the western North Pacific Ocean (Ito, 2011). With plumes of Siberian forest fires observed as far east as the western United States and Canada (Bertschi et al., 2004; Cottle et al., 2014), it is likely that aerosols from such fires are also deposited in the eastern North Pacific Ocean. In this chapter, I present evidence that aerosols from forest fires in Siberia were deposited at Ocean Station PAPA (OSP; 50°N and 145°W) in the HNLC northeast subarctic Pacific Ocean in May 2012. Contrary to expectations, however, the addition of the aerosols did not elicit a detectable response from the resident phytoplankton.

5.3 Methods

Analytical methods are outlined in Appendix C.

5.4 Evidence for an aerosol deposition event

Several independent lines of evidence suggest that an aerosol deposition event occurred at OSP in the spring of 2012. Firstly, the dFe and Fe(II) data from June 3, 2012, show an anomaly at depth that suggests an external supply of Fe (Figure 5.1 A and B). In the depth range 400–1000 m, dFe is markedly elevated relative to historic data for OSP. Similarly, Fe(II) exhibits an increase with depth that is well above Fe(II) concentrations measured at other offshore stations in the HNLC subarctic Pacific on the same cruise (Figure 5.1B). The increase in Fe(II) corresponds to decreasing dissolved oxygen concentrations and longer Fe(II) half-lives (Figure 5.1C), suggesting that a near-constant Fe(II) supply with depth, such as might be expected from settling particles, could lead to the observed distribution. A reductive dissolution mechanism for particles could produce the observed Fe(II) and dFe profiles.

The principal external sources of dFe and particulate Fe to the NE subarctic Pacific Ocean include the passage of mesoscale eddies generated near shore (Brown et al., 2012; Johnson et al., 2005; Lippiatt et al., 2011), isopycnal transport from the continental margins (Lam and Bishop, 2008; Lam et al., 2006), and atmospheric deposition of aerosols (Bishop et al., 2002; Boyd et al., 1998; Crusius et al., 2011; Hamme et al., 2010). The shipboard CTD data as well as satellite images of sea surface height show no indication that an eddy was present at or near OSP in June 2012 (see Figure C.2 in Appendix C). It is also highly unlikely that the Fe enhancement to a depth of 1000 m stems from the continental margins, as particulate Fe that is

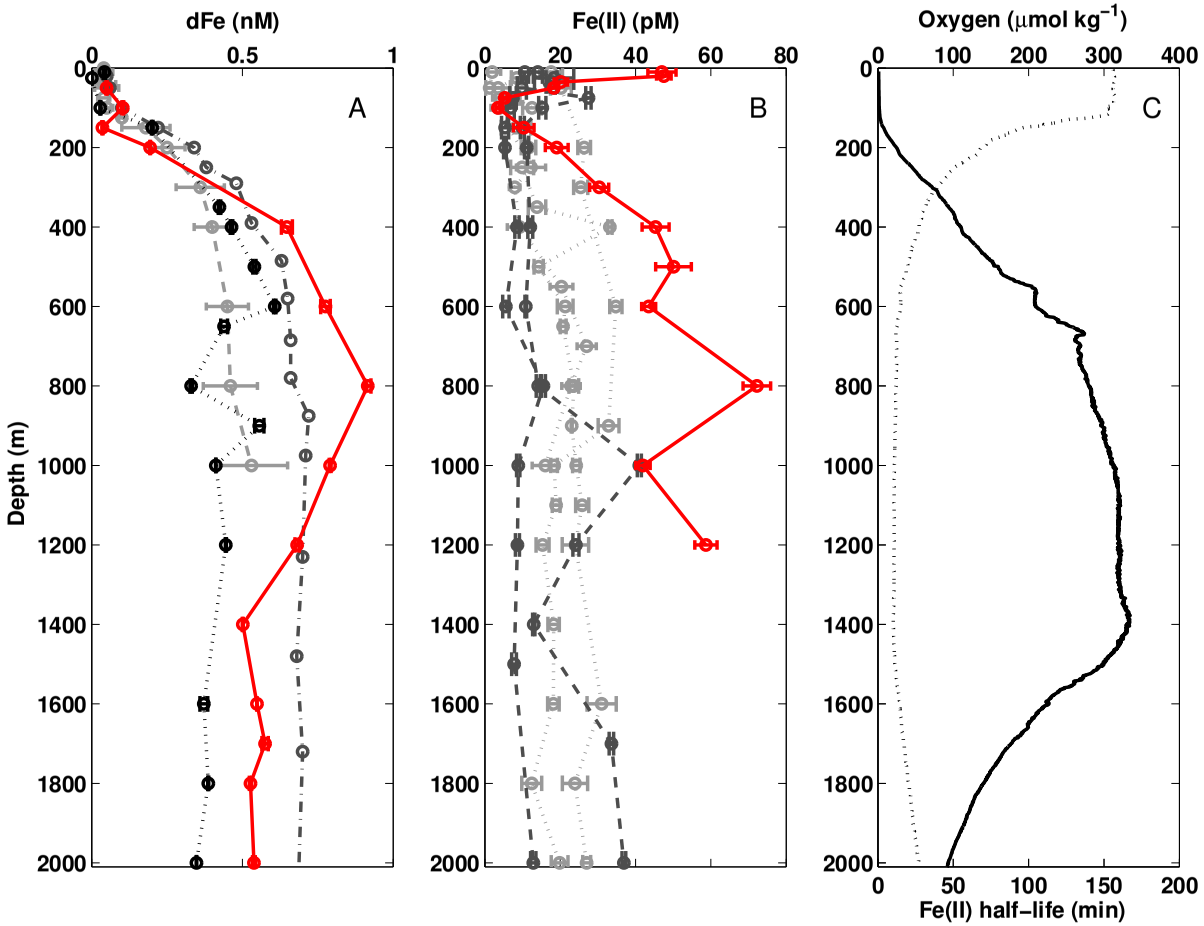

Figure 5.1: Concentrations of dFe (A), Fe(II) (B) and dissolved oxygen and calculated Fe(II) half-life (C) at OSP in June 2012. All error bars correspond to a single standard deviation. Panel A shows dFe concentrations from June 3, 2012, in red; historic OSP data are shown in grey and black as follows: average dFe concentrations measured by the Institute of Ocean Sciences, Sidney, Canada, between 2000 and 2011, with error bars corresponding to a single standard deviation (light-grey dashed line); VERTEX data from Martin et al. (1989) (dark-grey dash-dot); August 2013 data from Schallenberg et al. (2015a) (black dotted line). Panel B shows Fe(II) concentrations at OSP from June 2012 in red, together with other offshore data from the NE subarctic Pacific for comparison: P16 and P20 from June 2012 in dark grey (dashed) and P16, P20 and P26 from August 2013 in light grey (dotted); all data from Schallenberg et al. (2015a): P16 (light-grey dotted) and P20 (dark-grey dashed). Panel C shows dissolved oxygen concentrations (dotted) and calculated Fe(II) half-life from Schallenberg et al. (2015a) (solid line, bottom axis).

presumably associated with this source has its maximum around 200 m (Lam and Bishop, 2008; Lam et al., 2006). I therefore propose that an aerosol deposition event is the most likely source of the deep dFe and Fe(II) anomaly in June 2012.

The average UV aerosol index from the satellite-mounted Ozone Monitoring Instrument (OMI) for a 4×10° area centered at OSP shows a local maximum in early May 2012 (Figure 5.2) that is well above the seasonal average and is the only distinguished event that year, indicating the presence of UV-absorbing aerosols such as dust and soot. The decline of the UV aerosol index for areal bins along a southwest-to-northeast trajectory (i.e. the most likely transport direction for this aerosol cloud, see below) suggests aerosol deposition to the ocean. An investigation into the origin and movement of the aerosol cloud indicates that the material likely stemmed from forest fires in Siberia (Figure 5.3). Aerosols from Siberian forest fires are frequently transported across the Pacific Ocean between April and August (e.g., Bertschi et al., 2004; Cottle et al., 2014; Tomshin and Solovyev, 2014), and deposition of aerosols from biomass burning to the ocean has been proposed to constitute an important localized source of soluble Fe (Guieu, 2005; Ito, 2011; Luo et al., 2008). Wet deposition co-occurring with precipitation is a common mode of aerosol delivery to the ocean (Raiswell and Canfield, 2012). The NOAA-PMEL mooring at OSP (http://www.pmel.noaa.gov/OCS/data/disdel_v2/disdel_v2.html) detected precipitation as well as a decrease in sea surface salinity on May 10–11, 2012, coincident with the passage of the aerosol cloud (see Figure C.3 in Appendix C).

Knowing the timing of the aerosol deposition event, it is possible to further examine the possibility that the deep dFe enhancement measured on June 3 stems from settling particles. Following dust deposition in the oligotrophic North Atlantic, particle-settling velocities in the range 32–44 m d^{-1} have been observed (e.g., Brust et al., 2011; Neuer et al., 2004), while estimates from artificial dust seeding experiments span from ∼24 to 86 m d^{-1} (Bressac et al., 2011). Assuming that the dFe maximum measured at 800 m on June 3 resulted from dissolution of particles that were deposited on May 12, a particle settling velocity ≥36 m d^{-1} is required, consistent with the data from the literature. The deep dFe enhancement evident in the presented data could therefore result from the dissolution of sinking Fe-containing particles.

Another indicator for an aerosol deposition event at OSP in spring 2012 comes from ^{234}Th measurements reported by Mackinson et al. (2014). Mackinson and colleagues deployed sediment traps at OSP for ∼3 days in June 2012 and found ^{234}Th

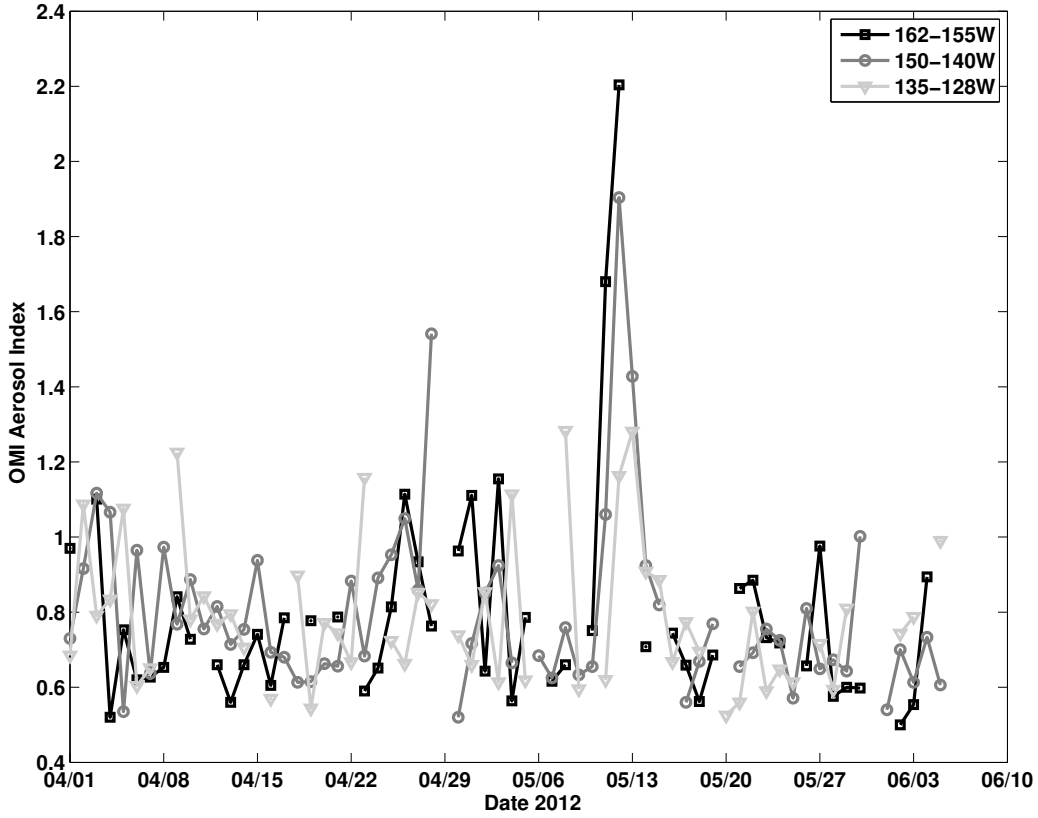

Figure 5.2: Averaged UV aerosol index from the satellite-mounted Ozone Monitoring Instrument (OMI) for 3 area bins around OSP. Assuming a SW-NE trajectory of the aerosol cloud in May 2012 (Figure 5.3), the bins were chosen as follows: centred at OSP (dark-grey; 140–150°W, 48–52°N), south-west of OSP (black; 155–162°W, 45–48°N) and north-east of OSP (light-grey; 128–135°W, 52–55°N).

fluxes close to 4000 dpm m^{-2} d^{-1} at 200 m. This flux is almost twice as high as the ^{234}Th flux measured at the same location, with the same traps, in June 2011 (Mackinson et al., 2014), and is more than twice as high as the ^{234}Th flux measured in sediment traps at station K2 in the northwest Pacific Ocean in July 2005 (Buesseler et al., 2009). The POC/^{234}Th ratio of the particles intercepted by the traps is only 1.3 in June 2012, compared to 3.7 in June 2011 (Mackinson et al., 2014), indicating that the sinking material in June 2012 contains a higher fraction of inorganic matter.

However, Mackinson et al. (2014) report the results from two kinds of measurements for particle export, and there is a slight discrepancy in the results. While the sediment trap data mentioned above show higher particle export in June 2012 compared to June 2011, the ^{234}Th deficit measured in the water column, which is a

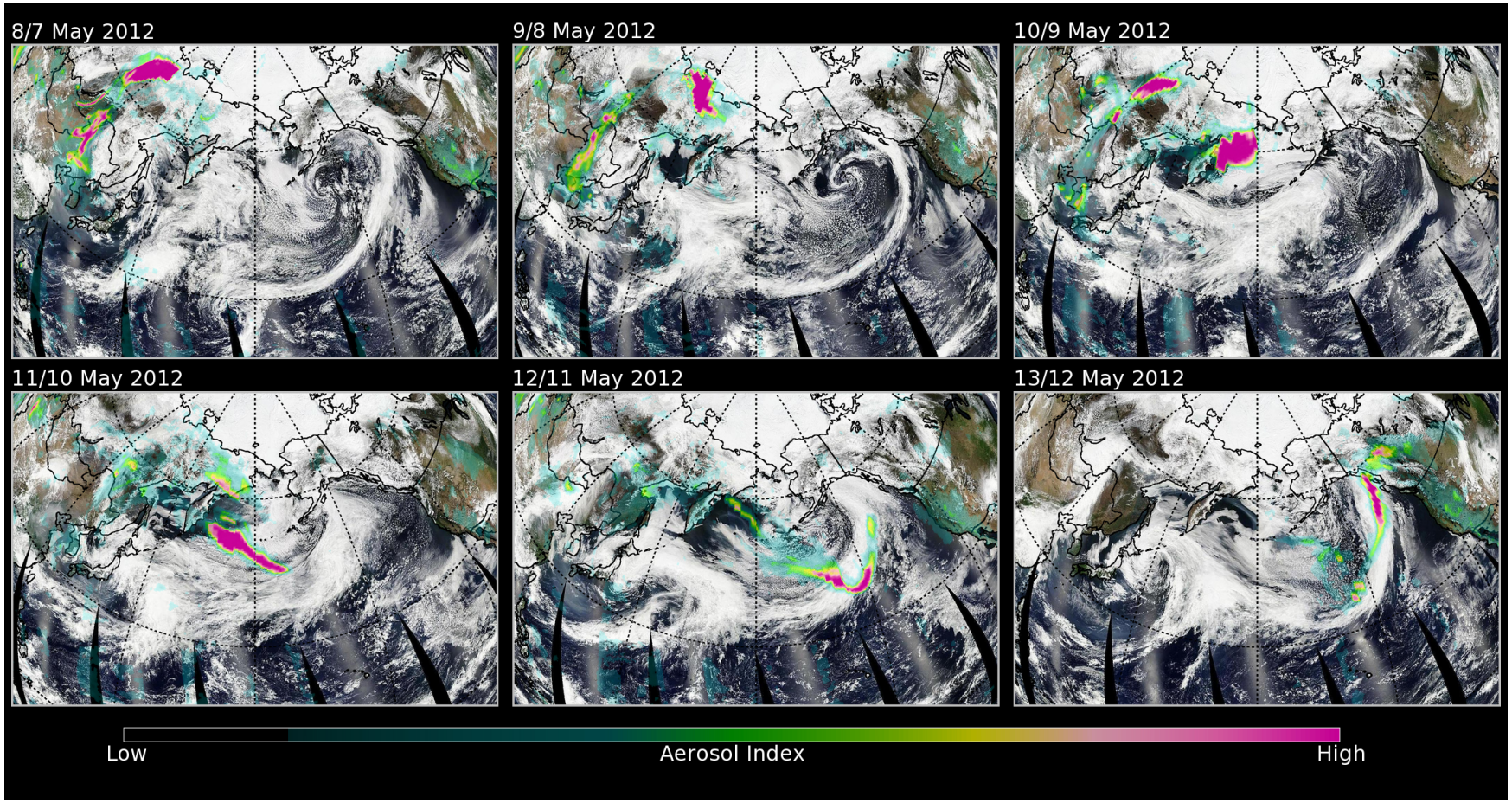

Figure 5.3: True-colour satellite images from May 2012 overlain with a false-colour rendering of the UV aerosol index, showing an aerosol cloud emanating from forest fires in Siberia and being transported across the North Pacific Ocean. Image downloaded from http://www.nasa.gov/mission_pages/fires/main/siberia-smoke.html. Credit: NASA/Suomi NPP/Colin Seftor.

more indirect indicator of particle export, suggests that particle export in June 2012 was similar to, but not larger than in June 2011. Sediment traps may oversample particles, especially when horizontal velocities are high (Buesseler et al., 2007), but there is no reason to suspect that horizontal velocities differed between the June 2011 and 2012 trap deployments at OSP. Interpretation of the ^{234}Th deficit, on the other hand, is subject to a catalog of biases of its own. For example, it assumes that in the absence of particle export ^{234}Th is in equilibrium with its parent ^{238}U, whose concentration is usually determined as a function of salinity (Savoye et al., 2006). However, in the context of aerosol deposition from a forest fire, the assumption that ^{238}U behaves conservatively with salinity may not hold, as ^{238}U can be enriched in fly ash from biomass burning (e.g., Carvalho et al., 2014).

The ^{234}Th deficit in the water column also integrates over much larger time and spatial scales than sediment traps, which has led Cochran et al. (2009) to conclude that flux estimates based on sediment trap data and ^{234}Th deficits in the water column are complementary, but not always directly comparable. Furthermore, conversion of the ^{234}Th deficit into a flux frequently assumes steady state — an assumption that is violated by episodic aerosol deposition events (Cochran et al., 2009). Cochran et al. (2009) speculate that flux calculations based on the ^{234}Th deficit would underestimate a dust deposition event compared to ^{234}Th fluxes from sediment traps. The sediment trap data are thus considered more conclusive in the context of the aerosol deposition event.

Based on the evidence outlined above, it is likely that an aerosol deposition event occurred at OSP in early May 2012, and that the deposited material originated from forest fires in Siberia.

5.5 Lack of a biological response to the aerosol deposition event

Profiling float 7601StnP stayed in the vicinity of OSP from February 2012 well into 2013, allowing for a year-to-year comparison of the recorded nitrate and chlorophyll *a* [chl *a*] data. Interpretation of chl *a* derived from fluorescence measurements (see Figure C.1 in Appendix C) is prone to a number of biases (see Appendix C for a discussion), hence I concentrate on nitrate drawdown as an indicator of phytoplankton growth. The data from the profiling float show only minimal nitrate drawdown in

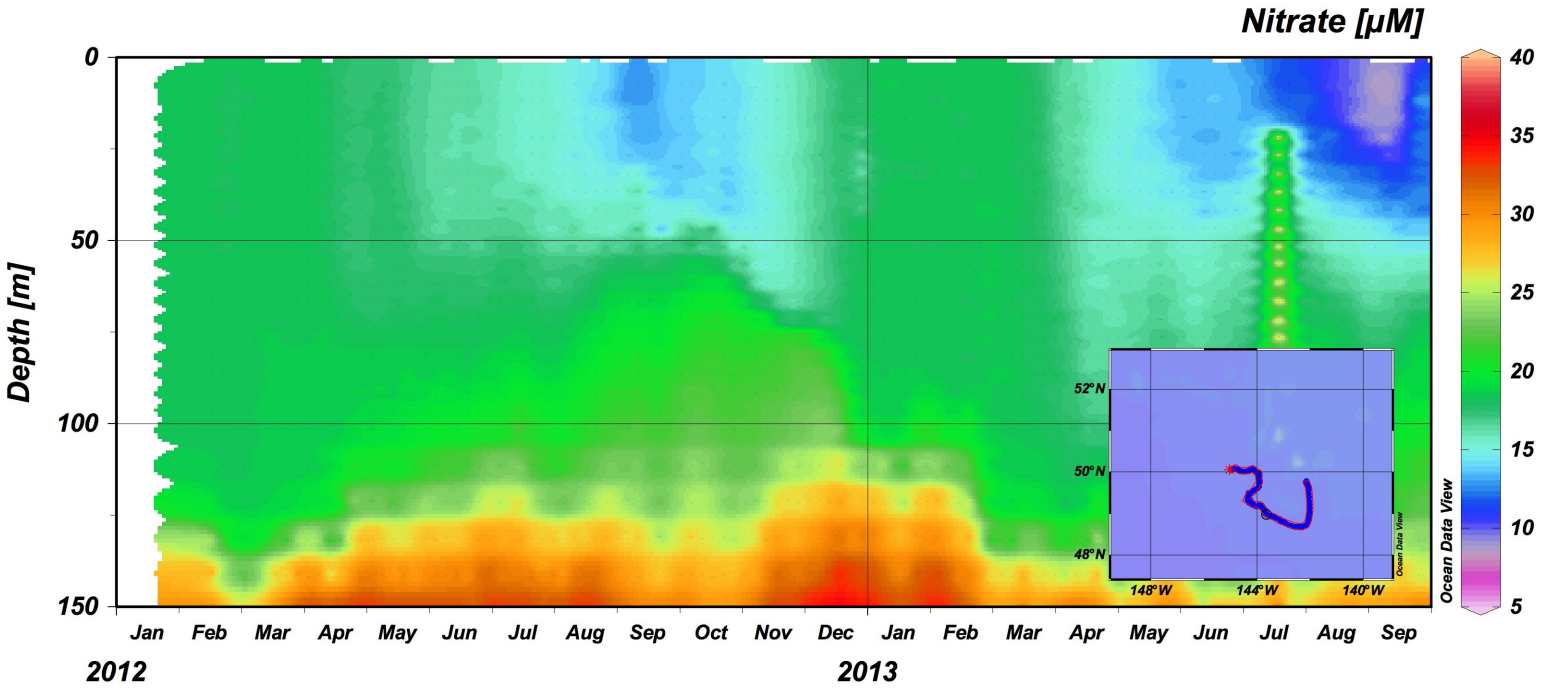

Figure 5.4: Nitrate concentrations (μM) in the upper 150 m as measured by APEX float 7601StnP deployed in February 2012 near OSP. Float location during the deployment is indicated on the map insert; the float travelled from West to East. Data courtesy of MBARI.

May 2012 compared to considerable drawdown in May 2013 (Figure 5.4). This is consistent with very little phytoplankton growth in May 2012. Similarly, the surface macronutrient data measured on discrete samples in June 2012 (nitrate, phosphate and silicic acid) do not show any sign of a deficit relative to the historic average (silicic acid shown in Figure 5.5).

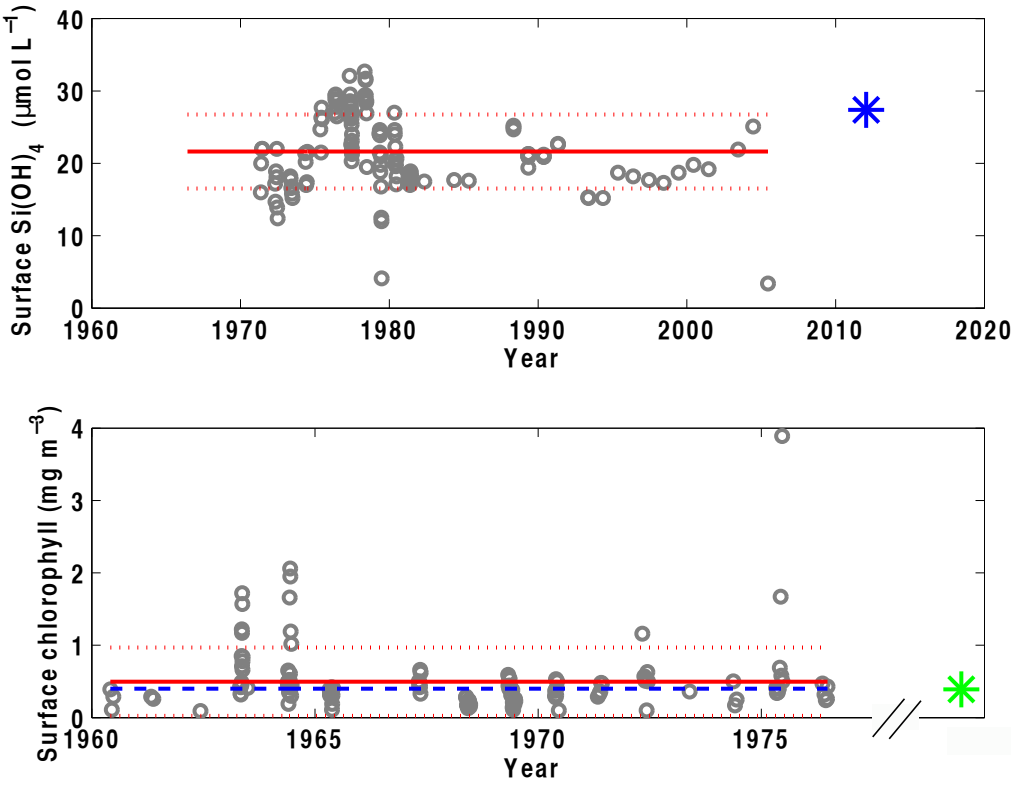

Figure 5.5: Comparison of shipboard silicic acid ($Si(OH)_4$, top panel) and chl *a* (bottom panel) surface data from June 2012 (blue and green star, respectively) with historical data for OSP from May and June (grey circles). Historical averages and their standard deviations (dashed lines) are indicated in red; for chl *a*, the historical median is also indicated in blue. Historical data courtesy of Frank Whitney, Institute of Ocean Sciences, Sidney.

Chlorophyll *a* concentrations measured aboard the CCGS John P. Tully in June 2012 were also unremarkable (0.4–0.6 mg L^{-1}), and Mackinson et al. (2014) report net primary production rates <50 mmol m^{-2} d^{-1} at OSP in June 2012, compared to 79–105 mmol m^{-2} d^{-1} in June 2011. Additional evidence comes from MODIS satellite imagery for May 2012 that shows no sign of elevated chl *a* concentrations in

the area surrounding OSP (see Figure C.4 in Appendix C).

It is important to point out, however, that with the available data I cannot exclude the possibility of any kind of response by the biota to the aerosol deposition event, I can only assert that there did not appear to be a large phytoplankton bloom. In experiments with water from an oligotrophic freshwater lake, Mackey et al. (2013) observed that the addition of forest fire aerosols favored picoplankton growth, which can enhance primary productivity without causing a strong increase in chlorophyll *a* concentration (Mackey et al., 2013). In addition, given that heterotrophic bacteria can account for up to 45% of biological Fe uptake in the HNLC subarctic Pacific (Tortell et al., 1996), it is possible that non-photosynthetic organisms were the main beneficiaries of the aerosol deposition event, but would have been missed in the presented analysis.

5.6 Explanations for lack of a detectable biological response

One obvious explanation for the lack of a phytoplankton response would be deep mixing or subduction of the water mass that received the aerosol deposition. Estimates of mixed layer depth at OSP based on temperature distribution in the upper ocean do not indicate a deepening of the mixed layer, but rather a shoaling due to rising sea surface temperatures throughout May (see Figure C.3 in Appendix C). There were no strong wind events recorded in May 2012 at OSP, and no mesoscale eddies were present within a radius of several hundred kilometres (see Figures C.2 and C.3 in Appendix C). Deep mixing and subduction are therefore unlikely explanations for the absence of a biological response.

The notion that an aerosol deposition event should lead to a biological response in an HNLC ocean assumes that the event causes an increase in surface dFe concentrations, temporarily alleviating the Fe limitation of resident phytoplankton. Although there is evidence from the field that the fertilizing effect of aerosol Fe can elicit a biological response (e.g., Bishop et al., 2002; DiTullio and Laws, 1991; Hamme et al., 2010; Young et al., 1991), in situ dFe concentrations were not directly measured in these events.

It is possible that the aerosol, which presumably originated mainly from wildfires, simply did not contain enough readily soluble Fe to elicit a strong response in the

phytoplankton. In a re-analysis of several published studies, Boyd et al. (2010) found that the estimated dFe addition from dust deposition events was frequently insufficient to cause a phytoplankton bloom, and that biological signatures had been falsely attributed to dust deposition. Interestingly, the authors discovered in one case study that the aerosol observed in conjunction with enhanced carbon dioxide drawdown in the Southern Ocean (Brévière et al., 2006) stemmed from bushfires in Australia and not — as had been assumed — from a dust storm (Boyd et al., 2010). Although this technically led to a false attribution of a phytoplankton response to dust deposition, it may provide evidence that aerosols from biomass burning can alleviate Fe limitation in HNLC areas of the ocean.

This suggestion is further supported by several studies reporting considerable Fe solubility for aerosols from biomass burning. For example, Guieu (2005) found 2% fractional Fe solubility for aerosols from pyrogenic emissions in the Mediterranean, and they attribute a 0.4 nM surface dFe enrichment in local waters to the deposition of aerosols from forest fires. Although not distinguishing between coal and biomass burning, Sholkovitz et al. (2012) report increased fractional Fe solubility in aerosols from combustion sources compared to crustal sources in a global dataset. In the African Sahel, Paris et al. (2010) observed increased Fe solubility in aerosols that were impacted by biomass burning, though the source of the Fe was found to be mainly internally mixed dust. Pyro-convection in large fires frequently causes the entrainment of dust and soil particles into the aerosol cloud (Gaudichet et al., 1995). It is thus likely that the material deposited at OSP contained both crustal particles and aerosols directly originating from biomass burning, with fractional Fe solubility at least equal to, and possibly higher than that of lithogenic particles not impacted by biomass burning. The evidence thus suggests that Fe fertilization is a likely result of aerosol deposition originating from wildfires. This begs the question: why was there no phytoplankton bloom observed in response to the aerosol deposition event in May 2012?

One possible explanation is that Fe scavenging onto particles decreased dFe concentrations in surface waters. Croot et al. (2004b) report very short residence times for dissolved and particulate Fe in surface waters of the equatorial North Atlantic after dust deposition from the Sahara, suggesting that added Fe is rapidly removed by scavenging, aggregation and sinking. In the same region but in a different year, Rijkenberg et al. (2008) observed only a slight dFe enhancement following a Saharan dust event, with concentrations increasing from 0.20 (initial) to 0.25 nM. Mesocosm

studies have found that the seeding with atmospheric dust may decrease the dFe inventory in surface waters (Wagener et al., 2010; Wuttig et al., 2013), presumably due to scavenging onto sinking particles (Ye et al., 2011). These mesocosm studies were carried out in Fe-replete waters, so their results may not be directly applicable to the HNLC subarctic ocean, where dFe concentrations are generally low. However, dominance of particle scavenging over dissolution in the upper water column, where particle aggregation and subsequent export are most pronounced (Ohnemus and Lam, 2015), could explain the low dFe concentrations (<0.2 nM) measured to a depth of 200 m at OSP in June 2012 (Figure 5.1A), and it could also explain the absence of a biological response to the aerosol deposition event.

Another possibility is that the aerosols had a toxic effect on the biota, as was observed by Paytan et al. (2009) for marine phytoplankton exposed to African aerosols. Additional testing led the authors to suggest that copper (Cu) toxicity was the most likely explanation, though they could not rule out the possibility that other elements present in the aerosols and/or their synergistic effects contributed as well (Paytan et al., 2009). Biomass burning has been observed to contribute more than 90% of the measured Cu in aerosols of the African Savanna (Gaudichet et al., 1995), and Sholkovitz et al. (2010) report relatively high fractional solubility (>40%) for Cu in combustion aerosols, compared to 1–7% for Saharan dust. It is thus possible that aerosol toxicity — in relation to Cu and/or other elements — prevented a phytoplankton bloom in response to the aerosol deposition event, but other factors, such as particle scavenging discussed above, cannot be ruled out.

5.7 Conclusions and Implications

The lack of a clear phytoplankton response to an aerosol deposition event in the HNLC subarctic Pacific Ocean provides evidence from the field that the deposition of aerosols in an HNLC ocean may not lead to an increase in biomass, possibly due to a lack of Fe fertilization. This is consistent with the analysis of Boyd et al. (2010), which concluded that dust-induced phytoplankton blooms in the world's oceans are probably rare because of slow dissolution of the particles. The available evidence suggests that the impact of aerosol deposition events on surface ocean biology depends strongly on aerosol composition and fate. Clearly, more research is needed on how factors such as aerosol source and atmospheric processing control the biological response to aerosol deposition. Paytan et al. (2009) observed that toxic effects from aerosols were

not uniform across phytoplankton taxonomic groups, highlighting the possibility that aerosol deposition may influence community composition, with possible effects on the biological carbon pump.

The depth distribution of dFe following the aerosol deposition event suggests that the aerosols deposited in the NE subarctic Pacific in May 2012 likely had a short residence time in the surface ocean, evident in the lack of enhanced dFe concentrations in the upper 200 m of the water column. The dFe increase relative to background concentrations in the 400–1000 m depth range implies that particles reached this depth in 22 days, and also dissolved to some extent while transiting through the water column. Measures et al. (2008) observed similar dFe distributions with depth — although higher overall dFe concentrations — in the ODZ of the tropical North Atlantic Ocean. They attributed the dFe enhancement at depth to atmospheric deposition of mineral dust originating from the Sahara (Measures et al., 2008).

The Fe(II) profile accompanying the dFe data holds intriguing additional information about the dissolution process of the aerosol particles. The increase in Fe(II) concentrations between 150 and 500 m depth corresponds well with the increase in calculated Fe(II) half-life in that same depth range (Figure 5.1 B and C). This suggests that a constant supply of Fe(II) from sinking particles could be responsible for the shape of the Fe(II) profile, leading to elevated Fe(II) concentrations where Fe(II) half-life is longest. Furthermore, the Fe(II) distribution hints at a reductive dissolution process on the particles, where the generation of Fe(II) is the intermediate step leading to the observed dFe maximum. With the present data it is impossible to distinguish whether the observed Fe speciation reflects the speciation present in the parent aerosol, or whether it is the result of reductive processes associated with the particles. Such processes could be directly related to the low oxygen concentrations in the ODZ, and/or they may be mediated by microbes populating the sinking particles.

Chapter 6

Conclusions

6.1 Summary

In this thesis, I have presented an investigation into dFe and Fe(II) sources to different HNLC regions. Chapters 2 and 3 document dFe and Fe(II) distributions under the seasonal pack ice in the Southern Ocean and along a transect in the subarctic NE Pacific, respectively. The Southern Ocean data from the SIPEX-2 study highlight the role of sea ice in supplying dFe to surface waters in this oceanic region. This Fe source, in combination with the stratifying effect of the melting sea ice, is expected to be important for the formation of the spring bloom that develops each year as the ice retreats (Fitch and Moore, 2007; Smith and Nelson, 1986).

Fe(II) concentrations under the sea ice were very low in spring, likely due to a lack of electron donors in the water column and very limited biological activity this early in the season. In addition, the snow-covered sea ice reduced the amount of solar radiation reaching the underlying water column, thus limiting the available light energy for Fe(II) generation. These observations are consistent with the known sources and production mechanisms for Fe(II) in surface waters, requiring either biological activity and/or the availability of sunlight combined with the presence of light-absorbing electron donors such as CDOM (Maldonado and Price, 2001; Rijkenberg et al., 2005).

The observed spatial and depth distribution of dFe during the SIPEX-2 study indicates that in addition to sea ice, the continental shelf around Antarctica is also a significant Fe source. The influence of this sedimentary Fe source is most pronounced at depth and near the continent, and is also reflected in elevated Fe(II) concentrations. There is evidence that offshore transport of waters from near the shelf may distribute

sediment-derived dFe farther offshore.

The importance of dFe supply from sediments is also apparent in the data from the HNLC subarctic Pacific presented in Chapter 3. The sedimentary influence can be observed several hundred kilometres from the shelf in the Fe(II) data, but it does not extend to the farther offshore stations along the Line P transect. As is the case for the Antarctic data set, elevated Fe(II) at depth nearer to shore serves as an indicator of Fe input from reducing sediments.

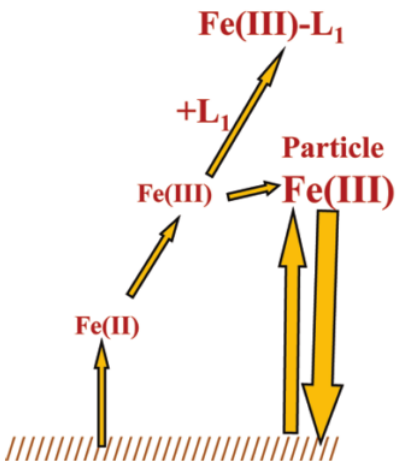

Figure 6.1: Schematic of the transformation of Fe(II) in the water column after leaving the sediment or particle surface. Adapted from Lohan and Bruland (2008).

Even in areas of low oxygen concentration, such as the ODZ in the subarctic Pacific, Fe(II) is best viewed as an intermediate in the conversion of particulate Fe in the sediment to dFe in the water column (see Figure 6.1 for an illustration). After re-oxidation, some of the Fe(III) will be stabilized by organic Fe ligands in the seawater, thus remaining in the dFe pool, while another part will be lost to renewed particle formation or scavenging to particle surfaces. In an indirect way, this process is evident in the data from P4 (see Chapter 3), where both Fe(II) and dFe are highly elevated at depth, most likely indicating a reductive sedimentary source for Fe. While continuous Fe(II) release from the sediments is expected to feed into the dFe pool over time (Figure 6.1), the Fe(II) present at any given time makes up only a small fraction of dFe, i.e. the Fe(II) percentage at P4 is not elevated compared to other stations.

Several indicators in the Line P data set point to particles as a potential source of Fe(II). Offshore in the HNLC subarctic Pacific, particle-associated remineralization

processes appear to generate transient Fe(II) maxima in the ODZ. Closer to shore, pronounced Fe(II) maxima at P12 are best explained by continuous Fe(II) release from sedimentary particles that are transported from the shelf break. In addition, aerosol particles may also be implicated as an Fe(II) source, as discussed in more detail in Chapter 5. Dust deposition is considered an important Fe source to HNLC regions (e.g., Jickells et al., 2005; Moore and Braucher, 2008), which led me to further investigate the Fe solubility from dust sources in the experiment described in Chapter 4.

The experimental results are not straightforward to interpret, not least because of the high, unexpected SOTS-1 treatment blank (see Chapter 4). Superoxide is an ephemeral reactive oxygen species that is challenging to work with at the best of times, and the experimental results further confirm its reputation of being "complicated". Regardless of the difficulties, the results of the experiment indicate that O_2^- may promote the dissolution of Fe contained in dust particles from a range of source regions. Hence O_2^-, and its generation by heterotrophic bacteria throughout the water column, is one more thing to take into consideration when contemplating the many factors affecting Fe dust dissolution in the ocean. This finding implies that Fe addition from particles could occur at all depths of the ocean, not just in the surface layer where solar irradiance drives photochemical reactions.

The work presented in Chapter 5 suggests that Fe(II) and dFe addition at depth may indeed occur as a result of aerosol deposition, transient though it may be due to the stochastic nature of dust input. This observation has implications for the dust-associated Fe cycle, with processes at depth possibly playing a larger role than previously assumed (Boyd et al., 2010). In addition, the absence of a strong phytoplankton response to the aerosol deposition event indicates that it may be necessary to consider the possibility of aerosol toxicity when contemplating the fertilizing effect of aerosols. In summary, the results from Chapters 4 and 5 add more questions to the already well-established catalogue of questions related to dust-associated Fe fertilization in the surface ocean. The acknowledged uncertainties include dust dissolution rates, Fe solubility, atmospheric processing of particles, particle scavenging, and the role of organic ligands, among others (e.g., Boyd et al., 2010). My work adds to this list by introducing the potential for subsurface dFe and Fe(II) anomalies attributable to aerosol deposition events and the possibility of toxic effects associated with aerosol deposition, suppressing phytoplankton growth.

6.2 Future directions

More work is required to understand the role of particles in the cycling of Fe, and particularly the possibility that particles may constitute a source of Fe(II). Clearly, this is a promising field for future work, but particles are difficult to study, as laboratory work has its limitations in how well it can imitate processes occurring in the ocean. In the oceanic environment, simultaneous sampling of particles and measurement of Fe(II) in the water column will help us to evaluate whether indeed particles are a likely source of Fe(II). This kind of work will also help us assess whether different kinds of particles, and/or different kinds of environments are more or less likely to produce Fe(II). However, it remains challenging to identify the processes happening at particle surfaces, in particular with regards to the microbial community. The field of "omics", i.e. the study of the genome, proteome and metabolome, may be promising in this respect, as it provides clues about the metabolic capabilities of microbes associated with particles, thus shedding light on the range of possible microbe-mediated processes (e.g., Wright et al., 2012). For example, one could search for genomic evidence that microbes in the ODZ of the subarctic NE Pacific are capable of Fe-reduction. It may also be possible to probe whether particle-associated Fe(II) production results from microbial activity by comparing Fe(II) accumulation in poisoned and un-poisoned sediment traps, similar to the approach employed by Karl and Tilbrook (1994) to investigate particle-associated methane.

The study of iron stable isotopes is another powerful tool that allows fingerprinting of iron sources to the ocean (e.g., Conway and John, 2014; Homoky et al., 2013; John et al., 2012). Dissolved Fe supplied by reductive processes has a lighter isotopic signature than dFe from non-reductive sources. With the stable isotope composition of lithogenic material well constrained, the in situ stable isotope composition in the water column or in pore waters can thus be used to estimate the influence of reductive processes relative to non-reductive processes (Conway and John, 2014; Homoky et al., 2013; John et al., 2012). Applying this approach in the ODZ of the subarctic NE Pacific could be very informative indeed. In addition, iron stable isotopes in the sedimentary record can be applied to investigate Fe sources to the ocean on geological time scales, as recently illustrated by Horner et al. (2015). This kind of approach may in the future allow us to better understand the connections between Fe supply mechanisms and climate.

Particles released from sea ice are another area where more research is needed.

Pertinent questions include the following: What are particles in sea ice made of, where do they come from and how do they form? How fast do these particles sink after being released into the water column? How bio-available is the Fe contained in the particles? This last question could be answered with incubation experiments, while the question regarding sinking velocities requires sediment traps or cameras and a time series approach.

The field of O_2^- research offers many open questions waiting to be answered. However, O_2^- remains an elusive species that is extremely difficult to measure reliably in the field. SOTS-1 is a promising candidate for experiments investigating the role of O_2^- in a range of processes, as demonstrated in Chapter 4. However, the high Fe(II) treatment blank makes it challenging to interpret experimental results pertaining to Fe. Likewise, the lower-than-expected steady-state concentrations in SOTS-1 solutions, which could be explained by rapid O_2^- decay due to a contaminant (see Section 4.4.2), is suspicious. I therefore recommend that trace element concentrations of SOTS-1 be better characterized before employing this reagent in future experiments.

The fast decay rate of O_2^- makes measurements in the field very challenging with current methods. However, the measurement apparatus for O_2^- detection is surprisingly simple, the MCLA reagent is very specific for O_2^-, and the chemiluminescence reaction that allows quantification of O_2^- is fast (reaction rate $\sim$5 x 10^5 M^{-1} s^{-1}; Burns et al., 2012). It should thus be possible to build a submersible superoxide detector that could be towed from a ship or lowered through the water column. While it may be difficult to properly calibrate such an instrument, and temperature as well as pH effects need to be taken into consideration, it could be deployed to provide insight into the spatial and depth variations in O_2^- concentrations in different environments, as well as the day-and-night cycle of this reactive oxygen species in surface waters. This type of information would help us to better constrain the processes that generate O_2^- in the ocean and would greatly improve biogeochemical models of Fe speciation in the surface ocean, which frequently assume that O_2^- is an intermediate in the redox cycling of Fe (e.g., Fan, 2008; Weber, 2005).

Finally, the observation that both Fe(II) and dFe appear to be elevated in the ODZ after an aerosol deposition event (see Chapter 5) begs an intriguing question to be answered: Are the low oxygen concentrations in the ODZ a prerequisite for this dFe addition to occur at depth? In other words: would there be no comparable dFe addition at depth if the same aerosol deposition event occurred over a fully oxygenated water column? To answer these questions, we need to learn more about the Fe

solubilization processes at work on particles. For example, if microbial Fe reduction plays an important role, then low ambient oxygen concentrations may indeed be essential, as microbial Fe reduction requires an anoxic micro-environment (e.g., Weber et al., 2006). Particle-associated microzones void of oxygen are more likely to occur in a suboxic water column (Wright et al., 2012). Thus, if ODZs were indeed found to enhance the Fe solubilization of particles, then the ongoing de-oxygenation of the oceans on a global scale (Keeling et al., 2010) may in the long term result in increased dFe fluxes from particles to ocean waters.

Appendix A

Data Table for Chapter 2

Stn	Date 2012	Lat	Lon	Depth (m)	NO_3 +NO_2 (µM)	PO_4 (µM)	$Si(OH)_4$ (µM)	dFe (nM)	SD dFe (nM)	Fe(II) (pM)	SD Fe(II) (pM)
0	24.9.	62° 31' S	121° 29' E	15	31.21	2.16	61.57	0.51	0.01	-	-
				30	31.43	2.16	63.24	0.14	0.01	-	-
Bottom depth > 3500 m				50	31	2.2	63.24	0.3	0.01	-	-
				75	31.29	2.2	63.24	0.18	0.01	-	-
				100	31.29	2.2	68.23	0.17	0.01	-	-
				125	32.79	2.36	76.55	0.17	0	-	-
				150	32.64	2.32	81.54	0.39	0.05	-	-
				200	32.5	2.32	86.54	0.25	0.01	-	-
				300	32.14	2.32	88.2	0.21	0.01	-	-
				500	31.43	2.16	91.53	0.25	0.01	-	-
				750	31.07	2.16	96.52	0.29	0.02	-	-
				1000	31.64	2.2	103.18	0.44	0.02	-	-
1	25.9.	63° 53' S	119° 55' E	15	31.29	2.2	99.85	0.38	0.02	-	-
				50	30.86	2.1	63.24	0.6	0.01	-	-
Bottom depth > 3500 m				75	30.86	2.16	64.9	0.45	0.02	-	-
				100	30.79	2.16	64.9	3.05	0.14	-	-
				125	31.57	2.23	73.22	1.31	0.03	-	-
				150	32.29	2.29	84.87	0.34	0.01	-	-
				200	32.21	2.26	86.54	0.36	0.01	-	-
				300	32.14	2.32	88.2	0.36	0.01	-	-
				500	31.86	2.26	89.87	1.04	0.03	-	-
				750	31.43	2.23	91.53	0.48	0	-	-
				1000	31.5	2.26	114.83	0.59	-	-	-
2	29.9.	64° 27' S	119° 52' E	15	30.64	2.16	64.9	0.47	0.01	< d.l.	< d.l.
				30	30.64	2.16	64.9	0.19	0.02	< d.l.	< d.l.
Bottom depth 3500 m				50	30.64	2.16	64.9	0.2	0.02	1.9	1.1
				75	30.64	2.2	66.57	1.04	0.06	< d.l.	< d.l.
				100	30.93	2.2	69.9	0.47	0.01	< d.l.	< d.l.
				150	31.86	2.26	79.88	0.17	0.01	< d.l.	< d.l.
				200	32.07	2.29	84.87	0.13	0.01	< d.l.	< d.l.
				300	31.93	2.29	88.2	0.12	0.01	< d.l.	< d.l.
				500	31.57	2.26	89.87	0.24	0.01	< d.l.	< d.l.
				750	31.29	2.26	96.52	0.25	0.01	< d.l.	< d.l.
				1000	31.5	2.26	104.84	0.18	0.01	< d.l.	< d.l.

Continued on the next page

Stn	Date 2012	Lat	Lon	Depth (m)	NO_3 +NO_2 (µM)	PO_4 (µM)	$Si(OH)_4$ (µM)	dFe (nM)	SD dFe (nM)	Fe(II) (pM)	SD Fe(II) (pM)
4	9.10.	65° 08' S	120° 38' E	15	30.57	2.2	59.91	1.04	0.03	< d.l.	< d.l.
				30	30.64	2.23	58.25	0.54	0.07	< d.l.	< d.l.
Bottom depth 3000 m				50	30.57	2.23	58.25	0.53	0.06	< d.l.	< d.l.
				75	30.64	2.16	61.57	0.57	0.06	< d.l.	< d.l.
				100	30.71	2.23	64.9	0.31	0.06	< d.l.	< d.l.
				125	30.71	2.2	69.9	0.28	0.01	< d.l.	< d.l.
				150	30.79	2.26	66.57	0.43	0.05	-	-
				200	31.21	2.23	76.55	0.42	0.02	-	-
				300	31.5	2.29	88.2	0.45	0.04	-	-
				500	31.43	2.23	96.52	1	0.12	-	-
				750	31.36	2.26	108.17	0.46	0.03	-	-
5	12.10.	65° 13' S	120° 08' E	15	30.5	2.26	59.91	0.17	0.01	17.0	0.5
				30	30.57	2.26	59.91	0.14	0	7.9	1.8
Bottom depth 3000 m				50	30.5	2.26	59.91	0.11	0.01	5.8	2.0
				75	30.5	2.23	59.91	0.1	0.01	6.4	2.1
				100	31.29	2.2	59.91	0.09	0.01	7.6	1.5
				125	30.36	2.2	58.25	0.13	0.01	5.8	2.6
				150	30.29	2.2	59.91	0.14	0.01	< d.l.	< d.l.
				200	30.64	2.23	66.57	0.16	0.01	< d.l.	< d.l.
				300	31.64	2.29	84.87	0.19	0.01	< d.l.	< d.l.
				500	31.29	2.23	93.19	0.21	0.01	< d.l.	< d.l.
				750	31.36	2.29	98.19	0.26	0.01	5.7	2.6
				1000	31.71	2.32	104.84	0.26	0.01	-	-
6	13.10.	65° 15' S	120° 00' E	15	30.5	2.29	58.25	0.16	0.01	< d.l.	< d.l.
				30	30.5	2.26	58.25	0.15	0.01	< d.l.	< d.l.
Bottom depth ~ 2600 m				50	30.5	2.26	59.91	0.13	0.01	< d.l.	< d.l.
				75	30.43	2.29	59.91	0.2	0.01	< d.l.	< d.l.
				100	30.36	2.26	58.25	0.16	0	< d.l.	< d.l.
				125	30.14	2.26	56.58	0.21	0.01	-	-
				150	30.14	2.23	58.25	0.2	0.01	-	-
				200	30.36	2.26	63.24	0.27	0.01	< d.l.	< d.l.
				300	31.57	2.36	81.54	0.29	0.02	< d.l.	< d.l.
				500	31.29	2.39	88.2	0.36	0.02	3.8	2.1
				750	31.43	2.39	101.51	0.38	0.01	< d.l.	< d.l.
				1000	31.64	2.36	104.84	0.57	0.01	32.6	1.6
7	19.10.	65° 16' S	118° 59' E	15	30.57	1.97	58.25	0.69	0.04	4.1	0.5
				30	30.21	1.94	59.91	0.62	0.02	< d.l.	< d.l.
Bottom depth ~ 2000 m				50	30.43	1.87	58.25	0.77	0.03	4.3	1.0
				75	30.5	2.1	59.91	0.63	0.03	< d.l.	< d.l.
				100	30.43	2.1	59.91	0.62	0.01	< d.l.	< d.l.
				125	31.14	1.97	59.91	0.63	0.02	-	-
				150	19.64	1.71	58.25	0.66	0.04	< d.l.	< d.l.
				200	30.29	1.97	59.91	0.72	0.03	3.2	1.5
				300	31.36	2.39	76.55	0.83	0.03	7.2	1.6
				500	31.36	2.39	89.87	1.04	0.02	4.1	0.6
				750	31.57	2.39	101.51	0.86	0.03	4.6	1.6
				1000	32.07	2.49	116.49	0.96	0.04	21.9	1.2

Table A.1: Station dates and locations, bottom depths and concentrations of macronutrients, dFe and Fe(II). The reported Fe(II) concentrations are not adjusted (see Section 2.3.5), hence a lot of data fall below the detection limit (d.l.). Single standard deviations (SD) are shown for dFe and Fe(II) and are based on replicate analyses of the same sample. Fe(II) was not determined at all stations and depths, resulting in missing values in the table.

Appendix B

Supplementary material for Chapter 3

B.1 Fe(II) determination with and without injection valve

Fe(II) data from three different cruises is presented, with slight modifications to the instrumental set-up between cruises as outlined in Section 3.3.4. In particular, the introduction of an injection valve for the August 2013 cruise deserves mention. The advantage of using an injection valve is that baseline drift is inherently accounted for because the baseline is always subtracted from the signal. I therefore did not measure any blanks to control drift during analysis when an injection valve was used.

However, on the cruises where an injection valve was not used, blanks in the form of aged seawater were frequently measured throughout the analysis to keep track of baseline fluctuations. For the most part, the blank showed some minor variability around 0 pM, and the blank average for the two 2012 cruises is 2.6 ± 4.1 pM (n=37). Only in one instance did I observe significant instrument drift (P12, August 2012); in that case, the blank (interpolated for the duration of analysis) was subtracted from the Fe(II) data and is not included in the blank average above. As a whole, I find that using an injection valve for Fe(II) determination simplifies the analysis and eliminates baseline drift as a source of error, and is therefore preferred.

B.2 Replicate Fe(II) measurements from same GO-FLO

Throughout the Fe(II) analyses, I took repeat samples from select GO-FLO bottles and during pumping events to verify that my results were reproducible. The standard deviation of all measurements made on repeat samples during the 3 cruises is 1.8 ± 1.2 pM (n=20), which compares well to the mean absolute standard deviation of replicate measurements made on the same sample, i.e. 2.4 ± 0.4 pM and 2.3 ± 2.5 pM with and without the injection valve, respectively. In my data presentation, I therefore do not distinguish whether error bars represent the standard deviation of replicate measurements from the same physical sample or from the same GO-FLO bottle/pump depth. In other words: the majority of error bars in the figures of the main manuscript represent the standard deviation of replicate measurements on the same sample, but when more than one sample was drawn from the same GO-FLO or pump depth, the error bar represents the standard deviation of the replicate samples.

B.3 Two casts, one Fe(II) profile

At two stations during the August 2013 cruise (P12 and P26), Fe(II) was measured on two separate casts that were subsequently "spliced" together to yield the high-resolution Fe(II) profiles presented in the manuscript. In one case (P12), the profiles from the two casts fit together seamlessly (Figure B.1), and both show elevated Fe(II) concentrations at 1000 and 1100 m respectively, increasing confidence that the feature at this depth is real, and that similar features at other stations are real as well.

As can be seen in Figure B.2A, the individual profiles from P26 do not fit together as seamlessly as for P12. It is worth pointing out that the two casts were also spaced farther apart in time, i.e. 17 h rather than 4 h at P12. It is thus possible that the difference between profiles is not analytical but reflects true variability at P26, especially when considering how seamlessly the two profiles could be combined at P12. However, for ease of presentation, each profile was shifted by 3 pM Fe(II) towards the other, which yields a reasonably smooth combined profile (Figure B.2B). The resulting "adjusted" profile is the profile that is shown throughout the main manuscript.

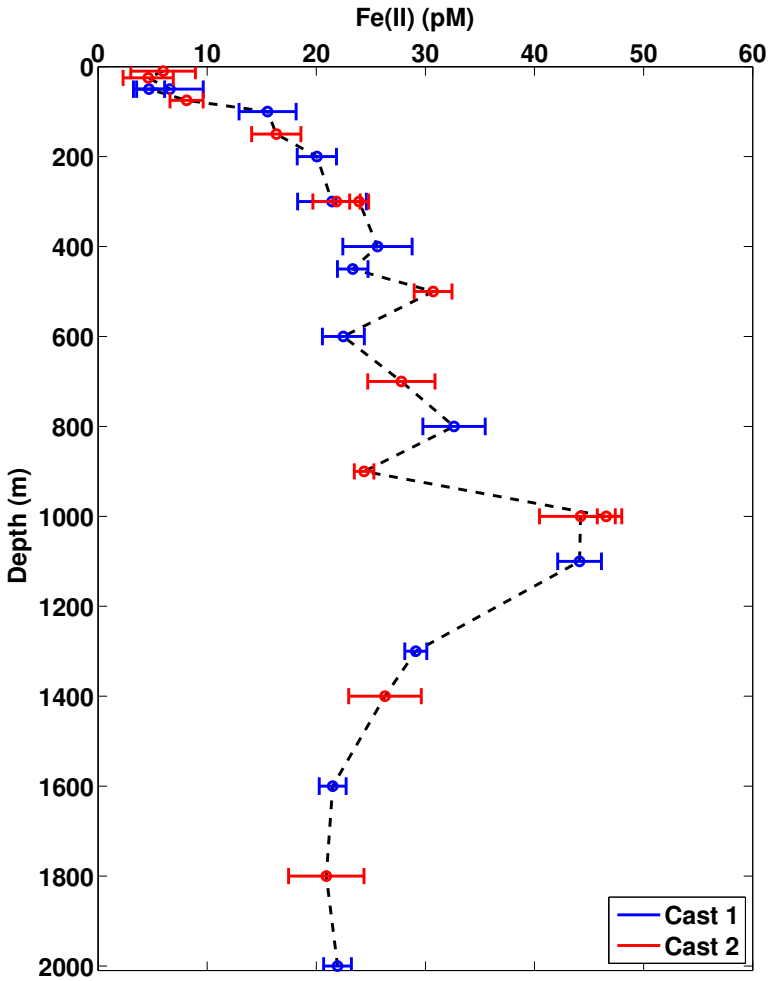

Figure B.1: Fe(II) profile from station P12 in August 2013. Red and blue colours indicate data from different casts that were ∼4 h apart.

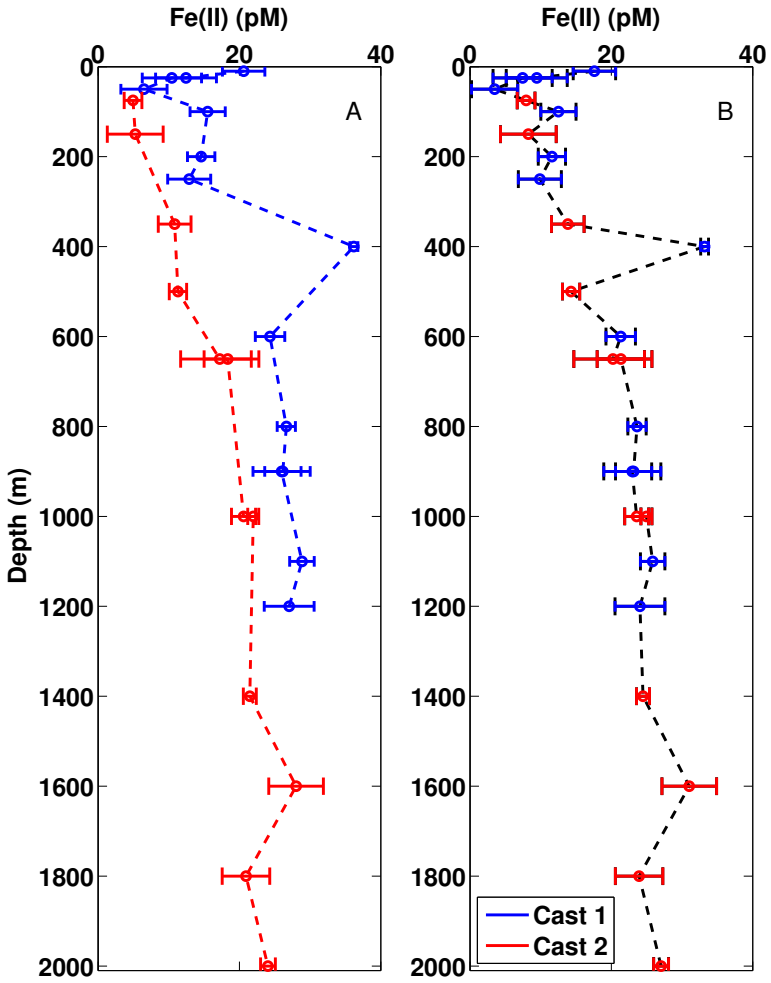

Figure B.2: Fe(II) profiles from station P26 in August 2013. Red and blue indicate data from different casts that were ∼17 h apart. The individual casts are displayed in panel A, while panel B shows the combined profile. For ease of presentation, i.e. in order to "smooth" the combined profile, data from cast 1 were adjusted by subtracting 3 pM Fe(II), and data from cast 2 had 3 pM added to yield the profile shown in panel B.

B.4 Fe(II) half-life calculation

Millero et al. (1987) report that the oxidation of Fe(II) by O_2 is strongly dependent on pH and O_2 concentration as follows:

$$-\frac{d\mathrm{Fe(II)}}{dt} = k'[\mathrm{Fe(II)}] \tag{B.1}$$

where

$$k' = k[\mathrm{OH^-}]^2[\mathrm{O_2}] \tag{B.2}$$

The rate constant k can be calculated for a given temperature and ionic strength (Millero et al., 1987). For the June 2012 cruise, $[O_2]$ was measured by an O_2 probe on the shipboard CTD, and $[OH^-]$ is calculated from pH measured at discrete depths and linearly interpolated to match the CTD data. Calculation of $[OH^-]$ requires the dissociation constant for water, K_w, which was calculated for in situ pressure (Millero, 1995), temperature and ionic strength (Millero et al., 1987). Likewise, the measured pH was adjusted to in situ temperature and pressure with the CO2SYS carbonate equilibrium program, using DIC data from a Line P cruise in June 2007. See the MATLAB® code in Figure B.4 for details regarding the calculation, and see Supplementary Table B.2 for a list of input and calculated parameters at P26 in June 2012.

My results for the half-life calculation differ markedly from the estimates by Hansard et al. (2009) for the NE Pacific, especially at depth. Hansard et al. (2009) estimate maximum half-lives in the ODZ of ∼12 h, while I estimate half-lives close to 170 h at the station closest to theirs, i.e. P26. There a two big differences between their approach and mine: Firstly, Hansard et al. (2009) referred to Trapp and Millero (2007) to calculate the Fe(II) oxidation rate with O_2, while I used the equations from Millero et al. (1987), which are much simpler and don't require dissolved inorganic carbon (not currently available for the 2012 data set) as an input parameter. Secondly, Hansard et al. (2009) included Fe(II) oxidation by H_2O_2 in their half-life estimates, and I did not (because H_2O_2 was not determined on our cruises). So I am unable to directly compare my half-life calculations to those of Hansard et al. (2009), but the respective estimates for the rate constant of the Fe(II) oxidation with O_2 can be compared.

Referring to the Supplementary material of Hansard et al. (2009), I calculated k' for the oxidation of Fe(II) by O_2 using their input parameters, i.e. $[OH^-]$, temperature,

ionic strength and oxygen concentration, but following the approach of Millero et al. (1987) as I did for my own data. The result is shown as the grey dashed line in Figure B.3A. For comparison, the k' calculated by Hansard et al. (2009) with the same input data but using the Trapp and Millero (2007) model is shown in red. This k' is specific to the oxidation by O_2 and is taken directly from the Supplementary material of Hansard et al. (2009). I also show k' calculated after Millero et al. (1987) using data from P26 (blue line).

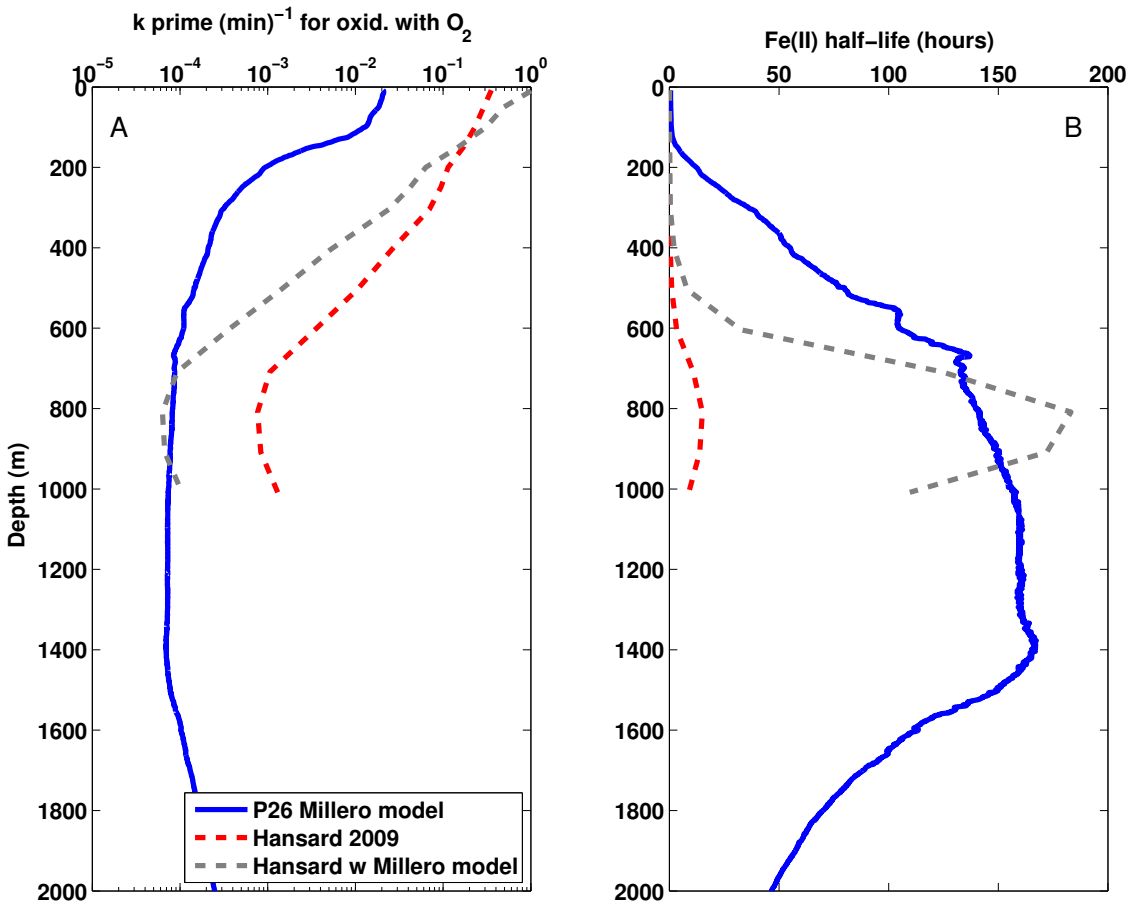

Figure B.3: Calculated k' (min^{-1}) for the oxidation of Fe(II) by O_2 (A) and the corresponding Fe(II) half-lives (hours; B). Blue line uses input data from OSP in June 2012, while the grey and red lines use input data from Hansard et al. (2009) but with different models. See text for details.

It is obvious that the choice of model has considerable influence on the outcome, especially at depth (i.e. comparing the red and grey dashed lines). It is beyond the scope of this manuscript to delve into the model details that may cause the

discrepancy, but this analysis illustrates the uncertainty associated with these half-life calculations. I would like to point out that in the depth range of the ODZ, the half-life calculation following Millero et al. (1987) yields longer half-lives than the model by Trapp and Millero (2007) for the same input parameters (compare the grey and red lines in Figure B.3B). Since I used the approach of Millero et al. (1987) in this analysis, my half-life estimates can therefore be considered upper limits.

	Calculated Fe(II) half-life (min)					Δ_t between bottle closing and analysis (min)	
Sample depth (m)	**P4**	**P12**	**P16**	**P20**	**P26**	**TMR**	**GO-FLOs on Kevlar**
10	8	20	25	31	33	10-15	120-150
20	11	20	26	31	34	12-20	120-150
35	20	20	28	31	35	15-30	120-150
50	31	24	30	31	38	20-35	120-150
75	40	31	38	39	47	25-40	120-150
100	60	37	57	56	54	30-45	120-150
150	249	118	227	253	225	35-50	115-150
200	254	206	529	425	742	40-60	115-140
400	2532	2031	3459	2551	3311	45-65	115-140
600	10438	7598	8912	6593	6268	50-70	110-140
800	20110	15759	13850	10529	8419	55-75	110-130
1000	17603	21419	20076	15488	9407	60-80	100-120
1200	11274	16566	17595	16576	9625	70-90	100-120
1500	-	6851	9073	8572	8923	80-100	90-120
2000	-	2477	2692	2686	2806	90-110	90-120

Table B.1: Calculated Fe(II) half-lives for a subset of depths at all stations, and the corresponding estimated time that elapsed between closing of GO-FLO bottles and Fe(II) analysis (Δ_t). Calculated half-lives are for June 2012, see Section B.4 for details of the calculation. Variability between cruises is not expected to be large compared to the variability with depth and between stations.

Sample depth (m)	Temperature [1] (°C)	Ionic strength [2]	pH [3]	K_w [4]	$[OH^-]$ [5] (mol kg^{-1})	$[O_2]$ [6] (µmol kg^{-1})	k [7]	k' [8] (min^{-1})	Fe(II) half-life [9] (min)
10	6.8	0.67	8.04	14.31	5.40E-07	311.7	2.31E+14	2.11E-02	33
20	6.5	0.67	8.04	14.32	5.34E-07	313.1	2.28E+14	2.04E-02	34
35	6.2	0.67	8.05	14.33	5.25E-07	314.8	2.26E+14	1.96E-02	35
50	6.0	0.67	8.05	14.34	5.14E-07	312.8	2.23E+14	1.84E-02	38
75	5.3	0.67	8.04	14.37	4.68E-07	312.8	2.16E+14	1.48E-02	47
100	4.9	0.67	8.02	14.38	4.44E-07	304.4	2.13E+14	1.28E-02	54
150	4.5	0.69	7.84	14.39	2.79E-07	192.7	2.05E+14	3.08E-03	225
200	4.1	0.70	7.67	14.41	1.83E-07	139.0	2.00E+14	9.35E-04	742
400	3.9	0.70	7.55	14.41	1.40E-07	54.0	1.97E+14	2.09E-04	3311
600	3.7	0.71	7.54	14.40	1.37E-07	30.2	1.94E+14	1.11E-04	6268
800	3.2	0.71	7.54	14.41	1.34E-07	24.1	1.90E+14	8.23E-05	8419
1000	2.9	0.71	7.55	14.42	1.34E-07	21.9	1.86E+14	7.37E-05	9407
1200	2.6	0.71	7.55	14.42	1.35E-07	21.4	1.84E+14	7.20E-05	9625
1500	2.3	0.71	7.56	14.42	1.37E-07	22.8	1.81E+14	7.77E-05	8923
2000	1.9	0.71	7.62	14.41	1.60E-07	54.1	1.77E+14	2.47E-04	2806

1) Measured with the shipboard CTD
2) Calculated based on salinity after Millero et al. (1987)
3) in situ pH on the total scale, calculated from discrete pH measurements using CO2SYS software
4) Dissociation constant of water corrected for pressure effects; calculated after Millero et al. (1987) and Millero (1995)
5) Free OH^- concentration calculated from K_w and pH
6) Oxygen concentration measured by an O_2 probe on the shipboard CTD
7) Overall rate constant for the oxidation of Fe(II) by O_2, calculated after Millero et al. (1987)
8) Pseudo-f rst-order rate constant for the oxidation of Fe(II) by O_2, calculated after Millero et al. (1987)
9) Fe(II) half-life calculated from the pseudo-f rst-order rate constant

Table B.2: Key input parameters for the Fe(II) half-life calculation at P26 in June 2012

```
% use CO2SYS to calculate in situ pH (column 18 in RESULT files)

[P4_RESULTS] = CO2SYS(pH_1(:,1),P4_1(:,4),3,2,june12_ctd.sal(:,1),25,...
    june12_ctd.temp(:,1),0,june12_ctd.pres(:,1),P4_1(:,3),P4_1(:,2),1,4,1);

[P12_RESULTS] = CO2SYS(pH_1(:,2),P12_1(:,4),3,2,june12_ctd.sal(:,2),25,...
    june12_ctd.temp(:,2),0,june12_ctd.pres(:,2),P12_1(:,3),P12_1(:,2),1,4,1);

[P16_RESULTS] = CO2SYS(pH_1(:,3),P16_1(:,4),3,2,june12_ctd.sal(:,3),25,...
    june12_ctd.temp(:,3),0,june12_ctd.pres(:,3),P16_1(:,3),P16_1(:,2),1,4,1);

[P20_RESULTS] = CO2SYS(pH_1(:,4),P20_1(:,4),3,2,june12_ctd.sal(:,4),25,...
    june12_ctd.temp(:,4),0,june12_ctd.pres(:,4),P20_1(:,3),P20_1(:,2),1,4,1);

[P26_RESULTS] = CO2SYS(pH_1(:,5),P26_1(:,4),3,2,june12_ctd.sal(:,5),25,...
    june12_ctd.temp(:,5),0,june12_ctd.pres(:,5),P26_1(:,3),P26_1(:,2),1,4,1);

% now pull out the in situ pH, i.e. column 18:
pH_situ = [P4_RESULTS(:,18),P12_RESULTS(:,18),P16_RESULTS(:,18),...
    P20_RESULTS(:,18),P26_RESULTS(:,18)];

% to get OH- concentration from pH, calculate Kw ==========================

% need T and I as input:
% temperature
T = 273.15 + june12_ctd.temp;    % K

% ionic strength based on salinity; eqn from Millero et al. 1987, Table 1:
I = 19.9201.*june12_ctd.sal./(10.^3 - 1.00488.*june12_ctd.sal);

% then calculate Kw following Millero et al. 1987, eqn 33;
ln_Kw = 148.9802 - 13847.26./T - 23.6521.*log(T) + 2.*(sqrt(I)./(1+1.2.*sqrt(I)))...
    + 1.667.*log(1+1.2.*sqrt(I))) .* (-5.8901 + 228.2338./T + 0.968144.*log(T))...
    - I.*(20.6365 - 945.556./T - 3.00298.*log(T)) - 0.18602.*(1-(1+2.*sqrt(I)...
     - 2.*I).*exp(-2.*sqrt(I))) - (I.^2).*(-0.05346 + 17.6216./T);
Kw = exp(ln_Kw);

% then correct Kw for pressure effects following Millero 1995;
% first the relevant constants from eqns 91 and 92:
del_V = -25.6 + 0.2324.*june12_ctd.temp - 3.6246.*0.001.*(june12_ctd.temp.^2);
del_K = (-5.13 + 0.0794.*june12_ctd.temp) .* 0.001;
% order of magnitude correction of del_K based on Millero 2001, p.372
R = 83.131;                         % Millero 1995
P = 0.1.*june12_ctd.pres;           % bar
% and then the equation to calculate corrected Kw (Millero 1995, eqn 90):
ln_KwP = -(del_V./(R.*T)).*P + (0.5.*del_K./(R.*T)).*(P.^2) + ln_Kw;
KwP = exp(ln_KwP);

% finally use Kw to calculate OH- concentration from pH:
OH = KwP ./ (10.^-pH_situ);

% calculate k for Fe(II) oxidation by O2, then Fe(II) half-lives =========

% calculate k, according to Millero et al. 1987 (eqns in the abstract):
logk = (21.56 - (1545./T)) - 3.29.*sqrt(I) + (1.52.*I);
k = 10.^logk;

% get the oxygen concentration in the right units, from CTD data
O2 = june12_ctd.oxy.*1e-6;

% and then calculate k_prime, also based on Millero et al. 1987, eqn 2:
k_prime = k.*(OH.^2).*O2;

% then use k_prim to calculate Fe(II) half-life:
t_half = 0.693./(k_prime);          % minutes
t_half = t_half./60;                % hours
```

Figure B.4: MATLAB code for calculation of Fe(II) half-lives following Millero et al. (1987)

Appendix C

Methods and Supplementary Figures for Chapter 5

C.1 Dissolved Fe and Fe(II)

The methods for the measurement of dFe and Fe(II) in June 2012 and August 2013 are described in Chapter 3, Sections 3.3.3 and 3.3.4. The historic dFe data from OSP were measured at sea by the Institute of Ocean Sciences in Sidney, Canada, on 16 cruises between 2000 and 2011 on filtered samples (0.2 μm) that had been buffered to pH 3.2 for 1–2 h prior to measurement (see Johnson et al., 2005). Comparisons to dFe data measured following GEOTRACES protocols show that the two measurements are comparable (Ross et al., manuscript in preparation).

C.2 Dissolved Oxygen and Fe(II) half-life

Dissolved oxygen concentrations were measured with a Sea-Bird Electronics dissolved oxygen sensor (SBE 43) on the CTD package of the CCGS John P. Tully in June 2012, which was calibrated against Winkler titration measurements. The calculation of Fe(II) half-life is described in detail in Section B.4.

C.3 Silicic acid and chlorophyll *a*

Silicic acid ($Si(OH)_4$) concentrations were measured on fresh samples at sea using a Technicon AutoAnalyzer (Barwell-Clarke and Whitney, 1996; Strickland and Parsons,

1972). Samples for discrete chlorophyll *a* analysis were filtered onto Whatman GF/F filters and extracted with 90% acetone prior to fluorometric analysis (Strickland and Parsons, 1972).

C.4 UV Aerosol Index

UV Aerosol Index data were downloaded from the Giovanni OMI/Aura Online Visualization and Analysis website. The UV Aerosol Index is calculated based on the difference between observations and model calculations of spectral radiance ratios in the UV (see http://disc.sci.gsfc.nasa.gov/giovanni/additional/data-holdings/PIP/aerosol_index.shtml for details). This index indicates the presence of aerosols such as dust and soot that absorb in the UV.

C.5 Profiling float

Quality-controlled data for profiling float 7601StnP were downloaded from http://www.mbari.org/chemsensor/FloatViz.htm. The float was equipped with a WETLabs fluorometer/backscatter sensor (ECO FLbb-AP2) and an in situ ultraviolet spectrophotometer (ISUS) for nitrate measurements (Johnson and Coletti, 2002). Floats are programmed to profile the upper 1000 m of the water column every 5–6 days.

Chl *a* concentrations were estimated from fluorescence measurements using the scale factor supplied by the manufacturer as follows: Chlorophyll *a* [μg L^{-1}] = (sensor output − dark counts) [counts] * scale factor [μg chl *a* L^{-1} $count^{-1}$]. No attempt was made to correct for daytime fluorescence quenching. Near the surface, nonphotochemical quenching may reduce phytoplankton fluorescence (Xing et al., 2012), which can lead to an underestimation of near-surface chl *a* concentrations that we have not accounted for in our analysis. However, the bias would apply to the entire dataset, so a comparison between data from 2012 and 2013 is still valid. A relief of Fe limitation following the aerosol deposition event could also decrease the fluorescence emission per unit chlorophyll (Behrenfeld et al., 2009; Westberry et al., 2013), which would again cause an underestimation of chl *a* concentration by the float.

C.6 Sea surface height anomaly

The sea surface height anomaly (SSHA) image for June 3 was downloaded from the Colorado Center for Astrodynamics Research (CCAR) Global Historical Gridded SSH Data Viewer website. The SSHA product merges data from multiple altimetry satellites.

C.7 Mooring data

Data from the NOAA-PMEL mooring at OSP were downloaded at http://www.pmel.noaa.gov/OCS/data/disdel_v2/disdel_v2.html. The mooring was equipped with a rain gage, a Gill sonic anemometer, and a number of Sea-Bird Electronics temperature, conductivity and pressure sensors (SBE 37 TC, SBE 51 TC, SBE 39 TP).

C.8 Satellite chlorophyll *a*

The MODIS near-surface chl *a* composite for May 8 − June 1, 2012, was downloaded using the Giovanni Ocean Color data portal. The algorithm for deriving chl *a* from the MODIS satellite sensor (OC3M) is based on reflectance ratios in the blue and green wavelengths of the visible spectrum and is thus not susceptible to the quenching-related biases that fluorescence-based chl *a* estimates suffer from.

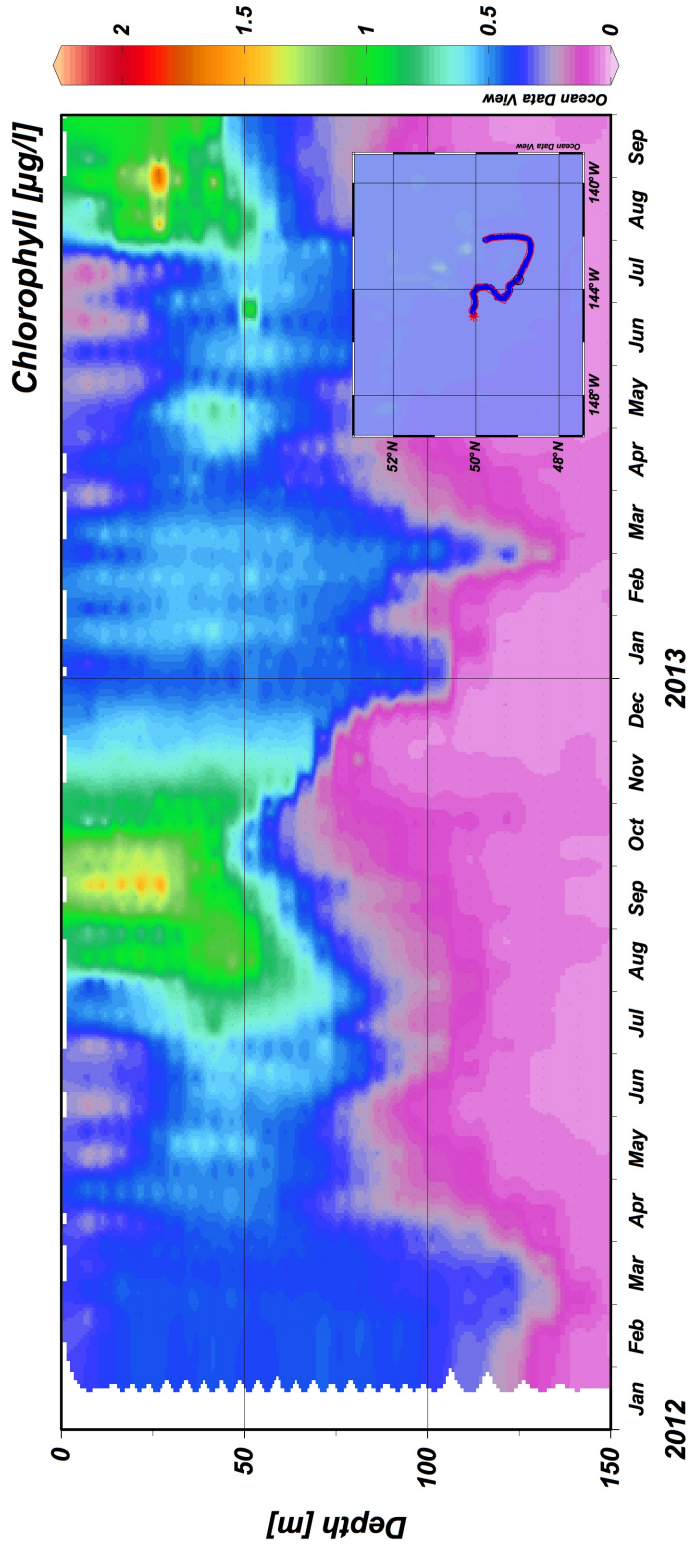

Figure C.1: Chlorophyll a concentration (μg L^{-1}) in the upper 150 m as measured by APEX float 7601StnP deployed in February 2012 near OSP. Float location during the deployment is indicated on the map insert. Data courtesy of MBARI.

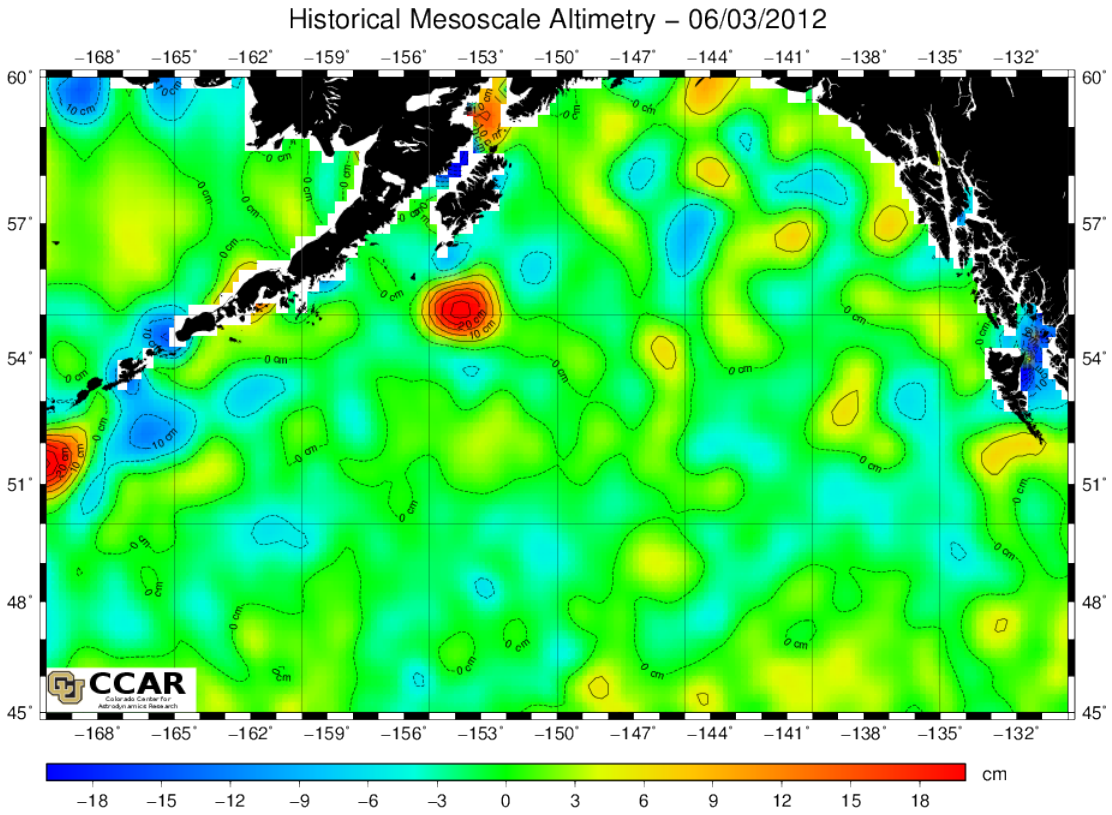

Figure C.2: Sea surface height anomaly (SSHA) image for the subarctic NE Pacific from June 3, 2012. Note the absence of an eddy signature at OSP (50°N, 145°W). The weak SSHA feature south-west of OSP first appeared in mid-April 2012 and is not a remnant eddy.

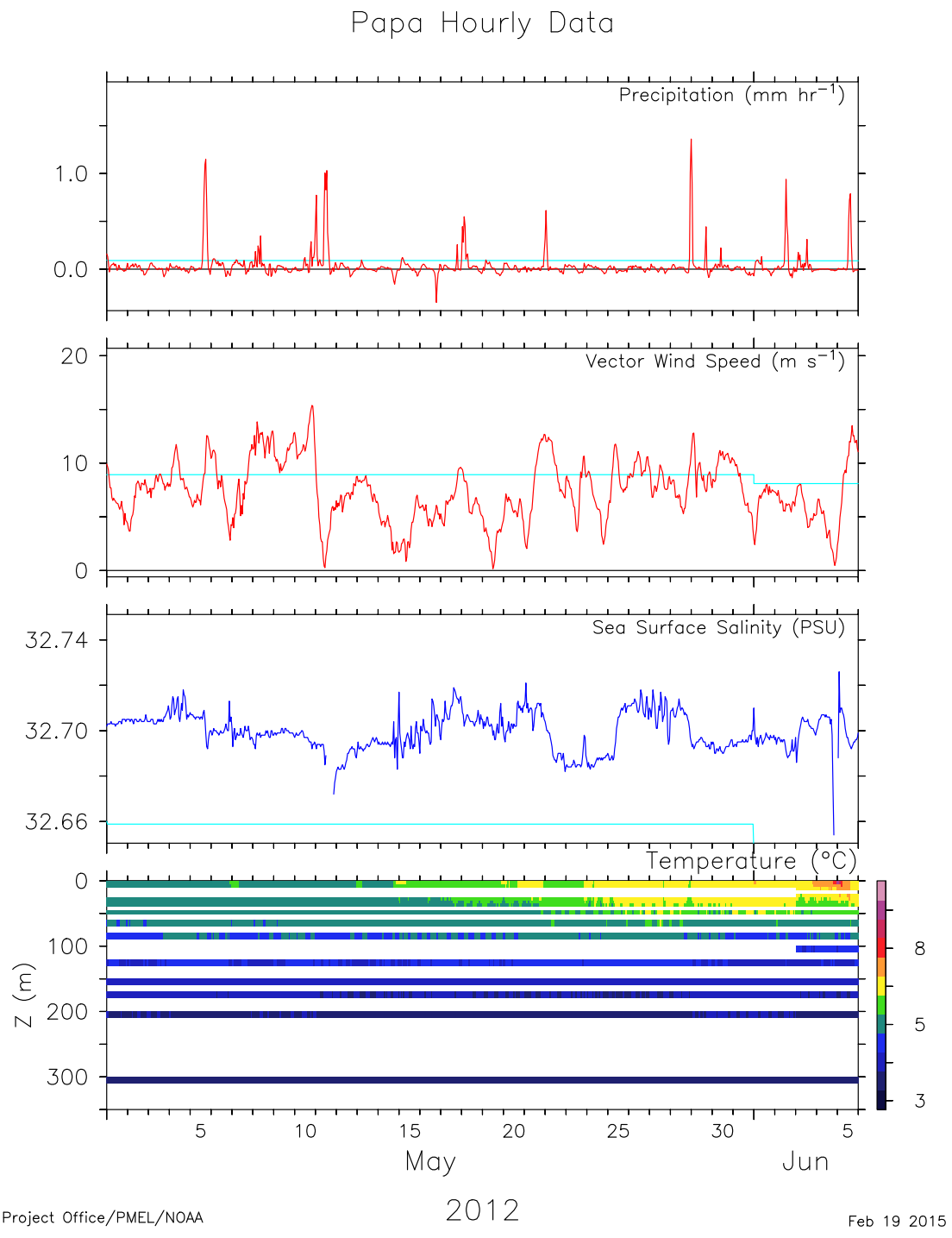

Figure C.3: Time series data from the NOAA-PMEL mooring at OSP for May and early June 2012: Precipitation, wind speed, sea surface salinity and temperature in the top 300 m of the water column. Cyan lines on top 3 panels indicate monthly climatologies (for details, see http://www.pmel.noaa.gov/tao/clim/clim-info.html). Data downloaded from http://www.pmel.noaa.gov/OCS/data/disdel_v2/disdel_v2.html.

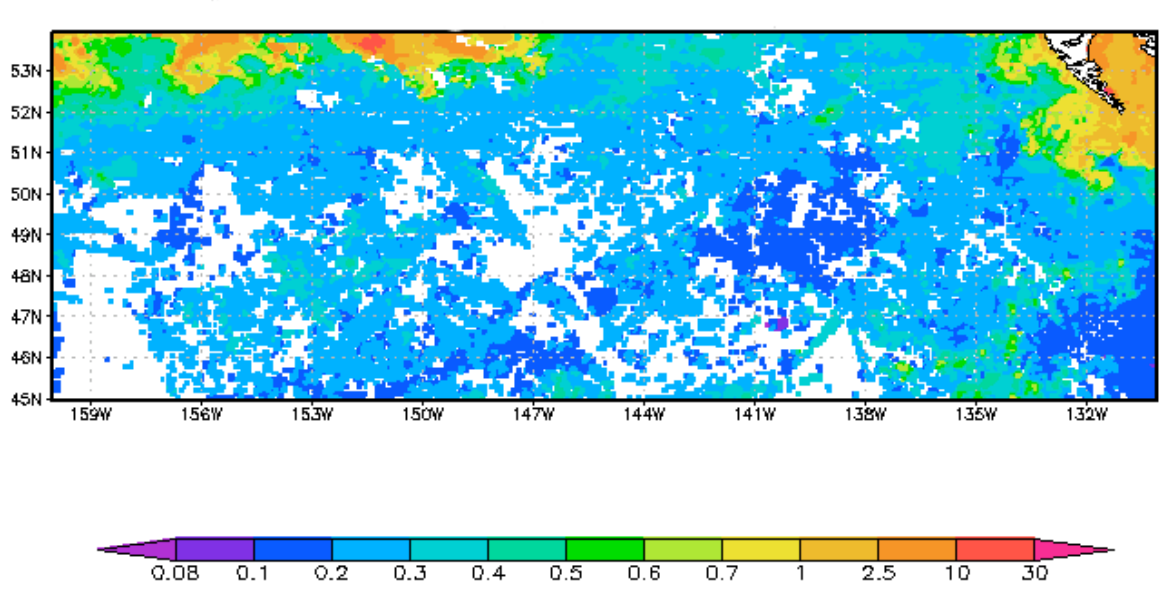

Figure C.4: MODIS near-surface chl a (mg m^{-3}) composite for May 8 – June 1, 2012

Bibliography

Aguilar-Islas, A. M., Wu, J., Rember, R., Johansen, A. M., and Shank, L. M. (2010). Dissolution of aerosol-derived iron in seawater: Leach solution chemistry, aerosol type, and colloidal iron fraction. *Marine Chemistry*, 120(1-4):25–33, doi:10.1016/j.marchem.2009.01.011.

Arrigo, K. R. and van Dijken, G. L. (2011). Secular trends in Arctic Ocean net primary production. *Journal of Geophysical Research*, 116(C09011), doi:10.1029/2011JC007151.

Arrigo, K. R., van Dijken, G. L., and Bushinsky, S. (2008). Primary production in the Southern Ocean, 19972006. *Journal of Geophysical Research*, 113(C8):C08004, doi:10.1029/2007JC004551.

Baker, A. and Croot, P. (2010). Atmospheric and marine controls on aerosol iron solubility in seawater. *Marine Chemistry*, 120:4–13, doi:10.1016/j.marchem.2008.09.003.

Barbeau, K., Rue, E. L., Bruland, K. W., and Butler, A. (2001). Photochemical cycling of iron in the surface ocean mediated by microbial iron(III)-binding ligands. *Nature*, 413:409–13, doi:10.1038/35096545.

Barnes, P. W. and Lien, R. (1988). Icebergs rework shelf sediments to 500 m off Antarctica. *Geology*, 16:1130–1133, doi:10.1130/0091-7613(1988)016¡1130.

Barwell-Clarke, J. and Whitney, F. (1996). Institute of Ocean Sciences nutrient methods and analysis. *Canadian Technical Report of Hydrography and Ocean Sciences*, 182.

Behrenfeld, M. J., Westberry, T. K., Boss, E. S., O'Malley, R. T., Siegel, D. a., Wiggert, J. D., Franz, B. a., McClain, C. R., Feldman, G. C., Doney, S. C., Moore,

J. K., Dall'Olmo, G., Milligan, a. J., Lima, I., and Mahowald, N. (2009). Satellite-detected fluorescence reveals global physiology of ocean phytoplankton. *Biogeosciences*, 6(5):779–794, doi:10.5194/bg-6-779-2009.

Berelson, W., McManus, J., Coale, K., Johnson, K., Burdige, D., Kilgore, T., Colodner, D., Chavez, F., Kudela, R., and Boucher, J. (2003). A time series of benthic flux measurements from Monterey Bay, CA. *Continental Shelf Research*, 23(5):457–481, doi:10.1016/S0278-4343(03)00009-8.

Bergquist, B. A., Wu, J., and Boyle, E. A. (2007). Variability in oceanic dissolved iron is dominated by the colloidal fraction. *Geochimica et Cosmochimica Acta*, 71(12):2960–2974, doi:10.1016/j.gca.2007.03.013.

Bertschi, I. T., Jaffe, D. A., Jaeglé, L., Price, H. U., and Dennison, J. B. (2004). PHOBEA/ITCT 2002 airborne observations of transpacific transport of ozone, CO, volatile organic compounds, and aerosols to the northeast Pacific: Impacts of Asian anthropogenic and Siberian boreal fire emissions. *Journal of Geophysical Research: Atmospheres*, 109(D23S12):1–16, doi:10.1029/2003JD004328.

Bielski, B., Cabelli, D., Arudi, R., and Ross, A. (1985). Reactivity of HO_2/O_2^- radicals in aqueous solutions. *J Phys Chem Ref Data*, 14(4).

Bindoff, N., Rosenberg, M., and Warner, M. (2000). On the circulation and water masses over the Antarctic continental slope and rise between 80 and 150°E. *Deep-Sea Research II*, 47:2299–2326.

Bishop, J. K. B., Davis, R. E., and Sherman, J. T. (2002). Robotic observations of dust storm enhancement of carbon biomass in the North Pacific. *Science*, 298(5594):817–21, doi:10.1126/science.1074961.

Blain, S., Quéguiner, B., Armand, L., Belviso, S., Bombled, B., Bopp, L., Bowie, A., Brunet, C., Brussaard, C., Carlotti, F., Christaki, U., Corbière, A., Durand, I., Ebersbach, F., Fuda, J.-L., Garcia, N., Gerringa, L., Griffiths, B., Guigue, C., Guillerm, C., Jacquet, S., Jeandel, C., Laan, P., Lefèvre, D., Lo Monaco, C., Malits, A., Mosseri, J., Obernosterer, I., Park, Y.-H., Picheral, M., Pondaven, P., Remenyi, T., Sandroni, V., Sarthou, G., Savoye, N., Scouarnec, L., Souhaut, M., Thuiller, D., Timmermans, K., Trull, T., Uitz, J., van Beek, P., Veldhuis, M., Vincent, D.,

Viollier, E., Vong, L., and Wagener, T. (2007). Effect of natural iron fertilization on carbon sequestration in the Southern Ocean. *Nature*, 446(7139):1070–4, doi:10.1038/nature05700.

Borer, P. M., Sulzberger, B., Reichard, P., and Kraemer, S. M. (2005). Effect of siderophores on the light-induced dissolution of colloidal iron(III) (hydr)oxides. *Marine Chemistry*, 93(2-4):179–193, doi:10.1016/j.marchem.2004.08.006.

Bowie, A., Achterberg, E. E. P., Sedwick, P., Ussher, S., and Worsfold, P. (2002). Real-time monitoring of picomolar concentrations of iron(II) in marine waters using automated flow injection-chemiluminescence instrumentation. *Environmental science & technology*, 36:4600–4607.

Bowie, A. R., Lannuzel, D., Remenyi, T. a., Wagener, T., Lam, P. J., Boyd, P. W., Guieu, C., Townsend, A. T., and Trull, T. W. (2009). Biogeochemical iron budgets of the Southern Ocean south of Australia: Decoupling of iron and nutrient cycles in the subantarctic zone by the summertime supply. *Global Biogeochemical Cycles*, 23, doi:10.1029/2009GB003500.

Boyd, P., Law, C., Wong, C., Nojiri, Y., Tsuda, A., Levasseur, M., Takeda, S., Rivkin, R., Harrison, P., Strzepek, R., Gower, J., McKay, R., Abraham, E., Arychuk, M., Barwell-Clarke, J., Crawford, W., Crawford, D., Hale, M., Harada, K., Johnson, K., Kiyosawa, H., Kudo, I., Marchetti, A., Miller, W., Needoba, J., Nishioka, J., Ogawa, H., Page, J., Robert, M., Saito, H., Sastri, A., Sherry, N., Soutar, T., Sutherland, N., Taira, Y., Whitney, F., Wong, S.-K. E., and Yoshimura, T. (2004). The decline and fate of an iron-induced subarctic phytoplankton bloom. *Nature*, 428:549–553, doi:10.1029/2001JB001129.

Boyd, P., Mackie, D., and Hunter, K. (2010). Aerosol iron deposition to the surface ocean — Modes of iron supply and biological responses. *Marine Chemistry*, 120(1-4):128–143, doi:10.1016/j.marchem.2009.01.008.

Boyd, P., Watson, A., Law, C., Abraham, E., Trull, T., Murdoch, R., Bakker, D., Bowie, A., Buesseler, K., Chang, H., Charette, M., Croot, P., Downing, K., Frew, R., Gall, M., Hadfield, M., Hall, J., Harvey, M., Jameson, G., LaRoche, J., Liddicoat, M., Ling, R., Maldonado, M., McKay, R., Nodder, S., Pickmere, S., Pridmore, R., Rintoul, S., Safi, K., Sutton, P., Strzepek, R., Tanneberger, K., Turner, S., Waite, A., and Zeldis, J. (2000). A mesoscale phytoplankton bloom

in the polar Southern Ocean stimulated by iron fertilization. *Nature*, 407:695–702, doi:10.1038/35037500.

Boyd, P., Wong, C., Merrill, J., Whitney, F., Snow, J., Harrison, P., and Gower, J. (1998). Atmospheric iron supply and enhanced vertical carbon flux in the NE subarctic Pacific: Is there a connection? *Global Biogeochemical Cycles*, 12(3):429–441.

Boyd, P. W. and Ellwood, M. J. (2010). The biogeochemical cycle of iron in the ocean. *Nature Geoscience*, 3:675–682, doi:10.1038/ngeo964.

Boyd, P. W., Jickells, T., Law, C. S., Blain, S., Boyle, E. A., Buesseler, K. O., Coale, K. H., Cullen, J. J., de Baar, H. J. W., Follows, M., Harvey, M., Lancelot, C., Levasseur, M., Owens, N. P. J., Pollard, R., Rivkin, R. B., Sarmiento, J., Schoemann, V., Smetacek, V., Takeda, S., Tsuda, A., Turner, S., and Watson, A. J. (2007). Mesoscale iron enrichment experiments 1993-2005: Synthesis and future directions. *Science*, 315(5812):612–7, doi:10.1126/science.1131669.

Boye, M., van den Berg, C. M., de Jong, J. T., Leach, H., Croot, P., and de Baar, H. J. (2001). Organic complexation of iron in the Southern Ocean. *Deep-Sea Research I*, 48:1477–1497, doi:10.1016/S0967-0637(00)00099-6.

Boyle, E., Edmond, J., and Sholkovitz, E. (1977). The mechanism of iron removal in estuaries. *Geochimica et Cosmochimica Acta*, 41(9):1313–1324, doi:10.1016/0016-7037(77)90075-8.

Bressac, M., Guieu, C., Doxaran, D., Bourrin, F., Obolensky, G., and Grisoni, J.-M. (2011). A mesocosm experiment coupled with optical measurements to assess the fate and sinking of atmospheric particles in clear oligotrophic waters. *Geo-Marine Letters*, 32(2):153–164, doi:10.1007/s00367-011-0269-4.

Brévière, E., Metzl, N., Poisson, A., and Tilbrook, B. (2006). Changes of the oceanic CO_2 sink in the Eastern Indian sector of the Southern Ocean. *Tellus B*, 58(5):438–446, doi:10.1111/j.1600-0889.2006.00220.x.

Brown, M. T., Lippiatt, S. M., Lohan, M. C., and Bruland, K. W. (2012). Trace metal distributions within a Sitka eddy in the northern Gulf of Alaska. *Limnology and Oceanography*, 57(2):503–518, doi:10.4319/lo.2012.57.2.0503.

Brust, J., Schulz-Bull, D. E., Leipe, T., Chavagnac, V., and Waniek, J. J. (2011). Descending particles: From the atmosphere to the deep ocean—A time series study in the subtropical NE Atlantic. *Geophysical Research Letters*, 38(6), doi:10.1029/2010GL045399.

Buck, C. S., Landing, W. M., and Resing, J. (2013). Pacific Ocean aerosols: Deposition and solubility of iron, aluminum, and other trace elements. *Marine Chemistry*, 157:117–130, doi:10.1016/j.marchem.2013.09.005.

Buck, C. S., Landing, W. M., Resing, J. a., and Lebon, G. T. (2006). Aerosol iron and aluminum solubility in the northwest Pacific Ocean: Results from the 2002 IOC cruise. *Geochemistry, Geophysics, Geosystems*, 7(4):n/a–n/a, doi:10.1029/2005GC000977.

Buck, K. N., Lohan, M. C., Berger, C. J. M., and Bruland, K. W. (2007). Dissolved iron speciation in two distinct river plumes and an estuary: Implications for riverine iron supply. *Limnology and Oceanography*, 52(2):843–855.

Buesseler, K., Pike, S., Maiti, K., Lamborg, C., Siegel, D., and Trull, T. (2009). Thorium-234 as a tracer of spatial, temporal and vertical variability in particle flux in the North Pacific. *Deep-Sea Research I*, 56(7):1143–1167, doi:10.1016/j.dsr.2009.04.001.

Buesseler, K. O., Antia, A. N., Chen, M., Fowler, S. W., Gardner, W. D., Gustafsson, O., Harada, K., Michaels, A. F., Rutgers van der Loeff, M., Sarin, M., Steinberg, D. K., and Trull, T. (2007). An assessment of the use of sediment traps for estimating upper ocean particle fluxes. *Journal of Marine Research*, 65(3):345–416, doi:10.1357/002224007781567621.

Burns, J. M., Cooper, W. J., Ferry, J. L., King, D. W., DiMento, B. P., McNeill, K., Miller, C. J., Miller, W. L., Peake, B. M., Rusak, S. A., Rose, A. L., and Waite, T. D. (2012). Methods for reactive oxygen species (ROS) detection in aqueous environments. *Aquatic Sciences*, 74(4):683–734, doi:10.1007/s00027-012-0251-x.

Butler, A. and Theisen, R. M. (2010). Iron(III)-siderophore coordination chemistry: Reactivity of marine siderophores. *Coordination chemistry reviews*, 254(3-4):288–296, doi:10.1016/j.ccr.2009.09.010.

Canfield, E. (1988). Reactive iron in marine sediments. *Geochimica et Cosmochimica Acta*, 53:619–632.

Carvalho, F., Oliveira, J., and Malta, M. (2014). Exposure to radionuclides in smoke from vegetation fires. *Science of The Total Environment*, 472:421–424.

Chase, Z., Hales, B., Cowles, T., Schwartz, R., and van Geen, A. (2005a). Distribution and variability of iron input to Oregon coastal waters during the upwelling season. *Journal of Geophysical Research*, 110:1–14, doi:10.1029/2004JC002590.

Chase, Z., Johnson, K. S., Elrod, V. A., Plant, J. N., Fitzwater, S. E., Pickell, L., and Sakamoto, C. M. (2005b). Manganese and iron distributions off central California influenced by upwelling and shelf width. *Marine Chemistry*, 95:235–254, doi:10.1016/j.marchem.2004.09.006.

Chase, Z., Strutton, P. G., and Hales, B. (2007). Iron links river runoff and shelf width to phytoplankton biomass along the U.S. West Coast. *Geophysical Research Letters*, 34, doi:10.1029/2006GL028069.

Chen, H., Laskin, A., Baltrusaitis, J., Gorski, C. a., Scherer, M. M., and Grassian, V. H. (2012). Coal fly ash as a source of iron in atmospheric dust. *Environmental science & technology*, 46(4):2112–20, doi:10.1021/es204102f.

Chen, M. and Wang, W.-X. (2001). Bioavailability of natural colloid-bound iron to marine plankton: Influences of colloidal size and aging. *Limnology and Oceanography*, 46(8):1956–1967, doi:10.4319/lo.2001.46.8.1956.

Chen, Y. and Siefert, R. L. (2003). Determination of various types of labile atmospheric iron over remote oceans. *Journal of Geophysical Research: Atmospheres*, 108(D24), doi:10.1029/2003JD003515.

Chever, F., Bucciarelli, E., Sarthou, G., Speich, S., Arhan, M., Penven, P., and Tagliabue, A. (2010). Physical speciation of iron in the Atlantic sector of the Southern Ocean along a transect from the subtropical domain to the Weddell Sea Gyre. *Journal of Geophysical Research*, 115(C10059), doi:10.1029/2009JC005880.

Coale, K. H., Gordon, M. R., and Wang, X. (2005). The distribution and behavior of dissolved and particulate iron and zinc in the Ross Sea and Antarctic circumpolar current along 170°W. *Deep-Sea Research I*, 52:295–318, doi:10.1016/j.dsr.2004.09.008.

Coale, K. H., Johnson, K. S., Chavez, F. P., Buesseler, K. O., Barber, R. T., Brzezinski, M. A., Cochlan, W. P., Millero, F. J., Falkowski, P. G., Bauer, J. E., Wanninkhof, R. H., Kudela, R. M., Altabet, M. A., Hales, B. E., Takahashi, T., Landry, M. R., Bidigare, R. R., Wang, X., Chase, Z., Strutton, P. G., Friederich, G. E., Gorbunov, M. Y., Lance, V. P., Hilting, A. K., Hiscock, M. R., Demarest, M., Hiscock, W. T., Sullivan, K. F., Tanner, S. J., Gordon, R. M., Hunter, C. N., Elrod, V. A., Fitzwater, S. E., Jones, J. L., Tozzi, S., Koblizek, M., Roberts, A. E., Herndon, J., Brewster, J., Ladizinsky, N., Smith, G., Cooper, D., Timothy, D., Brown, S. L., and Selph, K. E. (2004). Southern Ocean iron enrichment experiment: Carbon cycling in high- and low-Si waters. *Science*, 304:408–414.

Cochran, J. K., Miquel, J. C., Armstrong, R., Fowler, S. W., Masqué, P., Gasser, B., Hirschberg, D., Szlosek, J., Rodriguez y Baena, A. M., Verdeny, E., and Stewart, G. M. (2009). Time-series measurements of ^{234}Th in water column and sediment trap samples from the northwestern Mediterranean Sea. *Deep-Sea Research II*, 56(18):1487–1501, doi:10.1016/j.dsr2.2008.12.034.

Comiso, J. (2010). Variability and trends of the global sea ice cover. In Thomas, D. and Dieckmann, G., editors, *Sea Ice*, pages 205–246. Wiley-Blackwell, Oxford.

Conway, T. M. and John, S. G. (2014). Quantification of dissolved iron sources to the North Atlantic Ocean. *Nature*, 511(7508):212–215, doi:10.1038/nature13482.

Cottle, P., Strawbridge, K., and McKendry, I. (2014). Long-range transport of Siberian wildfire smoke to British Columbia: Lidar observations and air quality impacts. *Atmospheric Environment*, 90:71–77, doi:10.1016/j.atmosenv.2014.03.005.

Crawford, R. and Dewey, R. K. (1989). Turbulence and mixing: Sources of nutrients on the Vancouver Island continental shelf. *Atmosphere Ocean*, 27(2):428–442.

Croot, P., Bowie, A., Frew, R., Maldonado, M., Hall, J., Safi, K., La Roche, J., Boyd, P., and Law, C. (2001). Retention of dissolved iron and FeII in an iron induced Southern Ocean phytoplankton bloom. *Geophysical Research Letters*, 28(18):3425–3428.

Croot, P. L., Andersson, K., Öztürk, M., and Turner, D. R. (2004a). The distribution and speciation of iron along 6°E in the Southern Ocean. *Deep-Sea Research II*, 51:2857–2879, doi:10.1016/j.dsr2.2003.10.012.

Croot, P. L., Bluhm, K., Schlosser, C., Streu, P., Breitbarth, E., Frew, R., and Van Ardelan, M. (2008). Regeneration of Fe(II) during EIFeX and SOFeX. *Geophysical Research Letters*, 35(L19606), doi:10.1029/2008GL035063.

Croot, P. L., Frew, R. D., Sander, S., Hunter, K. A., Ellwood, M. J., Pickmere, S. E., Abraham, E. R., Law, C. S., Smith, M. J., and Boyd, P. W. (2007). Physical mixing effects on iron biogeochemical cycling: FeCycle experiment. *Journal of Geophysical Research*, 112(C06015), doi:10.1029/2006JC003748.

Croot, P. L. and Laan, P. (2002). Continuous shipboard determination of Fe(II) in polar waters using flow injection analysis with chemiluminescence detection. *Analytica Chimica Acta*, 466:261–273, doi:10.1016/S0003-2670(02)00596-2.

Croot, P. L., Streu, P., and Baker, A. R. (2004b). Short residence time for iron in surface seawater impacted by atmospheric dry deposition from Saharan dust events. *Geophysical Research Letters*, 31(23), doi:10.1029/2004GL020153.

Crusius, J., Schroth, A. W., Gassó, S., Moy, C. M., Levy, R. C., and Gatica, M. (2011). Glacial flour dust storms in the Gulf of Alaska: Hydrologic and meteorological controls and their importance as a source of bioavailable iron. *Geophysical Research Letters*, 38(6), doi:10.1029/2010GL046573.

Cullen, J. T., Bergquist, B. A., and Moffett, J. W. (2006). Thermodynamic characterization of the partitioning of iron between soluble and colloidal species in the Atlantic Ocean. *Marine Chemistry*, 98(2-4):295–303, doi:10.1016/j.marchem.2005.10.007.

Cullen, J. T., Chong, M., and Ianson, D. (2009). British Columbian continental shelf as a source of dissolved iron to the subarctic northeast Pacific Ocean. *Global Biogeochemical Cycles*, 23(4):GB4012, doi:10.1029/2008GB003326.

Cutter, G., Andersson, P., Codispoti, L., Croot, P., Francois, R., Lohan, M., Obata, H., and Rutgers van der Loeff, M. (2010). Sampling and sample-handling protocols for GEOTRACES cruises. Technical Report December.

de Baar, H., de Jong, J., Bakker, D., Löscher, B., Veth, C., Bathmann, U., and Smetacek, V. (1995). Importance of iron for plankton blooms and carbon dioxide drawdown in the Southern Ocean. *Nature*, 373:412–415.

de Jong, J., den Das, J., Bathmann, U., Stoll, M., Kattner, G., Nolting, R., and de Baar, H. (1998). Dissolved iron at subnanomolar levels in the Southern Ocean as determined by ship-board analysis. *Analytica Chimica Acta*, 377:113–124, doi:10.1016/S0003-2670(98)00427-9.

de Jong, J., Schoemann, V., Lannuzel, D., Croot, P., de Baar, H., and Tison, J.-L. (2012). Natural iron fertilization of the Atlantic sector of the Southern Ocean by continental shelf sources of the Antarctic Peninsula. *Journal of Geophysical Research*, 117(G01029), doi:10.1029/2011JG001679.

de Jong, J., Schoemann, V., Maricq, N., Mattielli, N., Langhorne, P., Haskell, T., and Tison, J.-L. (2013). Iron in land-fast sea ice of McMurdo Sound derived from sediment resuspension and wind-blown dust attributes to primary productivity in the Ross Sea, Antarctica. *Marine Chemistry*, 157:24–40, doi:10.1016/j.marchem.2013.07.001.

DeVries, T., Deutsch, C., Primeau, F., Chang, B., and Devol, A. (2012). Global rates of water-column denitrification derived from nitrogen gas measurements. *Nature Geoscience*, 5(8):547–550, doi:10.1038/ngeo1515.

Diaz, J., Hansel, C., and Voelker, B. (2013). Widespread production of extracellular superoxide by heterotrophic bacteria. *Science*, 1223-1226, doi:10.1126/science.1237331.

Dickson, A., Sabine, C., and Christian, J. (2007). Guide to best practices for ocean CO_2 measurements. North Pacific Marine Science Organization, Sidney.

DiTullio, G. and Laws, E. (1991). Impact of an atmospheric-oceanic disturbance on phytoplankton community dynamics in the North Pacific Central Gyre. *Deep-Sea Research A*, 38(10):1305–1329.

Dowdeswell, J. and Bamber, J. (2007). Keel depths of modern Antarctic icebergs and implications for sea-floor scouring in the geological record. *Marine Geology*, 243:120–131, doi:10.1016/j.margeo.2007.04.008.

Duce, R. and Tindale, N. (1991). Atmospheric transport of iron and its deposition in the ocean. *Limnology and Oceanography*, 36(8):1715–1726.

Elrod, V., Berelson, W., Coale, K., and Johnson, K. K. (2004). The flux of iron from continental shelf sediments: A missing source for global budgets. *Geophysical Research Letters*, 31(L12307), doi:10.1029/2004GL020216.

Falkowski, P. G., Barber, R., and Smetacek, V. (1998). Biogeochemical controls and feedbacks on ocean primary production. *Science*, 281:200–206, doi:10.1126/science.281.5374.200.

Fan, S.-M. (2008). Photochemical and biochemical controls on reactive oxygen and iron speciation in the pelagic surface ocean. *Marine Chemistry*, 109(1-2):152–164, doi:10.1016/j.marchem.2008.01.005.

Fitch, D. T. and Moore, J. K. (2007). Wind speed influence on phytoplankton bloom dynamics in the Southern Ocean Marginal Ice Zone. *Journal of Geophysical Research*, 112(C8):C08006, doi:10.1029/2006JC004061.

Fu, H., Cwiertny, D. M., Carmichael, G. R., Scherer, M. M., and Grassian, V. H. (2010). Photoreductive dissolution of Fe-containing mineral dust particles in acidic media. *Journal of Geophysical Research*, 115(D11):D11304, doi:10.1029/2009JD012702.

Fu, H. B., Shang, G. F., Lin, J., Hu, Y. J., Hu, Q. Q., Guo, L., Zhang, Y. C., and Chen, J. M. (2014). Fractional iron solubility of aerosol particles enhanced by biomass burning and ship emission in Shanghai, East China. *The Science of the total environment*, 481:377–91, doi:10.1016/j.scitotenv.2014.01.118.

Fujii, M., Rose, A. L., Waite, T. D., and Omura, T. (2006). Superoxide-mediated dissolution of amorphous ferric oxyhydroxide in seawater. *Environmental science & technology*, 40(3):880–7.

Fujimori, K., Nakajima, H., Akutsu, K., Mitani, M., Sawada, H., and Nakayama, M. (1993). Chemiluminescence of Cypridina Luciferin Analogues. Part 1. Effect of pH on rates of spontaneous autoxidation of CLA in aqueous buffer solutions. *J. Chem. Soc. Perkin Trans.*, 2:2405–2409.

Garg, S., Rose, A. L., Godrant, A., and Waite, T. D. (2007a). Iron uptake by the ichthyotoxic *Chattonella marina* (Raphidophyceae): impact of superoxide generation[1]. *Journal of Phycology*, 43(5):978–991, doi:10.1111/j.1529-8817.2007.00394.x.

Garg, S., Rose, A. L., and Waite, T. D. (2007b). Superoxide mediated reduction of organically complexed iron(III): comparison of non-dissociative and dissociative reduction pathways. *Environmental science & technology*, 41(9):3205–12.

Gaudichet, A., Echalar, F., and Chatenet, B. (1995). Trace elements in tropical African Savanna biomass burning aerosols. *Journal of Atmospheric Chemistry*, 22:19–39.

Gerringa, L., Alderkamp, A.-C., Laan, P., Thuróczy, C.-E., de Baar, H. J., Mills, M. M., van Dijken, G. L., van Haren, H., and Arrigo, K. R. (2012). Iron from melting glaciers fuels the phytoplankton blooms in Amundsen Sea (Southern Ocean): Iron biogeochemistry. *Deep-Sea Research II*, 71-76:16–31, doi:10.1016/j.dsr2.2012.03.007.

Gerringa, L., Blain, S., Laan, P., Sarthou, G., Veldhuis, M., Brussaard, C., Viollier, E., and Timmermans, K. (2008). Fe-binding dissolved organic ligands near the Kerguelen Archipelago in the Southern Ocean (Indian sector). *Deep-Sea Research II*, 55:606–621, doi:10.1016/j.dsr2.2007.12.007.

Gledhill, M. and Buck, K. N. (2012). The organic complexation of iron in the marine environment: a review. *Frontiers in microbiology*, 3:1–17, doi:10.3389/fmicb.2012.00069.

Gledhill, M. and van den Berg, C. M. (1994). Determination of complexation of iron(III) with natural organic complexing ligands in seawater using cathodic stripping voltammetry. *Marine Chemistry*, 47:41–54, doi:10.1016/0304-4203(94)90012-4.

Golden, K., Ackley, S., and Lytle, V. (1998). The percolation phase transition in sea Ice. *Science*, 282:2238–41.

Goldstone, J. and Voelker, B. (2000). Chemistry of superoxide radical in seawater: CDOM associated sink of superoxide in coastal waters. *Environmental science & technology*, 34(6):1043–1048.

Guieu, C. (2005). Biomass burning as a source of dissolved iron to the open ocean? *Geophysical Research Letters*, 32(19):L19608, doi:10.1029/2005GL022962.

Hamme, R. C., Webley, P. W., Crawford, W. R., Whitney, F. A., DeGrandpre, M. D., Emerson, S. R., Eriksen, C. C., Giesbrecht, K. E., Gower, J. F. R., Kavanaugh, M. T., Peña, M. A., Sabine, C. L., Batten, S. D., Coogan, L. A., Grundle, D. S., and Lockwood, D. (2010). Volcanic ash fuels anomalous plankton bloom in subarctic northeast Pacific. *Geophysical Research Letters*, 37(19):1–5, doi:10.1029/2010GL044629.

Hansard, S. and Landing, W. (2009). Determination of iron(II) in acidified seawater samples by luminol chemiluminescence. *Limnology and Oceanography: Methods*, 7:222–234.

Hansard, S., Landing, W., Measures, C., and Voelker, B. (2009). Dissolved iron(II) in the Pacific Ocean: Measurements from the PO2 and P16N CLIVAR/CO2 repeat hydrography expeditions. *Deep-Sea Research I*, 56(7):1117–1129, doi:10.1016/j.dsr.2009.03.006.

Hansard, S., Vermilyea, A., and Voelker, B. (2010). Measurements of superoxide radical concentration and decay kinetics in the Gulf of Alaska. *Deep-Sea Research I*, 57(9):1111–1119, doi:10.1016/j.dsr.2010.05.007.

Hassler, C., Alasonati, E., Manusco Nichols, C., and Slaveykova, V. (2011a). Exopolysaccharides produced by bacteria isolated from the pelagic Southern Ocean Role in Fe binding, chemical reactivity, and bioavailability. *Marine Chemistry*, 123:88–98, doi:10.1016/j.marchem.2010.10.003.

Hassler, C., Schoemann, V., Mancuso Nichols, C., Butler, E., and Boyd, P. (2011b). Saccharides enhance iron bioavailability to Southern Ocean phytoplankton. *PNAS*, 108(3):1076–81, doi:10.1073/pnas.1010963108.

Hatta, M., Measures, C., Selph, K., Zhou, M., and Hiscock, W. (2013). Iron fluxes from the shelf regions near the South Shetland Islands in the Drake Passage during the austral-winter 2006. *Deep-Sea Research II*, 90:89–101, doi:10.1016/j.dsr2.2012.11.003.

Heller, M. and Croot, P. (2011). Superoxide decay as a probe for speciation changes during dust dissolution in Tropical Atlantic surface waters near Cape Verde. *Marine Chemistry*, 126(1-4):37–55, doi:10.1016/j.marchem.2011.03.006.

Heller, M. I. and Croot, P. L. (2010a). Application of a superoxide (O_2^-) thermal source (SOTS-1) for the determination and calibration of O_2^- fluxes in seawater. *Analytica chimica acta*, 667(1-2):1–13, doi:10.1016/j.aca.2010.03.054.

Heller, M. I. and Croot, P. L. (2010b). Kinetics of superoxide reactions with dissolved organic matter in tropical Atlantic surface waters near Cape Verde (TENATSO). *Journal of Geophysical Research*, 115(C12):C12038, doi:10.1029/2009JC006021.

Heller, M. I. and Croot, P. L. (2010c). Superoxide decay kinetics in the Southern Ocean. *Environmental science & technology*, 44(1):191–6, doi:10.1021/es901766r.

Hickey, B. and Banas, N. (2008). Why is the northern end of the California current system so productive ? *Oceanography*, 21(4):90–107.

Homoky, W. B., John, S. G., Conway, T. M., and Mills, R. A. (2013). Distinct iron isotopic signatures and supply from marine sediment dissolution. *Nature communications*, 4:2143, doi:10.1038/ncomms3143.

Homoky, W. B., Severmann, S., McManus, J., Berelson, W. M., Riedel, T. E., Statham, P. J., and Mills, R. A. (2012). Dissolved oxygen and suspended particles regulate the benthic flux of iron from continental margins. *Marine Chemistry*, 134-135:59–70, doi:10.1016/j.marchem.2012.03.003.

Hong, H. and Kester, D. (1986). Redox state of iron in the offshore waters of Peru. *Limnol. Oceanogr*, 31(3):512–524.

Hopkinson, B. M. and Barbeau, K. A. (2007). Organic and redox speciation of iron in the eastern tropical North Pacific suboxic zone. *Marine Chemistry*, 106(1-2):2–17, doi:10.1016/j.marchem.2006.02.008.

Hopwood, M. J., Statham, P. J., Tranter, M., and Wadham, J. L. (2014). Glacial flours as a potential source of Fe(II) and Fe(III) to polar waters. *Biogeochemistry*, doi:10.1007/s10533-013-9945-y.

Horner, T. J., Williams, H. M., Hein, J. R., Saito, M. A., Burton, K. W., and Halliday, A. N. (2015). Persistence of deeply sourced iron in the Pacific Ocean. *PNAS*, 112(5):1292–1297, doi:10.1073/pnas.1420188112/-/DCSupplemental.www.pnas.org/cgi/doi/10.1073/pnas.1420188112.

Hwang, H. and Ro, C.-u. (2006). Single-particle characterization of Asian Dust certified reference materials using low-Z particle electron probe X-ray microanalysis. *Spectrochimica Acta Part B*, 61(4):400–406, doi:10.1016/j.sab.2006.01.013.

Ibisanmi, E., Sander, S. G., Boyd, P. W., Bowie, A. R., and Hunter, K. A. (2011). Vertical distributions of iron-(III) complexing ligands in the Southern Ocean. *Deep-Sea Research II*, 58:2113–2125, doi:10.1016/j.dsr2.2011.05.028.

Ingold, K. U., Paul, T., Young, M. J., and Doiron, L. (1997). Invention of the first azo compound to serve as a superoxide thermal source under physiological conditions: Concept, synthesis, and chemical properties. *J. Am. Chem. Soc.*, 119(11):12364–12365.

Ito, A. (2011). Mega fire emissions in Siberia: potential supply of bioavailable iron from forests to the ocean. *Biogeosciences*, 8(6):1679–1697, doi:10.5194/bg-8-1679-2011.

Jenkins, A. (1999). The impact of melting ice on ocean waters. *Journal of Physical Oceanography*, 29:2370–2381.

Jickells, T. D., An, Z. S., Andersen, K. K., Baker, A. R., Bergametti, G., Brooks, N., Cao, J. J., Boyd, P. W., Duce, R. A., Hunter, K. A., Kawahata, H., Kubilay, N., LaRoche, J., Liss, P. S., Mahowald, N., Prospero, J. M., Ridgwell, A. J., Tegen, I., and Torres, R. (2005). Global iron connections between desert dust, ocean biogeochemistry, and climate. *Science*, 308:67–71, doi:10.1126/science.1105959.

John, S. G., Mendez, J., Moffett, J., and Adkins, J. (2012). The flux of iron and iron isotopes from San Pedro Basin sediments. *Geochimica et Cosmochimica Acta*, 93:14–29, doi:10.1016/j.gca.2012.06.003.

Johnson, K., Chavez, F., and Friederich, G. (1999). Continental-shelf sediment as a primary source of iron for coastal phytoplankton. *Nature*, 398:697–700.

Johnson, K. S. and Coletti, L. J. (2002). In situ ultraviolet spectrophotometry for high resolution and long-term monitoring of nitrate, bromide and bisulfide in the ocean. *Deep-Sea Research I*, 49(7):1291–1305, doi:10.1016/S0967-0637(02)00020-1.

Johnson, K. W., Miller, L. A., Sutherland, N. E., and Wong, C. (2005). Iron transport by mesoscale Haida eddies in the Gulf of Alaska. *Deep-Sea Research II*, 52(7-8):933–953, doi:10.1016/j.dsr2.2004.08.017.

Journet, E., Desboeufs, K. V., Caquineau, S., and Colin, J.-L. (2008). Mineralogy as a critical factor of dust iron solubility. *Geophysical Research Letters*, 35(7), doi:10.1029/2007GL031589.

Karl, D. and Tilbrook, B. (1994). Production and transport of methane in oceanic particulate organic matter. *Nature*, 368:732–734.

Keeling, R. F., Körtzinger, A., and Gruber, N. (2010). Ocean deoxygenation in a warming world. *Annual Review of Marine Science*, 2(1):199–229, doi:10.1146/annurev.marine.010908.163855.

Keller, M. D., Bellows, W. K., and Guillard, R. R. L. (1988). Microwave treatment for sterilization of phytoplankton culture media. *J. Exp. Mar. Biol. Ecol.*, 117:279–283.

Kieber, D., Toole, D., and Kiene, R. (2009). Chromophoric dissolved organic matter cycling during a Ross Sea *Phaeocystis antarctica* bloom. *Smithsonian at the Poles*, pages 319–333.

Klunder, M., Laan, P., Middag, R., De Baar, H., and van Ooijen, J. (2011). Dissolved iron in the Southern Ocean (Atlantic sector). *Deep-Sea Research II*, 58:2678–2694, doi:10.1016/j.dsr2.2010.10.042.

Klymak, J. M., Crawford, W., Alford, M. H., Mackinnon, J. A., and Pinkel, R. (2015). Along-isopycnal variability of spice in the North Pacific. *Journal of Geophysical Research: Oceans*, 120:1–21, doi:10.1002/2013JC009421.Received.

Kondo, Y. and Moffett, J. W. (2013). Dissolved Fe(II) in the Arabian Sea oxygen minimum zone and western tropical Indian Ocean during the inter-monsoon period. *Deep-Sea Research I*, 73:73–83, doi:10.1016/j.dsr.2012.11.014.

Kraemer, S. M. (2004). Iron oxide dissolution and solubility in the presence of siderophores. *Aquatic Sciences - Research Across Boundaries*, 66(1):3–18, doi:10.1007/s00027-003-0690-5.

Kranzler, C., Lis, H., Shaked, Y., and Keren, N. (2011). The role of reduction in iron uptake processes in a unicellular, planktonic cyanobacterium. *Environmental microbiology*, 13(11):2990–2999, doi:10.1111/j.1462-2920.2011.02572.x.

Kuma, K., Nishioka, J., and Matsunaga, K. (1996). Controls on iron(III) hydroxide solubility in seawater: The influence of pH and natural organic chelators. *Limnology and Oceanography*, 41(3):396–407.

Kustka, A. B., Shaked, Y., Milligan, A. J., King, D. W., and Morel, F. M. M. (2005). Extracellular production of superoxide by marine diatoms: Contrasting effects on iron redox chemistry and bioavailability. *Limnology and Oceanography*, 50(4):1172–1180, doi:10.4319/lo.2005.50.4.1172.

Lam, P. and Bishop, J. K. B. (2008). The continental margin is a key source of iron to the HNLC North Pacific Ocean. *Geophysical Research Letters*, 35(L07608), doi:10.1029/2008GL033294.

Lam, P., Bishop, J. K. B., Henning, C. C., Marcus, M. A., Waychunas, G. A., and Fung, I. Y. (2006). Wintertime phytoplankton bloom in the subarctic Pacific supported by continental margin iron. *Global Biogeochemical Cycles*, 20(GB1006), doi:10.1029/2005GB002557.

Lam, P. J., Ohnemus, D. C., and Marcus, M. A. (2012). The speciation of marine particulate iron adjacent to active and passive continental margins. *Geochimica et Cosmochimica Acta*, 80:108–124, doi:10.1016/j.gca.2011.11.044.

Lancelot, C., de Montety, A., Goosse, H., Becquevort, S., Schoemann, V., Pasquer, B., and Vancoppenolle, M. (2009). Spatial distribution of the iron supply to phytoplankton in the Southern Ocean: a model study. *Biogeosciences*, 6:2861–2878, doi:10.5194/bg-6-2861-2009.

Lannuzel, D., Bowie, A. R., Remenyi, T., Lam, P., Townsend, A., Ibisanmi, E., Butler, E., Wagener, T., and Schoemann, V. (2011). Distributions of dissolved and particulate iron in the sub-Antarctic and Polar Frontal Southern Ocean (Australian sector). *Deep-Sea Research II*, 58:2094–2112, doi:10.1016/j.dsr2.2011.05.027.

Lannuzel, D., Chever, F., van der Merwe, P. C., Janssens, J., Roukaerts, A., Cavagna, A.-J., Townsend, A. T., Bowie, A. R., and Meiners, K. M. (2014). Iron biogeochemistry in Antarctic pack ice during SIPEX-2. *Deep-Sea Research II*, pages 1–12, doi:10.1016/j.dsr2.2014.12.003.

Lannuzel, D., Schoemann, V., de Jong, J., Chou, L., Delille, B., Becquevort, S., and Tison, J.-L. (2008). Iron study during a time series in the western Weddell pack ice. *Marine Chemistry*, 108:85–95, doi:10.1016/j.marchem.2007.10.006.

Lannuzel, D., Schoemann, V., de Jong, J., Pasquer, B., van der Merwe, P., Masson, F., Tison, J.-L., and Bowie, A. (2010). Distribution of dissolved iron in Antarctic sea ice: Spatial, seasonal, and inter-annual variability. *Journal of Geophysical Research*, 115(G03022), doi:10.1029/2009JG001031.

Lannuzel, D., Schoemann, V., de Jong, J., Tison, J.-L., and Chou, L. (2007). Distribution and biogeochemical behaviour of iron in the East Antarctic sea ice. *Marine Chemistry*, 106:18–32, doi:10.1016/j.marchem.2006.06.010.

Lannuzel, D., Schoemann, V., Dumont, I., Content, M., Jong, J., Tison, J.-L., Delille, B., and Becquevort, S. (2013). Effect of melting Antarctic sea ice on the fate of microbial communities studied in microcosms. *Polar Biology*, 36(10):1483–1497, doi:10.1007/s00300-013-1368-7.

Learman, D. R., Voelker, B. M., Vazquez-Rodriguez, A. I., and Hansel, C. M. (2011). Formation of manganese oxides by bacterially generated superoxide. *Nature Geoscience*, 4(2):95–98, doi:10.1038/ngeo1055.

Lewis, E. and Wallace, D. (1998). Program developed for CO_2 sustem calculations. ORNL/CDIAC-105.

Lin, H., Rauschenberg, S., Hexel, C. R., Shaw, T., and Twining, B. (2011). Free-drifting icebergs as sources of iron to the Weddell Sea. *Deep-Sea Research II*, 58:1392–1406, doi:10.1016/j.dsr2.2010.11.020.

Lippiatt, S., Brown, M., Lohan, M. C., and Bruland, K. W. (2011). Reactive iron delivery to the Gulf of Alaska via a Kenai eddy. *Deep-Sea Research I*, 58(11):1091–1102, doi:10.1016/j.dsr.2011.08.005.

Lippiatt, S., Lohan, M. C., and Bruland, K. W. (2010). The distribution of reactive iron in northern Gulf of Alaska coastal waters. *Marine Chemistry*, 121(1-4):187–199, doi:10.1016/j.marchem.2010.04.007.

Lis, H., Shaked, Y., Kranzler, C., Keren, N., and Morel, F. M. M. (2014). Iron bioavailability to phytoplankton: an empirical approach. *The ISME Journal*, pages 1–11, doi:10.1038/ismej.2014.199.

Liu, X. and Millero, F. J. (2002). The solubility of iron in seawater. *Marine Chemistry*, 77:43–54, doi:10.1016/S0304-4203(01)00074-3.

Lohan, M., Aguilar-Islas, A., and Bruland, K. (2006). Direct determination of iron in acidified (pH 1.7) seawater samples by flow injection analysis with catalytic spectrophotometric detection: Application and intercomparison. *Limnology and Oceanography: Methods*, 4:164–171, doi:10.4319/lom.2006.4.164.

Lohan, M. and Bruland, K. (2008). Elevated Fe(II) and dissolved Fe in hypoxic shelf waters off Oregon and Washington: An enhanced source of iron to coastal upwelling regimes. *Environmental science & technology*, 42(17):6462–8.

Löscher, B., de Baar, H., de Jong, J., Veth, C., and Dehairs, F. (1997). The distribution of Fe in the Antarctic Circumpolar Current. *Deep-Sea Research II*, 44(1-2):143–187.

Luo, C., Mahowald, N., Bond, T., Chuang, P. Y., Artaxo, P., Siefert, R., Chen, Y., and Schauer, J. (2008). Combustion iron distribution and deposition. *Global Biogeochemical Cycles*, 22(1), doi:10.1029/2007GB002964.

MacFadyen, A., Hickey, B., and Cochlan, W. (2008). Influences of the Juan de Fuca Eddy on circulation, nutrients, and phytoplankton production in the northern California Current System. *Journal of Geophysical Research*, 113, doi:10.1029/2007JC004412.

Mackey, K. R. M., Hunter, D., Fischer, E. V., Jiang, Y., Allen, B., Chen, Y., Liston, A., Reuter, J., Schladow, G., and Paytan, A. (2013). Aerosol-nutrient-induced picoplankton growth in Lake Tahoe. *Journal of Geophysical Research: Biogeosciences*, 118, doi:10.1002/jgrg.20084.

Mackinson, B. L., Moran, S. B., Lomas, M. W., Stewart, G. M., and Kelly, R. P. (2014). Estimates of micro-, nano-, and picoplankton contributions to particle export in the northeast Pacific. *Biogeosciences Discussions*, 11(8):12631–12671, doi:10.5194/bgd-11-12631-2014.

Maldonado, M. and Price, N. (1999). Utilization of iron bound to strong organic ligands by plankton communities in the subarctic Pacific Ocean. *Deep-Sea Research II*, 46:2447–2473, doi:10.1016/S0967-0645(99)00071-5.

Maldonado, M. and Price, N. (2001). Reduction and transport of organically bound iron by *Thalassiosira oceanica* (Bacillariophyceae). *Journal of Phycology*, 37:298–309.

Maldonado, M., Strzepek, R., Sander, S., and Boyd, P. (2005). Acquisition of iron bound to strong organic complexes, with different Fe binding groups and photochemical reactivities, by plankton communities in Fe-limited subantarctic waters. *Global Biogeochemical Cycles*, 19(GB4S23), doi:10.1029/2005GB002481.

Marsay, C. M., Sedwick, P. N., Dinniman, M. S., Barrett, P. M., Mack, S. L., and Mcgillicuddy Jr., D. J. (2014). Estimating the benthic efflux of dissolved iron on the Ross Sea continental shelf. *Geophysical Research Letters*, 41:7576–7583, doi:10.1002/2014GL061684.Received.

Marshall, J.-A., Salas, M., Oda, T., and Hallegraeff, G. (2005). Superoxide production by marine microalgae. *Marine Biology*, 147(2):533–540, doi:10.1007/s00227-005-1596-7.

Martin, J. (1990). Glacial-interglacial CO_2 change: the iron hypothesis. *Paleoceanography*, 5(1):1–13.

Martin, J., Gordon, R., Fitzwater, S., and Broenkow, W. (1989). VERTEX: phytoplankton/iron studies in the Gulf of Alaska. *Deep-Sea Research*, 36(5):649–680.

Martin, J., Knauer, G., Karl, D., and Broenkow, W. (1987). VERTEX: Carbon cycling in the northeast Pacific. *Deep-Sea Research*, 34(2):267–285.

Measures, C. (1999). The role of entrained sediments in sea ice in the distribution of aluminium and iron in the surface waters of the Arctic Ocean. *Marine Chemistry*, 68:59–70.

Measures, C. and Vink, S. (2001). Dissolved Fe in the upper waters of the Pacific sector of the Southern Ocean. *Deep-Sea Research II*, 48:3913–3941, doi:10.1016/S0967-0645(01)00074-1.

Measures, C. I., Landing, W. M., Brown, M. T., and Buck, C. S. (2008). High-resolution Al and Fe data from the Atlantic Ocean CLIVAR-CO_2 repeat hydrography A16N transect: Extensive linkages between atmospheric dust and upper ocean geochemistry. *Global Biogeochemical Cycles*, 22(1):GB1005, doi:10.1029/2007GB003042.

Measures, C. I. C., Hatta, M., and Grand, M. M. (2012). Bioactive trace metal distributions and biogeochemical controls in the Southern Ocean. *Oceanography*, 25(3):122–133.

Micinski, E., Ball, L. A., and Zafiriou, O. C. (1993). Photochemical oxygen activation: Superoxide radical detection and production rates in the Eastern Caribbean. *Journal of Geophysical Research*, 98(C2):2299–2306.

Miller, W. L., King, D., Lin, J., and Kester, D. R. (1995). Photochemical redox cycling of iron in coastal seawater. *Marine Chemistry*, 50(1-4):63–77, doi:10.1016/0304-4203(95)00027-O.

Millero, F. and Sotolongo, S. (1989). The oxidation of Fe(II) with H_2O_2 in seawater. *Geochimica et Cosmochimica Acta*, 53(8):1867–1873, doi:10.1016/0016-7037(89)90307-4.

Millero, F., Sotolongo, S., and Izaguirre, M. (1987). The oxidation kinetics of Fe(II) in seawater. *Geochimica et Cosmochimica Acta*, 51:793–801, doi:10.1016/0016-7037(87)90093-7.

Millero, F. J. (1995). Thermodynamics of the carbon dioxide system in the oceans. *Geochimica et Cosmochimica Acta*, 59(4):661–677.

Moffett, J. W., Goepfert, T. J., and Naqvi, S. W. A. (2007). Reduced iron associated with secondary nitrite maxima in the Arabian Sea. *Deep-Sea Research I*, 54(8):1341–1349, doi:10.1016/j.dsr.2007.04.004.

Moore, J. and Braucher, O. (2008). Sedimentary and mineral dust sources of dissolved iron to the world ocean. *Biogeosciences*, 5:631–656.

Moore, J. K., Doney, S. C., Glover, D. M., and Fung, I. Y. (2002). Iron cycling and nutrient-limitation patterns in surface waters of the World Ocean. *Deep-Sea Research II*, 49:463–507.

Morel, F. and Hering, J. (1997). *Principles and Applications of Aquatic Chemistry*. Wiley & Sons, New York, NY.

Morgan, M., Trieste, P. V., and Garlick, S. (1988). Ultraviolet molar absorptivities of aqueous hydrogen peroxide and hydroperoxyl ion. *Analytica Chimica Acta*, 215:325–329.

Nelson, N., Siegel, D., and Michaels, A. (1998). Seasonal dynamics of colored dissolved material in the Sargasso Sea. *Deep-Sea Research I*, 45:931–957.

Nelson, N. B., Carlson, C. A., and Steinberg, D. K. (2004). Production of chromophoric dissolved organic matter by Sargasso Sea microbes. *Marine Chemistry*, 89:273–287, doi:10.1016/j.marchem.2004.02.017.

Neshyba, S. (1977). Upwelling by icebergs. *Nature*, 267:507–508.

Neuer, S., Torres-Padrón, M. E., Gelado-Caballero, M. D., Rueda, M. J., Hernández-Brito, J., Davenport, R., and Wefer, G. (2004). Dust deposition pulses to the eastern subtropical North Atlantic gyre: Does ocean's biogeochemistry respond? *Global Biogeochemical Cycles*, 18(4), doi:10.1029/2004GB002228.

Nishikawa, M., Hao, Q., and Morita, M. (2000). Preparation and evaluation of certified reference materials for Asian mineral dust. *Global Environ. Research*, 4(1):103–113.

Nishioka, J., Ono, T., Saito, H., Nakatsuka, T., Takeda, S., Yoshimura, T., Suzuki, K., Kuma, K., Nakabayashi, S., Tsumune, D., Mitsudera, H., Johnson, W. K., and Tsuda, A. (2007). Iron supply to the western subarctic Pacific: Importance of iron export from the Sea of Okhotsk. *Journal of Geophysical Research*, 112(C10):C10012, doi:10.1029/2006JC004055.

Nishioka, J., Takeda, S., Wong, C. S., and Johnson, W. K. (2001). Size-fractionated iron concentrations in the northeast Pacific Ocean: distribution of soluble and small colloidal iron. *Marine Chemistry*, 74:157–179.

Noffke, A., Hensen, C., Sommer, S., Scholz, F., Bohlen, L., Mosch, T., Graco, M., and Wallmann, K. (2012). Benthic iron and phosphorus fluxes across the Peruvian oxygen minimum zone. *Limnology and Oceanography*, 57(3):851–867, doi:10.4319/lo.2012.57.3.0851.

Norman, L., Thomas, D. N., Stedmon, C. A., Granskog, M. A., Papadimitriou, S., Krapp, R. H., Meiners, K. M., Lannuzel, D., van der Merwe, P., and Dieckmann, G. S. (2011). The characteristics of dissolved organic matter (DOM) and chromophoric dissolved organic matter (CDOM) in Antarctic sea ice. *Deep-Sea Research II*, 58:1075–1091, doi:10.1016/j.dsr2.2010.10.030.

Obata, H., Karatani, H., and Nakayama, E. (1993). Automated determination of iron in seawater by chelating resin concentration and chemiluminescence detection. *Analytical Chemistry*, 65:1524–1528.

Ohnemus, D. C. and Lam, P. J. (2015). Cycling of lithogenic marine particles in the US GEOTRACES North Atlantic transect. *Deep-Sea Research II*, pages 1–20, doi:10.1016/j.dsr2.2014.11.019.

Orsi, A. H., Whitworth III, T., and Nowlin Jr, W. D. (1995). On the meridional extent and fronts of the Antarctic Circumpolar Current. *Deep-Sea Research I*, 42(5):641–673.

Ortega-Retuerta, E., Reche, I., Pulido-Villena, E., Agustí, S., and Duarte, C. (2010a). Distribution and photoreactivity of chromophoric dissolved organic matter in the Antarctic Peninsula (Southern Ocean). *Marine Chemistry*, 118:129–139, doi:10.1016/j.marchem.2009.11.008.

Ortega-Retuerta, E., Siegel, D., Nelson, N., Duarte, C., and Reche, I. (2010b). Observations of chromophoric dissolved and detrital organic matter distribution using remote sensing in the Southern Ocean: Validation, dynamics and regulation. *Journal of Marine Systems*, 82:295–303, doi:10.1016/j.jmarsys.2010.06.004.

O'Sullivan, D., Hanson, A. K., and Kester, D. R. (1995). Stopped flow luminol chemiluminescence determination of Fe (II) and reducible iron in seawater at subnanomolar levels. *Marine Chemistry*, 49:65–77.

Paris, R., Desboeufs, K. V., Formenti, P., Nava, S., and Chou, C. (2010). Chemical characterisation of iron in dust and biomass burning aerosols during AMMA-SOP0/DABEX: implication for iron solubility. *Atmospheric Chemistry and Physics*, 10(9):4273–4282, doi:10.5194/acp-10-4273-2010.

Paytan, A., Mackey, K. R. M., Chen, Y., Lima, I. D., Doney, S. C., Mahowald, N., Labiosa, R., and Post, A. F. (2009). Toxicity of atmospheric aerosols on marine phytoplankton. *Proceedings of the National Academy of Sciences*, 106(12):4601–5, doi:10.1073/pnas.0811486106.

Planquette, H., Sanders, R. R., Statham, P. J., Morris, P. J., and Fones, G. R. (2011). Fluxes of particulate iron from the upper ocean around the Crozet Islands: A

naturally iron-fertilized environment in the Southern Ocean. *Global Biogeochemical Cycles*, 25(2):GB2011, doi:10.1029/2010GB003789.

Pollard, R. T., Salter, I., Sanders, R. J., Lucas, M. I., Moore, C. M., Mills, R. A., Statham, P. J., Allen, J. T., Baker, A. R., Bakker, D. C. E., Charette, M. A., Fielding, S., Fones, G. R., French, M., Hickman, A. E., Holland, R. J., Hughes, J. A., Jickells, T. D., Lampitt, R. S., Morris, P. J., Nédélec, F. H., Nielsdóttir, M., Planquette, H., Popova, E. E., Poulton, A. J., Read, J. F., Seeyave, S., Smith, T., Stinchcombe, M., Taylor, S., Thomalla, S., Venables, H. J., Williamson, R., and Zubkov, M. V. (2009). Southern Ocean deep-water carbon export enhanced by natural iron fertilization. *Nature*, 457(7229):577–80, doi:10.1038/nature07716.

Powers, L. C. and Miller, W. L. (2014). Blending remote sensing data products to estimate photochemical production of hydrogen peroxide and superoxide in the surface ocean. *Environmental science: Processes & impacts*, 16(4):792–806, doi:10.1039/c3em00617d.

Price, N. M., Harrison, G. I., Hering, J. G., Hudson, R. J., Nirel, P. M. V., Palenik, B., and Morel, F. M. M. (1989). Preparation and chemistry of the artificial algal culture medium Aquil. *Biological Oceanography*, 6(5-6):443–461, doi:10.1080/01965581.1988.10749544.

Raiswell, R. (2011). Iceberg-hosted nanoparticulate Fe in the Southern Ocean: Mineralogy, origin, dissolution kinetics and source of bioavailable Fe. *Deep-Sea Research II*, 58:1364–1375, doi:10.1016/j.dsr2.2010.11.011.

Raiswell, R., Benning, L. G., Tranter, M., and Tulaczyk, S. (2008). Bioavailable iron in the Southern Ocean: the significance of the iceberg conveyor belt. *Geochemical transactions*, 9(7), doi:10.1186/1467-4866-9-7.

Raiswell, R. and Canfield, D. (2012). The iron biogeochemical cycle past and present. In *Geochemical Perspectives*, pages 81–93.

Raiswell, R., Tranter, M., Benning, L. G., Siegert, M., Death, R., Huybrechts, P., and Payne, T. (2006). Contributions from glacially derived sediment to the global iron (oxyhydr)oxide cycle: Implications for iron delivery to the oceans. *Geochimica et Cosmochimica Acta*, 70(11):2765–2780, doi:10.1016/j.gca.2005.12.027.

Raven, J. A., Evans, M. C. W., and Korb, R. E. (1999). The role of trace metals in photosynthetic electron transport in O_2 - evolving organisms. *Photosynthesis Research*, 60:111–149.

Rijkenberg, M., Fischer, A., Kroon, J., Gerringa, L., Timmermans, K., Wolterbeek, H., and de Baar, H. (2005). The influence of UV irradiation on the photoreduction of iron in the Southern Ocean. *Marine Chemistry*, 93:119–129, doi:10.1016/j.marchem.2004.03.021.

Rijkenberg, M., Powell, C., and Dall'Osto, M. (2008). Changes in iron speciation following a Saharan dust event in the tropical North Atlantic Ocean. *Marine Chemistry*, 110(1-2):56–67, doi:10.1016/j.marchem.2008.02.006.

Rochelle-Newall, E. and Fisher, T. (2002). Production of chromophoric dissolved organic matter fluorescence in marine and estuarine environments: an investigation into the role of phytoplankton. *Marine Chemistry*, 77:7–21.

Rose, A. (2012). The influence of extracellular superoxide on iron redox chemistry and bioavailability to aquatic microorganisms. *Frontiers in Microbiology*, 3(124), doi:10.3389/fmicb.2012.00124.

Rose, A. L., Godrant, A., Furnas, M., and Waite, T. D. (2010). Dynamics of nonphotochemical superoxide production in the Great Barrier Reef lagoon. *Limnology and Oceanography*, 55(4):1521–1536, doi:10.4319/lo.2010.55.4.1521.

Rose, A. L., Salmon, T. P., Lukondeh, T., Neilan, B. a., and Waite, T. D. (2005). Use of superoxide as an electron shuttle for iron acquisition by the marine cyanobacterium *Lyngbya majuscula*. *Environmental science & technology*, 39(10):3708–15.

Rose, A. L. and Waite, T. D. (2001). Chemiluminescence of luminol in the presence of iron(II) and oxygen: oxidation mechanism and implications for its analytical use. *Analytical Chemistry*, 73:5909–5920.

Rose, A. L. and Waite, T. D. (2005). Reduction of organically complexed ferric iron by superoxide in a simulated natural water. *Environmental science & technology*, 39(8):2645–50.

Rose, A. L. and Waite, T. D. (2006). Role of superoxide in the photochemical reduction of iron in seawater. *Geochimica et Cosmochimica Acta*, 70(15):3869–3882, doi:10.1016/j.gca.2006.06.008.

Rose, A. L., Webb, E. A., Waite, T. D., and Moffett, J. W. (2008). Measurement and implications of nonphotochemically generated superoxide in the equatorial Pacific Ocean. *Environmental science & technology*, 42(7):2387–93.

Roy, E. and Wells, M. (2011). Evidence for regulation of Fe (II) oxidation by organic complexing ligands in the Eastern Subarctic Pacific. *Marine Chemistry*, 127(1-4):115–122, doi:10.1016/j.marchem.2011.08.006.

Roy, E. G., Wells, M. L., and King, D. W. (2008). Persistence of iron(II) in surface waters of the western subarctic Pacific. *Limnology and Oceanography*, 53(1):89–98, doi:10.4319/lo.2008.53.1.0089.

Rubin, M., Berman-Frank, I., and Shaked, Y. (2011). Dust- and mineral-iron utilization by the marine dinitrogen-fixer *Trichodesmium*. *Nature Geoscience*, 4:529–534, doi:10.1038/NGEO1181.

Rue, E. and Bruland, K. (1995). Complexation of iron(III) by natural organic ligands in the Central North Pacific as determined by a new competitive ligand equilibration/adsorptive cathodic stripping voltammetric method. *Marine Chemistry*, 50:117–138.

Rusak, S. A., Peake, B. M., Richard, L. E., Nodder, S. D., and Cooper, W. J. (2011). Distributions of hydrogen peroxide and superoxide in seawater east of New Zealand. *Marine Chemistry*, 127(1-4):155–169, doi:10.1016/j.marchem.2011.08.005.

Sackmann, B., Mack, L., Logsdon, M., and Perry, M. J. (2004). Seasonal and interannual variability of SeaWiFS-derived chlorophyll *a* concentrations in waters off the Washington and Vancouver Island coasts, 1998 - 2002. *Deep-Sea Research II*, 51(10-11):945–965, doi:10.1016/j.dsr2.2003.09.004.

Saragosti, E., Tchernov, D., Katsir, A., and Shaked, Y. (2010). Extracellular production and degradation of superoxide in the coral *Stylophora pistillata* and cultured *Symbiodinium*. *PLOS one*, 5(9):e12508, doi:10.1371/journal.pone.0012508.

Sarthou, G., Bucciarelli, E., Chever, F., Hansard, S., González-Dávila, M., Santana-Casiano, J., Planchon, F., and Speich, S. (2011). Labile Fe(II) concentrations in the Atlantic sector of the Southern Ocean along a transect from the subtropical domain to the Weddell Sea Gyre. *Biogeosciences*, 8:2461–2479, doi:10.5194/bg-8-2461-2011.

Savoye, N., Benitez-Nelson, C., Burd, A. B., Cochran, J. K., Charette, M., Buesseler, K. O., Jackson, G. A., Roy-Barman, M., Schmidt, S., and Elskens, M. (2006). ^{234}Th sorption and export models in the water column: A review. *Marine Chemistry*, 100(3-4):234–249, doi:10.1016/j.marchem.2005.10.014.

Schallenberg, C., Davidson, A. B., Simpson, K. G., Miller, L. A., and Cullen, J. T. (2015a). Iron(II) variability in the northeast subarctic Pacific Ocean. *Marine Chemistry*, doi:10.1016/j.marchem.2015.04.004.

Schallenberg, C., van der Merwe, P., Chever, F., Cullen, J. T., Lannuzel, D., and Bowie, A. R. (2015b). Dissolved iron and iron(II) distributions beneath the pack ice in the East Antarctic (120°E) during the winter/spring transition. *Deep-Sea Research II*, doi:dx.doi.org/10.1016/j.dsr2.2015.02.019.

Scholz, F., Mcmanus, J., Mix, A. C., Hensen, C., and Schneider, R. R. (2014). The impact of ocean deoxygenation on iron release from continental margin sediments. *Nature Geoscience*, 7(6):433–437, doi:10.1038/ngeo2162.

Schroth, A. W., Crusius, J., Sholkovitz, E. R., and Bostick, B. C. (2009). Iron solubility driven by speciation in dust sources to the ocean. *Nature Geoscience*, 2(5):337–340, doi:10.1038/ngeo501.

Sedwick, P., Bowie, A., and Trull, T. (2008). Dissolved iron in the Australian sector of the Southern Ocean (CLIVAR SR3 section): Meridional and seasonal trends. *Deep-Sea Research I*, 55:911–925, doi:10.1016/j.dsr.2008.03.011.

Sedwick, P. and DiTullio, G. (1997). Regulation of algal blooms in Antarctic shelf waters by the release if iron from melting sea ice. *Geophysical Research Letters*, 24(20):2515–2518.

Sedwick, P. N., DiTullio, G., and Mackey, D. J. (2000). Iron and manganese in the Ross Sea, Antarctica: Seasonal iron limitation in Antarctic shelf waters. *Journal of Geophysical Research*, 105(C5):11,321–11,336.

Sedwick, P. N., Sholkovitz, E. R., and Church, T. M. (2007). Impact of anthropogenic combustion emissions on the fractional solubility of aerosol iron: Evidence from the Sargasso Sea. *Geochemistry, Geophysics, Geosystems*, 8(10), doi:10.1029/2007GC001586.

Sedwick, P. N., Sohst, B., and Bowie, A. R. (2014). A zonal picture of the water column distribution of dissolved iron(II) during the U.S. GEOTRACES North Atlantic transect cruises. *Deep-Sea Research II*.

Severmann, S., McManus, J., Berelson, W. M., and Hammond, D. E. (2010). The continental shelf benthic iron flux and its isotope composition. *Geochimica et Cosmochimica Acta*, 74:3984–4004, doi:10.1016/j.gca.2010.04.022.

Shadwick, E. H., Rintoul, S. R., Tilbrook, B., Williams, G. D., Young, N., Fraser, A. D., Marchant, H., Smith, J., and Tamura, T. (2013). Glacier tongue calving reduced dense water formation and enhanced carbon uptake. *Geophysical Research Letters*, 40(5):904–909, doi:10.1002/grl.50178.

Shaked, Y., Kustka, A., and Morel, F. (2005). A general kinetic model for iron acquisition by eukaryotic phytoplankton. *Limnology and Oceanography*, 50(3):872–882.

Shaked, Y. and Lis, H. (2012). Disassembling iron availability to phytoplankton. *Frontiers in Microbiology*, 3, doi:10.3389/fmicb.2012.00123.

Sharpless, C. M. and Blough, N. V. (2014). The importance of charge-transfer interactions in determining chromophoric dissolved organic matter (CDOM) optical and photochemical properties. *Environmental science: Processes & impacts*, 16(4):654–71, doi:10.1039/c3em00573a.

Shelley, R. U., Morton, P. L., and Landing, W. M. (2015). Elemental ratios and enrichment factors in aerosols from the US-GEOTRACES North Atlantic transects. *Deep-Sea Research II*, doi:10.1016/j.dsr2.2014.12.005.

Shi, Z., Bonneville, S., Krom, M. D., Carslaw, K. S., Jickells, T. D., Baker, A. R., and Benning, L. G. (2011). Iron dissolution kinetics of mineral dust at low pH during simulated atmospheric processing. *Atmospheric Chemistry and Physics*, 11(3):995–1007, doi:10.5194/acp-11-995-2011.

Shigemitsu, M., Nishioka, J., Watanabe, Y., Yamanaka, Y., Nakatsuka, T., and Volkov, Y. (2013). Fe/Al ratios of suspended particulate matter from intermediate water in the Okhotsk Sea: Implications for long-distance lateral transport of particulate Fe. *Marine Chemistry*, 157:41–48, doi:10.1016/j.marchem.2013.07.003.

Sholkovitz, E. R., Sedwick, P. N., and Church, T. M. (2010). On the fractional solubility of copper in marine aerosols: Toxicity of aeolian copper revisited. *Geophysical Research Letters*, 37(20):n/a–n/a, doi:10.1029/2010GL044817.

Sholkovitz, E. R., Sedwick, P. N., Church, T. M., Baker, A. R., and Powell, C. F. (2012). Fractional solubility of aerosol iron: Synthesis of a global-scale data set. *Geochimica et Cosmochimica Acta*, 89:173–189, doi:10.1016/j.gca.2012.04.022.

Siedlecki, S. A., Mahadevan, A., and Archer, D. E. (2012). Mechanism for export of sediment-derived iron in an upwelling regime. *Geophysical Research Letters*, 39(3), doi:10.1029/2011GL050366.

Sigman, D. M. D. and Boyle, E. E. A. (2000). Glacial/interglacial variations in atmospheric carbon dioxide. *Nature*, 407:859–869.

Smetacek, V., Klaas, C., Strass, V. H., Assmy, P., Montresor, M., Cisewski, B., Savoye, N., Webb, A., D'Ovidio, F., Arrieta, J. M., Bathmann, U., Bellerby, R., Berg, G. M., Croot, P., Gonzalez, S., Henjes, J., Herndl, G. J., Hoffmann, L. J., Leach, H., Losch, M., Mills, M. M., Neill, C., Peeken, I., Röttgers, R., Sachs, O., Sauter, E., Schmidt, M. M., Schwarz, J., Terbrüggen, A., and Wolf-Gladrow, D. (2012). Deep carbon export from a Southern Ocean iron-fertilized diatom bloom. *Nature*, 487(7407):313–9, doi:10.1038/nature11229.

Smith, W. and Nelson, D. M. (1986). Importance of ice edge phytoplankton production in the Southern Ocean. *BioScience*, 36(4):251–257.

Sokolov, S. and Rintoul, S. R. (2007). On the relationship between fronts of the Antarctic Circumpolar Current and surface chlorophyll concentrations in the Southern Ocean. *Journal of Geophysical Research*, 112(C7):C07030, doi:10.1029/2006JC004072.

Statham, P., German, C., and Connelly, D. (2005). Iron (II) distribution and oxidation kinetics in hydrothermal plumes at the Kairei and Edmond vent sites, Indian Ocean. *Earth and Planetary Science Letters*, 236:588–596, doi:10.1016/j.epsl.2005.03.008.

Stephenson Jr., G. R., Sprintall, J., Gille, S. T., Vernet, M., Helly, J. J., and Kaufmann, R. S. (2011). Subsurface melting of a free-floating Antarctic iceberg. *Deep-Sea Research II*, 58:1336–1345, doi:10.1016/j.dsr2.2010.11.009.

Stookey, L. L. (1970). Ferrozine — a new spectrophotometric reagent for iron. *Analytical Chemistry*, 42(7):779–781, doi:10.1021/ac60289a016.

Strickland, J. and Parsons, T. (1972). *A practical handbook of seawater analysis, Fisheries Research Board of Canada Bulletin 167*. Ottawa, 2nd edition.

Strutton, P., Griffiths, F. B., Waters, R. L., Wright, S. W., and Bindoff, N. (2000). Primary productivity off the coast of East Antarctica (80-150°E): January to March 1996. *Deep-Sea Research II*, 47(2000):2327–2362.

Sullivan, J. M., Twardowski, M. S., Donaghay, P. L., and Freeman, S. A. (2005). Use of optical scattering to discriminate particle types in coastal waters. *Applied Optics*, 44(9):1667, doi:10.1364/AO.44.001667.

Sunda, W. G. (2010). Iron and the carbon pump. *Science*, 327:654–655, doi:10.1126/science.1186151.

Tagliabue, A., Aumont, O., and Bopp, L. (2014). The impact of different external sources of iron on the global carbon cycle. *Geophysical Research Letters*, 41, doi:10.1002/2013GL059059.

Tagliabue, A., Bopp, L., and Aumont, O. (2009). Evaluating the importance of atmospheric and sedimentary iron sources to Southern Ocean biogeochemistry. *Geophysical Research Letters*, 36(L13601), doi:10.1029/2009GL038914.

Tagliabue, A., Bopp, L., Dutay, J.-C., Bowie, A. R., Chever, F., Jean-Baptiste, P., Bucciarelli, E., Lannuzel, D., Remenyi, T., Sarthou, G., Aumont, O., Gehlen, M., and Jeandel, C. (2010). Hydrothermal contribution to the oceanic dissolved iron inventory. *Nature Geoscience*, 3(4):252–256, doi:10.1038/ngeo818.

Thomson, R., Hickey, B., and LeBlond, P. (1989). The Vancouver Island Coastal Current: Fisheries barrier and conduit. In McFarlane, G., editor, *Effects of ocean variability on recruitment and an evaluation of parameters used in stock assessment models*, pages 265–296. Can. Spec. Publ. Fish. Aquat. Sci.

Thuróczy, C.-E., Alderkamp, A.-C., Laan, P., Gerringa, L., Mills, M., Van Dijken, G., de Baar, H. J. W., and Arrigo, K. R. (2012). Key role of organic complexation of iron in sustaining phytoplankton blooms in the Pine Island and Amundsen Polynyas (Southern Ocean). *Deep-Sea Research II*, 71-76:49–60, doi:10.1016/j.dsr2.2012.03.009.

Thuróczy, C.-E., Gerringa, L., Klunder, M., Laan, P., and de Baar, H. (2011). Observation of consistent trends in the organic complexation of dissolved iron in the Atlantic sector of the Southern Ocean. *Deep-Sea Research II*, 58:2695–2706, doi:10.1016/j.dsr2.2011.01.002.

Tomshin, O. and Solovyev, V. (2014). The impact of large-scale forest fires on atmospheric aerosol characteristics. *International Journal of Remote Sensing*, 35(15):5742–5749, doi:10.1080/01431161.2014.945001.

Tortell, P., Maldonado, M., and Price, N. (1996). The role of heterotrophic bacteria in iron-limited ocean ecosystems. *Nature*, 383:330–332.

Trapp, J. M. and Millero, F. J. (2007). The oxidation of iron(II) with oxygen in NaCl brines. *Journal of Solution Chemistry*, 36(11-12):1479–1493, doi:10.1007/s10953-007-9192-8.

Tsuda, A., Kiyosawa, H., Kuwata, A., Mochizuki, M., Shiga, N., Saito, H., Chiba, S., Imai, K., Nishioka, J., and Ono, T. (2005). Responses of diatoms to iron-enrichment (SEEDS) in the western subarctic Pacific, temporal and spatial comparisons. *Progress in Oceanography*, 64(2-4):189–205, doi:10.1016/j.pocean.2005.02.008.

Twining, B. S. and Baines, S. B. (2013). The trace metal composition of marine phytoplankton. *Annual Review of Marine Science*, 5:191–215, doi:10.1146/annurev-marine-121211-172322.

Uematsu, M., Duce, R. A., Prospero, J. M., Chen, L., Merrill, J. T., and McDonald, R. L. (1983). Transport of mineral aerosol from Asia over the North Pacific Ocean. *Journal of Geophysical Research*, 88(C9):5343, doi:10.1029/JC088iC09p05343.

van de Vossenberg, J., Rattray, J. E., Geerts, W., Kartal, B., van Niftrik, L., van Donselaar, E. G., Sinninghe Damsté, J. S., Strous, M., and Jetten, M. S. M. (2008). Enrichment and characterization of marine anammox bacteria associated with global nitrogen gas production. *Environmental microbiology*, 10(11):3120–9, doi:10.1111/j.1462-2920.2008.01643.x.

van der Merwe, P., Lannuzel, D., Bowie, A., Mancuso Nichols, C., and Meiners, K. (2011a). Iron fractionation in pack and fast ice in East Antarctica: Temporal decoupling between the release of dissolved and particulate iron during spring melt. *Deep-Sea Research II*, 58:1222–1236, doi:10.1016/j.dsr2.2010.10.036.

van der Merwe, P., Lannuzel, D., Bowie, A. R., and Meiners, K. M. (2011b). High temporal resolution observations of spring fast ice melt and seawater iron enrichment in East Antarctica. *Journal of Geophysical Research*, 116(G03017), doi:10.1029/2010JG001628.

van der Merwe, P., Lannuzel, D., Mancuso Nichols, C., Meiners, K., Heil, P., Norman, L., Thomas, D. N., and Bowie, A. R. (2009). Biogeochemical observations during the winterspring transition in East Antarctic sea ice: Evidence of iron and exopolysaccharide controls. *Marine Chemistry*, 115:163–175, doi:10.1016/j.marchem.2009.08.001.

Vancoppenolle, M., Meiners, K., Michel, C., Bopp, L., Brabant, F., Carnat, G., Delille, B., Lannuzel, D., Madec, G., Moreau, S., Tison, J.-L., and van der Merwe, P. (2013). Role of sea ice in global biogeochemical cycles: Emerging views and challenges. *Quaternary Science Reviews*, 79:207–230.

Vermilyea, A. W., Hansard, S. P., and Voelker, B. M. (2010). Dark production of hydrogen peroxide in the Gulf of Alaska. *Limnology and Oceanography*, 55(2):580–588, doi:10.4319/lo.2009.55.2.0580.

Voelker, B., Sedlak, D., and Zafiriou, O. (2000). Chemistry of superoxide radical in seawater: Reactions with organic Cu complexes. *Environmental science & technology*, 34:1036–1042.

Vraspir, J. M. and Butler, A. (2009). Chemistry of marine ligands and siderophores. *Annual Review of Marine Science*, 1:43–63, doi:10.1146/annurev.marine.010908.163712.

Wadley, M. R., Jickells, T. D., and Heywood, K. J. (2014). The role of iron sources and transport for Southern Ocean productivity. *Deep-Sea Research I*, 87:82–94, doi:10.1016/j.dsr.2014.02.003.

Wagener, T., Guieu, C., and Leblond, N. (2010). Effects of dust deposition on iron cycle in the surface Mediterranean Sea: results from a mesocosm seeding experiment. *Biogeosciences*, 7(11):3769–3781, doi:10.5194/bg-7-3769-2010.

Watson, A., Bakker, D., Ridgwell, A., Boyd, P., and Law, C. (2000). Effect of iron supply on Southern Ocean CO_2 uptake and implications for glacial atmospheric CO_2. *Nature*, 407:730–733.

Weber, K. A., Achenbach, L. A., and Coates, J. D. (2006). Microorganisms pumping iron: anaerobic microbial iron oxidation and reduction. *Nature reviews. Microbiology*, 4(10):752–64, doi:10.1038/nrmicro1490.

Weber, L. (2005). Modeling the speciation and biogeochemistry of iron at the Bermuda Atlantic Time-series Study site. *Global Biogeochemical Cycles*, 19(1):GB1019, doi:10.1029/2004GB002340.

Westberry, T. K., Behrenfeld, M. J., Milligan, A. J., and Doney, S. C. (2013). Retrospective satellite ocean color analysis of purposeful and natural ocean iron fertilization. *Deep-Sea Research I*, 73:1–16, doi:10.1016/j.dsr.2012.11.010.

Westwood, K. J., Griffiths, F., Meiners, K. M., and Williams, G. D. (2010). Primary productivity off the Antarctic coast from 30-80°E; BROKE-West survey, 2006. *Deep-Sea Research II*, 57:794–814, doi:10.1016/j.dsr2.2008.08.020.

Whitney, F., Crawford, W., and Harrison, P. (2005). Physical processes that enhance nutrient transport and primary productivity in the coastal and open ocean of the subarctic NE Pacific. *Deep-Sea Research II*, 52(5-6):681–706, doi:10.1016/j.dsr2.2004.12.023.

Whitney, F. A., Freeland, H. J., and Robert, M. (2007). Persistently declining oxygen levels in the interior waters of the eastern subarctic Pacific. *Progress in Oceanography*, 75(2):179–199, doi:10.1016/j.pocean.2007.08.007.

Williams, G., Meijers, A., Poole, A., Mathiot, P., Tamura, T., and Klocker, A. (2011). Late winter oceanography off the Sabrina and BANZARE coast (117-128°E), East Antarctica. *Deep-Sea Research II*, 58:1194–1210, doi:10.1016/j.dsr2.2010.10.035.

Wright, J. J., Konwar, K. M., and Hallam, S. J. (2012). Microbial ecology of expanding oxygen minimum zones. *Nature reviews. Microbiology*, 10(6):381–94, doi:10.1038/nrmicro2778.

Wu, J., Boyle, E., Sunda, W., and Wen, L. (2001). Soluble and colloidal iron in the oligotrophic North Atlantic and North Pacific. *Science*, 293(5531):847–849.

Wu, J. and Luther III, G. W. (1995). Complexation of Fe(III) by natural organic ligands in the Northwest Atlantic Ocean by a competitive ligand equilibration method and a kinetic approach. *Marine Chemistry*, 50(1-4):159–177, doi:10.1016/0304-4203(95)00033-N.

Wuttig, K., Wagener, T., Bressac, M., Dammshäuser, A., Streu, P., Guieu, C., and Croot, P. L. (2013). Impacts of dust deposition on dissolved trace metal concentrations (Mn, Al and Fe) during a mesocosm experiment. *Biogeosciences*, 10(4):2583–2600, doi:10.5194/bg-10-2583-2013.

Xing, X., Claustre, H., Blain, S., Ortenzio, A., Josephine, R., and Guinet, C. (2012). Quenching correction for in vivo chlorophyll fluorescence acquired by autonomous platforms: A case study with instrumented elephant seals in the Kerguelen region (Southern Ocean). *Limnol. Oceanogr.: Methods*, 10:483–495, doi:10.4319/lom.2012.10.483.

Xiu, P., Palacz, A. P., Chai, F., Roy, E. G., and Wells, M. L. (2011). Iron flux induced by Haida eddies in the Gulf of Alaska. *Geophysical Research Letters*, 38(13):L13607, doi:10.1029/2011GL047946.

Xiu, P., Thomas, A. C., and Chai, F. (2014). Satellite bio-optical and altimeter comparisons of phytoplankton blooms induced by natural and artificial iron addition in the Gulf of Alaska. *Remote Sensing of Environment*, 145:38–46, doi:10.1016/j.rse.2014.02.004.

Ye, Y., Wagener, T., Völker, C., Guieu, C., and Wolf-Gladrow, D. A. (2011). Dust deposition: iron source or sink? A case study. *Biogeosciences*, 8:2107–2124, doi:10.5194/bg-8-2107-2011.

Young, R., Carder, K., Betzer, P., Costello, D., Duce, R., DiTullio, G., Tindale, N., Laws, E., Uematsu, M., Merrill, J., and Feely, R. (1991). Atmospheric iron inputs and primary productivity: phytoplankton responses in the North Pacific. *Global Biogeochemical Cycles*, 5(2):119–134.

Yuan, J. and Shiller, A. M. (2004). Hydrogen peroxide in deep waters of the North Pacific Ocean. *Geophysical Research Letters*, 31(1):L01310, doi:10.1029/2003GL018439.

Yuan, W. and Zhang, J. (2006). High correlations between Asian dust events and biological productivity in the western North Pacific. *Geophysical Research Letters*, 33(7):L07603, doi:10.1029/2005GL025174.

Zafiriou, O. C. (1990). Chemistry of superoxide ion-radical (O_2^-) in seawater. I. pK_a^* (HOO) and uncatalyzed dismutation kinetics studied by pulse radiolysis*. *Marine Chemistry*, 30(7142):31–43.

Zafiriou, O. C., Voelker, B. M., and Sedlak, D. L. (1998). Chemistry of the superoxide radical (O_2^-) in seawater: Reactions with inorganic copper complexes. *The Journal of Physical Chemistry A*, 102(28):5693–5700, doi:10.1021/jp980709g.